ISTANBUL TECHNICAL UNIVERSITY ★ GRADUATE SCHOOL OF SCIENCE ENGINEERING AND TECHNOLOGY

PROPERTIES AND CHARACTERIZATION OF $LiFePO_4$ NANO POWDERS PRODUCED IN NONAQUEOUS SOLUTION

M.Sc. THESIS

Yahya TOPRAK

Department of Nanoscience and Nanoengineering

Nanoscience and Nanoengineering Programme

JANUARY 2014

ISTANBUL TECHNICAL UNIVERSITY ★ GRADUATE SCHOOL OF SCIENCE ENGINEERING AND TECHNOLOGY

PROPERTIES AND CHARACTERIZATION OF $LiFePO_4$ NANO POWDERS PRODUCED IN NONAQUEOUS SOLUTION

M.Sc. THESIS

Yahya TOPRAK

(513101019)

Department of Nanoscience and Nanoengineering

Nanoscience and Nanoengineering Programme

Thesis Advisor: Prof. Dr. A. Sezai SARAÇ

29 JANUARY 2014

İSTANBUL TEKNİK ÜNİVERSİTESİ ★ FEN BİLİMLERİ ENSTİTÜSÜ

SUSUZ ORTAMDA $LiFePO_4$ NANO TOZ ÜRETİMİ VE KARAKTERİZASYONU

YÜKSEK LİSANS TEZİ

Yahya TOPRAK

(513101019)

Nanobilim ve Nanomühensislik Anabilim Dalı

Nanobilim ve Nanomühensislik Programı

Tez Danışmanı: Prof. Dr. A. Sezai SARAÇ

29 OCAK 2014

Yahya Toprak, a **M.Sc.** student of ITU **Nanoscience&Nanoengineering / Graduate School of Science, Engineering and Technology** student ID 513101019, successfully defended the **thesis** entitled "**PROPERTIES AND CHARACTERIZATION OF $LiFePO_4$ NANO POWDERS PRODUCED IN NONAQUEOUS SOLUTION**", which he prepared after fulfilling the requirements specified in the associated legislations, before the jury whose signatures are below.

Thesis Advisor :	**Prof. Dr. A. Sezai SARAÇ** Istanbul Technical University	.....
Jury Members :	**Prof. Dr. E. Sabri KAYALI** Istanbul Technical University	.....
	Prof. Dr. Yücel ŞAHİN Yıldız Technical University	.....

Date of Submission : 16 December 2013
Date of Defense : 22 January 2014

I would like to dedicate this thesis to my family,
supporting and believing me during all the time of my life,
my friends helping me to encourage and motivate to keep studying.
Also I thank for my friends during their help of my thesis.
Thanks for everybody who made my life better…

FOREWORD

Batteries are widely used in daily life for the portable electronic devices such as laptops and cell phones. Nowadays, the interest for high energy density batteries is increasing rapidly due to electrical vehicle applications. Lithium-ion (Li-ion) batteries are the most common rechargeable batteries in many industrial productions. High energy densities and longer cycle life of Li-ion batteries take the attention of academic researchers and manufacturers. However Li-ion batteries are still under investigation to improve their properties and efficiency.

Li-ion batteries are mainly made of anode and cathode electrodes which can be lithium metal or alloys of lithium with other metals. $LiFePO_4$ is one of the most important cathode material for Li-ion battery industry due to its high specific capacity (170 mAh/g), low toxicity and low cost with stable structure comparing to other commercial cathode materials ($LiCoO_2$, $LiMn_2O_4$, $LiNiO_2$). Although it has a low electronic conductivity (10^{-9} S/cm), producing powders in nanometer sizes and covering the particles with carbon additives enhanced better conductivity results. For this reason, a novel technique is developed to cover with conductive carbon layers (CCL) on the surface of particles (US 20110151112 A1) by Dr. Marcin Molenda and coworkers in order to improve the conductivity of powders.

In this work, nanosized $LiFePO_4$ powders are produced by anhydrous solution precipitation technique and microemulsion technique. Precursor powders are examined in TGA to determine calcination temperature and covered by conductive carbon layers after calcination as referred by Dr. Molenda. Crystal structure and phases of powders are examined by XRD measurements and surface properties are analyzed by N_2-BET. Conductivities are obtained by AC (33Hz) 4-probe technique between (-20) °C and (+40) °C. Also electrochemical performances are measured by using potentiostat.

This project is done by the collaboration of Jagiellonian University and Istanbul Technical University laboratories. I would like to gratitude for my supervisor Prof. Dr. A. Sezai Saraç, also for my co-advisors Dr. Marcin Molenda and Dr. Małgorzata Zaitz from Jagiellonian University/Poland, for their scientific help and letting me using their laboratories to finish my thesis. Also I thanks for my friends, Agnieszka Chojnacka, Monika Bakierska, Hüseyin Can Çoban, Dilek Suadiye, M. Giray Ersözoğlu, Cem Ünsal and Timuçin Balkan and other coworkers in the laboratory helping me to do the experiments. Finally, I would like to thank Jagiellonian University and Istanbul Technical University cooperation and foundation of ERASMUS for all kind of supports.

January 2014

Yahya TOPRAK
(Materials Engineer)

TABLE OF CONTENTS

Page

ABBREVIATIONS

AC	**:** Alternative Current
CCL	**:** Conductive Carbon Layer
CV	**:** Cyclic Voltammogram
EIS	**:** Electrochemical Impedance Spectroscopy
EV	**:** Electrical Vehicles
HEV	**:** Hybrid Electrical Vehicles
IUPAC	**:** International Union of Pure and Applied Chemistry
JCPDS	**:** Joint Committee on Powder Diffraction Standarts
SEM	**:** Scanning Electron Microscopy
USABC	**:** United States Advanced Battery Consortium

LIST OF TABLES

Page

LIST OF FIGURES

Page

PROPERTIES AND CHARACTERIZATION OF $LiFePO_4$ NANO POWDERS PRODUCED IN NONAQUEOUS SOLUTION

SUMMARY

Rechargable batteries have a very important part in our lives since the development of electrical vehicles which are used in daily life such as cell phones and laptops. Li-ion rechargeable batteries are suppressed the other type of batteries due to their high energy densities and longer cycle life. Li-ion batteries are now the most widely used rechargeable batteries in energy industries having the biggest market share. For this reason industrial companies and academic researches try to improve the properties and efficiency of Li-ion batteries. More suitable materials having higher capacity, high energy densities, low cost, stable and environmental friendly are still under investigation for the usage of next generation electrical devices as hybride electrical vehicles and other energy applications.

Li-ion batteries are made from four main components since they are developed for the first time, which are anode and cathode electrodes, electrolyte and separator. Cathode materials are mostly made from lithium metal or lithium alloys with other metal compounds. Because of the safety problems with lithium metal, researchers tried to develop alternative electrode materials for cathode materials. Although the cathodes made from alloys of lithium and other metals show better safety, they have low capacity and very expensive to produce commercially. In order to improve the capacity and stability of Li-ion batteries, there have been many approaches to produce better cathode materials.

In 1997, Lithium Iron Phosphate ($LiFePO_4$) was first developed by Goodenough and friends as an alternative cathode material having low cost and nontoxicity, stable structure. It took great interest by industrial companies due to its advantages comparing to other conventional cathode materials ($LiCoO_2$, $LiMn_2O_4$, and LiNiO2). This material has 3.4 V working voltage and high specific capacity (170 mAh/g) however has very low electronic conductivity (10^{-9} S/cm) related to highly oxidized structure. Researchers published many publications and reports for improving the conductivity of $LiFePO_4$ by lowering the particles sizes in nanometer range and carbon coating on particles.

Although many experimental results showed that carbon coating improved the conductivity of $LiFePO_4$, some carbon coatings dissolved in electrolyte and caused formation of solid electrolyte interphase (SEI) which is an insulator layer. After few cycles in battery, this layer eventually affects the rate and power capability, life time, performance and safety of batteries. For this purpose, a unique conductive carbon layer covering on nanoparticles is established by Marcin Molenda and coworkers by a patent (US20110151112 A1). In this process, produced powders are impregnated to

the polymer solutions of pyromellitic acid (PMA) and poly-N-vinylformamide (PNVF) and pyrolyzed to achieve carbon layers covers on nano particles.

In order to obtain homogenous $LiFePO_4$ powders without impurities, it is necessary to produce the powders in anhydrous solutions to avoid formation of Fe_2O_3. These impurities can be caused by the degradation of Fe (II) ions to Fe (III) due to high reactivity with oxygen. For this purpose, microemulsion is a useful technique to achieve uniform nanosized particles with high purity. In this technique, there is no need to use expensive or complicated devices. Precursor powders are dissolved in water and oil phase by the help of surfactant/cosurfactant materials. Particle sizes are easily controlled by the amount and ratios of materials. The calcination temperature and time also affect the sizes of the particles.

In this research, $LiFePO_4$ nanosized powders are produced by a novel anhydrous solution precipitation technique and also by microemulsion technique. From the experimental results, it is observed that producing pure nano powders with microemulsion technique is challenging and needs more research to understand and control the parameters during synthesis. For this reason powders are produced only by solution precipitation technique. Once the precursor nano powders are achieved, they are characterized by the thermo gravimetric analysis (TGA) in order to determine the calcination temperature. After the calcination of the powders under inert gas (Ar, N_2) atmosphere, powders are characterized in X-ray diffraction analysis (XRD) for structure and impurities. Homogenous and pure $LiFePO_4$ nanopowders are produced referred as standard JCPDS-83-2092 patterns within the range of 30-40 nm having well crystal olivine structure. Powders are covered in different ratios of (% 5-20) conductive carbon layers (CCL) as referred to Marcin et. al. Surface properties and porosity of powders are measured by Brunauer-Emmett-Teller technique under nitrogenous atmosphere (N_2-BET). Surface areas and pore sizes are calculated by Barret–Joyner–Halenda (BJH) model. Samples show IV type isotherms with H3 hysteresis loops which are referred to porous surfaces of plate shape particles. Specific surface area of samples are around 20-25 m^2/g and average pore sizes are between 5-20 nm that is mesoporous surface mentioned by IUPAC. Conductivities of the covered nanoparticles are measured between (-20) °C and (+40) °C with AC (33Hz) 4-probe technique. The conductivities of CCL/$LiFePO_4$ nanopowders (10^{-2} to 10^{-3} S/cm) are achieved much higher than bare $LiFePO_4$ (10^{-9} S/cm) and increased by CCL ratio.

Morphological and surface properties of $LiFePO_4$ powders are observed by SEM. It can be seen that as prepared particles are almost similar sized around 50-100 nm individually, however after calcination particles are agglomerated to each other and resulted irregular shaped larger particles. However, size differences causes to porous network surface resulting high surface area.

From Raman spectroscopy analysis, the small band at 950 cm^{-1} is related to symmetric PO_4 stretch vibration in the olivine $LiFePO_4$. The broad line in 1350 cm^{-1} is obtained from the structure of disordered modes of graphite which is called D (disordered) line, the broad line in 1585 cm^{-1} corresponds from optically allowed E_{2g} zone center mode of crystalline graphite which is called G (graphite) line of carbon. The results are also combined with EDAX analysis that our powders contain wt. % 9.42 C element which is attributed to residual carbon from the decomposition of

acetates. As a consequent, powders will be used as the form with C residuals and expected to have higher conductive and better cycle properties.

The electrochemical tests of $LiFePO_4$ are measured using CR 2032 coin cells assembled in a glove box under argon atmosphere. For this reason, $LiFePO_4$ powders are used as active material and mixed with acetylene black to improve conductivity and polyvinylidene fluoride (PVDF) as binder in different ratios (% wt 80:10:10 and 75:15:10).

To investigate potential dependent interface processes, double layer capacitances and charge transfer reactions, the assembled batteries are cycled galvanostatically using a potentiostat (Parstat) between a potential range of 2.5 V and 4.5 V (vs. Li/Li^+) for cyclic voltammogram analysis at a scan rate of 1 mV/s and 5 mV/s. Within these tests, it is observed the rate capability and cycle performances of the cells. The intensity and shape of the peaks in CV measurements change by the type and amount of the carbon additives. Carbon coated $LiFePO_4$ cathode electrodes show higher peaks than bare $LiFePO_4$ powders.

To understand the effect of different carbon additive intensively, electrochemical impedance spectroscopy (EIS) measurements are carried out with CR-2032 coin cells using potentiostat (Parstat 2263). During the analysis, AC voltage is applied to cells of frequency ranges between 10 mHz and 100 kHz at a scan rate of 5 mV at room temperature. When compared the plots of samples for the cells assembled with %wt. 10 and 15 carbon black (CB) additives, it is observed that the semicircle of 15 CB/ $LiFePO_4$ is smaller than the one for 10 CB/ $LiFePO_4$. That shows the decrease of charge transfer resistance with increase of additive CB amount due to increased conductivity. These improved results are attributed the small particle sizes and high surface area of our $LiFePO_4$ powders, which also enhances the short diffusion path way for Li^+ ion diffusion. As a conclusion, small particle sized powders exhibit reduced resistances during the cycling and they are expected to achieve higher capacity, fast charge/discharge capability rates and better electrochemical properties.

SUSUZ ORTAMDA $LiFePO_4$ NANO TOZ ÜRETİMİ VE KARAKTERİZASYONU

ÖZET

Piller, ilk icat edildikleri andan itibaren hayatımızda önemli bir yere sahip olmuş ve bu önem son yıllarda büyük bir hızla artarak devam etmiştir. Özellikle cep telefonu, dizüstü bilgisayarlar ve birçok diğer elektrikli eşyanın günlük hayatta kullanımı ile birlikte pillerin teknoloji üzerindeki etkisi giderek dikkat çekmiş ve araştırmacıları bu konuda çalışmaya teşvik etmiştir. Piyasada birçok çeşit pil bulunmasına rağmen, şarj edilebilir piller arasında lityum-iyon (Li-ion) piller ağırlık başına yüksek enerji yoğunluğu ve kapasiteye sahip olması, daha uzun ömürlü olması ve diğer pillere kıyasla daha karalı yapısı sayesinde en çok tercih edilen pil olmayı başarmıştır. Şarjlı elektronik cihazların artışı ile doğru orantılı olarak li-iyon pillerin de üretimi artış ve büyük bir pazar payına sahip olmuştur.

Son yıllarda yüksek enerji gerektiren elektrikli cihazlar ve hibrit elektrikli otomobil üretiminin artması, mevcut lityum iyon pillerin sahip olması gereken kapasitenin artması, daha güvenli ve uzun ömürlü olması, ucuz ve doğa dostu olması, hızlı şarj/deşarj olabilmesini gerektirmiştir. Bunun için hem akademik olarak araştırmacılar hem de pil üretici firmalar yeni üretim yöntemleri ve faklı malzemeler ile Li-iyon pilleri geliştirmeye çalışmaktadırlar.

Li-iyon piller temel olarak dört bileşenden oluşmaktadırlar. Bunlardan en önemli olanları anot ve katot elektrotları, diğer ikisi ise elektrolit ve ayırıcıdır (separatör). Anot malzemesi, pil içerisisinde negatif elektrot olarak görev yaparken deşarj sırasında kimyasal reaksiyonlar sonucu oksitlenerek lityum iyonlarını yapıya verir ve elektrolit yardımı ile bu iyonlar katot malzemesine taşınır. Bu sırada anot malzemesinden ayrılan elektronlar katot (pozitif elektrot) malzemesine ulaşarak elektrokimyasal indirgenme reaksiyonuna neden olur. Anot ve katot malzemesi arasındaki Li^+ iyonlarının alış verişi, sallanan sandalye (rocking chair) hareketi olarak ifade edilebilir. Burada elektrolit, anot ve katot arasındaki iyon iletimini sağlayan iletken bir sıvı-tuz çözeltisi (EC-DMC-$LiPF_6$), seperatör ise elektrotların direkt olarak teması sonucu kısa devre olmasını engelleyen, ancak iyon transferine engel olmayacak şekilde gözenekli polimerik folyolardır.

İlk üretilen Li-iyon pillerde anot ve katot malzemesi olarak lityum metali kullanılmış olsa da güvenlik problemleri nedeniyle diğer metaller ve/veya bunların lityum metali ile alaşımları sonucu alternatif elektot üretilmeye çalışılmıştır. Bunlardan ilk olarak karbon ve grafit içerikli anot malzemeleri kullanılmaya başlanmış, daha sonra Al, Ge, Sn, Si, Bi, Sb metalleri ile kompozit anotların geliştirilmesi devam etmiştir. Katot malzemesi ise, lityum iyonlarını tedarik eden, lityumun bir başka metal ile alaşımlaması sonrası oluşan malzemelerdir.

İlk katot malzemesi $LiCoO_2$ olarak kullanılmış, daha sonra diğer metaller (Mn, Ni, Fe) ile alaşımlanarak gelişmesi devam etmiştir. Günümüz piyasasında halen daha en çok kullanılan katot malzemesi $LiCoO_2$ olmasına rağmen, araştırmacılar daha iyi ve güvenli çevrim özelliklerine sahip, ucuz, yüksek enerji ve kapasiteye sahip katot malzemesi üretimi üzerine çalışmalara devam etmektedir. İyi bir katot malzemesi, iletkenliği yüksek olmalı, yüksek oranda Li^+ iyonlarının giriş/çıkışına ev sahipliği yapabilmeli, kolayca oksidasyon/indirgenme reaksiyonları yapabilmeli, çevrim sırasında elektrolit ile reaksiyona girmemeli ve çevrim sırasında yapısında değişiklik olmamalıdır.

Yeni nesil alternatif katot malzemeleri arasında, 1997 yılında Goodenough ve arkadaşları tarafından geliştirilen Lityum Demir Fosfat ($LiFePO_4$) malzemesi, sahip olduğu yüksek kapasite, güvenli, ucuz ve doğa dostu olması gibi birçok avantajı sayesinde hem ticari üreticilerin hem de akademik araştırmacıların büyük ilgisini toplamıştır. Kristal yapısı olivin tipinde, ortorombik simetriye ile kararlı bir yapıya sahip olan $LiFePO_4$ malzemesi, 3.4 V çalışma voltajı ve 170 mAs/g kapasitesini uzun çevrimler boyunca koruyabilmektedir. Ancak, yapısında bulunan oksijen atomları nedeniyle elektronik iletkenliği oldukça düşük (10^{-9} S/cm) seviyelerdedir. Buna rağmen, daha önceden yapılan araştırmalar sonucu, malzemenin partikül boyutunu düşürmek (nanometre), yapıya karbon ilavesi ve partikülleri karbon kaplamanın iletkeniği artırdığı kanıtlanmıştır.

Katot malzemelerinin iletkiniliğinin artırılması için daha önce yapılan araştırmaların birçoğunda yapıya karbon veya grafit ilave edildiği görülmüş, ancak bunların elektrolit içerisinde çözünerek malzeme ile elektrolit arasında yalıtkan bir tabaka oluşturarak iyonların iletimini engelleyerek ilerleyen çevrimlerde pilin ömrünü kısalttığı gözlenmiştir. Ayrıca, nano boyutta kompozit malzeme üretimi sırasında partikül yüzeylerinin kimyasal olarak çok aktif olması nedeniyle problemler gözlenmiştir. Bu nedenle, Dr. Marcin Molenda ve arkadaşlarının geliştirdiği patentli (US 20110151112 A1) özgün bir teknik sayesinde nano boyutlu partikül üretimi ve karbon kaplanması gerçekleştirilmiştir. Bu teknikte, üretilen nano partiküller, poli-N-vinil formamit (PNVF) ile modifiye edilen piromellitik asitin (PMA) saf su içerisinde belirli oranda çözündürülmesi ile oluşan çözeltiye daldırılması ile elde edilir. Parçaçıkların yüzeyinde bulunan polimerik çözelti daha sonra kurutulup, kontrollü piroliz işlemi yüksek sıcaklıkta yakılarak istenilen iletken karbon kaplamaların oluşması sağlanır.

Nano boyutta partikül üretimi için son yıllarda geliştirilmiş olan mikroemülsiyon, diğer tekniklere kıyasla pahalı düzenek ve cihazlar gerektirmeyen, homojen ve aynı boyutlara sahip nano malzeme üretimi için oldukça kullanışlı ve basit bir yöntemdir. Ayrıca, deney parametreleri değiştilerek partikül boyutları isteğe göre kolayca ayarlanabilmektedir. Bu yöntem, ilk olarak geliştirilmesinden bu yana birçok organik ve inorganik polimerik, metalik ve magnetik nanopartikül üretimi için kullanılmaktadır. Diğer bir üretim yöntemi de çözelti çöktürmesi ile malzeme üretimidir. Bu yöntem ile partiküller uygun çözelti içerisinde dağıtıldıktan sonra santrifüj yöntemi ile çöktürülüp kurutulduktan sonra nano boyutlu malzeme üretimi gerçekleştirilir.

Ancak, $LiFePO_4$ üretimisi sırasında başlangıç malzemeleri olarak Fe tozları oksijen ve neme karşı yüksek bir kimyasal reaksiyon potansiyeline sahip olmasından dolayı, su içeren çözeltileri sonucu Fe (II) iyonları oksijen ile indirgenerek Fe (III)

dönüşürerek Fe_2O_3 impüritelerini meydana çıkarak katot malzemesinin performansını olumsuz yönde etkilemektedir. Bu nedenle, hazırlanan çözeltiler mümkün olduğunca nemden ve sudan uzak, kontrollü ortam atmosferinde (Ar, N_2) hazırlanmalıdır.

Bu çalışmada, nanoboyutlu homojen $LiFePO_4$ partikülleri üretimi için, su içermeyen çözeltilerin çöktürmesi yöntemi ve mikroemülsiyon yöntemi kullanılarak elde edilen tozlar termogravimetrik analiz (TGA) yöntemi ile bozunma sıcaklık ve süreleri belirlenerek tüp fırında kontrollü atmosfer altında (Ar, N_2) kalsinasyonu gerçekleştilmiştir. Elde edilen bu tozlar, kristal yapısı ve fazlar incelenmek üzere X-ray diffraksiyonu (XRD) analizine tabi tutulmuştur. Buna göre, homojen partikül boyutlarına sahip ve impürite içermeyen, saf $LiFePO_4$ tozlarının 30-40 nm boyutlarında olivine kristal yapısına sahip olduğu ve elde edilen piklerin standart JCPDS-83-2092 ile örtüştüğü belirlenmiştir. Daha sonra bu tozlar daha önce belirtilen patentli yöntemde olduğu gibi polimerik çözeltilere daldırılarak faklı oranlarda (% 5-20) iletken karbon katmanları ile kaplanmıştır. Kaplama sonrası tozlar istenilen karbonların eldesi için önce hava ortamında etüvde kurutularak daha sonra tüp fırında kontrollü ortamda (Ar, N_2) piroliz edilmişlerdir.

Tozların yüzey özellikleri ve belirlenmek üzere, azot (N_2) gazı altında Brunauer-Emmett-Teller (N_2-BET) yöntemi ile ölçümler gerçekleştirilmiş ve gözenek boyutları Barret–Joyner–Halenda (BJH) modeline göre hesaplanmıştır. Buna göre, elde edilen tozların IV tipli eğrileri ve H3 histerisis döngülerine, dolayısıyla katmanlı yapıda gözenekli bir yüzeye sahip olduğu gözlenmiştir. Nano boyuttaki kompozit tozların özgül yüzey alanlarının 20-25 m^2/g ve ortalama gözenek boyutlarının 5-20 nanometre aralığında olduğu, bu verilere göre, daha önceki yapılan çalışmalar sonucu IUPAC'ın belirttiği üzere, malzemenin meso-gözenekli bir yüzeye sahip olduğu belirlenmiştir. Üretilen iletken karbon kaplı $LiFePO_4$ nano tozların elektriksel iletkenlik ölçümleri AC (33Hz) 4-uç tekniği ile (-20) °C ve (+40) °C arasında ölçülmüştür. Karbon tabakası kaplı tozların saf $LiFePO_4$ (10^{-9} S/cm) tozlarına kıyasla çok daha yüksek iletkenlik değerlerine (10^{-2} ile 10^{-3} S/cm) sahip olduğu ve bu değerlerin artan karbon kaplama oranı ile doğru orantılı olarak arttığı gözlenmiştir.

Tozların yüzey morfolojisi ve görüntüleri taramalı elektron miktoskopu (SEM) ile incelenmiştir. Partiküllerin boyutları birbirinden bağımsız olarak 50-100 nm civarında olduğu gözlenmiş, ancak ısıl işlem sırasında birbirine tutunarak topaklandığı ve daha büyük boyutlu partiküller oluşturduğu görülmüştür. Buna rağmen farklı boyuttaki parçacıklar gözenekli ve büyük alana sahip yüzey elde edilmesini sağlamıştır.

Raman spektroskopisi incelemelerine göre 950 cm^{-1} civarında görülen pik, $LiFePO_4$ malzemesinin içerisindeki PO_4 bağlarının titreşmesine bağlı olduğu, 1350 cm-1 ve 1585 cm-1 civarında görülen pikler ise sırasıyla düzensiz yapıdaki (D) ve kristalleşmiş karbonun grafit formu (G) olarak görülmüştür. Ayrıca, EDAX sonuçları ile de yapıda % 9.42 oranında karbon elementi görülmüştür. Bu karbonlar, ısıl işlem sırasında asetatların bozunması ile yapıya dahil olduğu düşünülmektedir, lakin grafit formda olan karbonların yapıya artı iletkenlik katacağı düşünülmektedir.

Elde edilen $LiFePO_4$ tozları farklı oranlarda (%wt. 10-15) siyah karbon (CB) ve bağlayıcı ile karıştırılarak ince film halinde alüminyum folyolar üzerine kaplanmış ve elektrot olarak üretilmişlerdir. Daha sonra bu elektrotlar argon (AR) atmosferi altında düğme pil halinde CR 2032 olarak üretilmiştir.

Malzemelerin potensiyel değişime karşılık gösterdiği tepkimeleri, kapasite ve yüklü iyon taşınımı reaksiyonlarını incelemek üzere piller 2.5 V ve 4.5 V (vs. Li/Li^+) arasında 1 mV/s ve 5 mV/s hızlarında çevrime tabi tutulmuştur. Bu çevrimler sırasında pillerin çevrim performansları incelenmiştir. Elde edilen grafiler incelendiğinde, piklerin şiddeti ve şekli direkt olarak karbon miktarı ile orantılı olduğu ve karbon miktarı arttıkça pik şiddetinin arttığı gözlenmiştir.

Karbon etkisi daha detaylı incelenmek üzere pillerin elektrokimyasal analizleri AC voltaj uygulanarak 10 mHz ile 100 kHz frekans arasında 5 mV tarama hızı ile oda sıcaklığında gerçekleştirilmiştir. Grafikler incelendiğinde, daha iyi iletkenlik özelliği sergileyen 15 CB/ $LiFePO_4$ malzemesinin, yüklü iyonların taşınması sırasında daha küçük direnç gösterdiği gözlenmiştir. Ayrıca, elde edilen tozlar, literatürde daha önceden üretilmiş $LiFePO_4$ tozlarına kıyasla daha iyi empedans özellikleri göstermiştir. Bu elektriksel özelliklerdeki gelişmelerin, nano boyutlardaki partiküllerin getirmiş olduğu yüksek yüzey alanı ve bu sayede Li^+ iyonlarının difüzyon mesafesinin kısalması ile gerçekleştiği gözlenmiştir. Sonuç olarak, elde edilen $LiFePO_4$ tozlarının daha yüksek kapasite, hızlı şarj/deşarj edilebilme ve daha iyi elektrokimyasal sonuçlar göstermesi beklenmektedir.

1. INTRODUCTION

Batteries have been widely used in our daily life since the last 50 years. They have been developed so fast due to improving interest of electrical devices such as mobile phones, laptops and electrical vehicles [1]. Although there are plenty of different kind of batteries in industrial applications, lithium-ion (Li-ion) batteries are dominated the others, due to its high power and energy density in terms of volumetric and gravimetric, longer cycle life and stability. Because of the increment of production electronic devices, nowadays Li-ion batteries have the biggest market share in energy industry [2-4].

There have been many researches to develop new types of batteries. The structure of batteries is still the same as they developed for the first time as cathode and anode electrodes within electrolyte between. Improvements of cathode and anode materials are still under research in order to achieve better stability and efficiency [1].

Lithium metal was used for both anode and cathode material since it was first invented. There have been such problems with the usage of lithium metal in batteries. The corrosion of lithium metal surface by the interaction with electrolyte causes dentrite formation and results in short-circuit of cell. So that, thermally expansion of lithium metal outcomes to an explosion and fire. Also, lithium metal is very reactive with oxygen, humidity. It needed to be handle and stored in contolled atmosphere such as glove boxes and clean rooms. So, many precuations should be taken for the usage, storage and transportation of lithium metal [4].

In order to solve these safety problems, lithium metal is altered by another metal such as carbon, tin, silisium etc. Lithium, as always being an active ion source, other metals are used as a counter electrode [4]. Also calling the battery as a combination of both anode and cathode electrodes integrated with electrolyte and assembled under a controlled atmosphere. The interaction mechanism of the lithium-ion battery is the mobility of Li^+ ions through anode and cathode materials during charge and discharge treatment.

2. BATTERIES

A battery is an electrochemical device that can store and convert the chemical energy into electrical energy by reversible oxidation-reduction reactions [5, 6].

The first approach of the battery was in 1800, by an Italian physicist, Alessandro Volta demonstrated and quantified his invention as voltaic pile. He proved the relationship between chemical reactions and electricity with two metals; zinc and silver. He used a cardboard as a separator having porous structure and a solution of salt water that resulted a controlled steady current flowing externally between the two electrodes [7, 8]. Since Volta's invention of battery, it has become an irrevocable part of electronic devices such as cell phones, laptops, and hybrid electric vehicles [9].

A cell (battery) is the combination of four major components that can provide the chemical energy and conversion to electrical energy; anode, cathode, and electrolyte, separator. Anode (negative) electrode, gives electrons to external circuit and oxidized [6], and cathode (positive) electrode, accepts electrons from the external circuit and being reduced during the electrochemical reaction [10, 11]. The cathode should be an efficiently oxidizing material, also having stability in contact with electrolyte and work in a high voltage range. Electrolyte is the ionic conductor and become the medium for the transfer of charge ions, between the anode and cathode. The electrolyte is generally a liquid, prepared by water or other solvents, within dissolved salts, acids, or alkalies to provide ionic conductivity [12]. Some batteries use such solid electrolytes, which are ionic conductors at the range of operating cell temperature. In order to prevent internal short circuit, electrolyte must have ionic conductivity but not electronically. Hence, the anode and cathode electrodes must be electronically isolated while surrounded by the electrolyte. So, an insulating material is used to separate electrodes. The seperator should be permeable for the electrolyte in order to achieve ionic conductivity and permit the migration of

charged ions to electrolyte [13]. Therefore, a porous and insulative material such as polymeric is used as a separator in the cells [14].

There are two types of cells that can be categorized into primary and secondary, depending on their ability and capability of being electrically re-charged [15]. Primary cells are not capable of being electrically rechargable. These cells involve only an irreversible reaction. So they can only be used for a discharge and discarded to the environment that causes hazards and depletion of natural sources. But as a consumer, these batteries are convenient, inexpensive, lightweight [5]. On the other hand, secondary cells are renewable and the chemical reaction is reversible [16]. These kinds of cells can provide economically and environmentally impact with the increasing demand on small portable devices. There are still some researches of having power sources with high gravimetric and volumetric energy densities that can operate wide temperature ranges and with good electrochemical stability. Therefore, secondary battery development and industrial applications will continue to grow in near future for the next generation electrical devices.

2.1 Rechargable Batteries

Since the first invention of secondary batteries, there have been many attempts to achieve better enery densities. For the most common used rechargeable batteries' gravimetric energy densities (Wh/kg) and volumetric energy densities (Wh/l) are shown in Figure 2.1 [17, 18]. From this plot, it can be clearly observed that the high power and energy density properties of lithium metal make it preferable to traditional battery systems. Low specific energy density and low working voltage range of conventional batteries such as lead-acid and Ni-Cd batteries become a problem applicable as power sources and consumer electronics.

Although the lithium metal battery is excellent in terms of both gravimetric and volumetric energy density, it is extreme unstable [19]. However, Li-ion and lithium polymer (PLi-ion) batteries show comparable energy and power densities to lithium metal with exceptional stability [20].

Li-ion batteries are the lightest in weight and smallest size in comparison for the same energy provided by different kinds of battery systems [17]. As a result, the Li-ion and nickel metal hydride (Ni-MH) batteries are become as advanced power

sources. They slowly substitute several conventional battery systems such as the lead acid and nickel cadmium (Ni-Cd) [18]. However, Ni-MH batteries has a close volumetric energy density to Li-ion batteries, as shown in Figure 2.1, discharge voltage of Ni-MH is only 1.2 V is just one third of the Li-ion batteries 3.7 V, and the gravimetric energy density of Li-ion batteries are superior to Ni-MH batteries [21, 19].

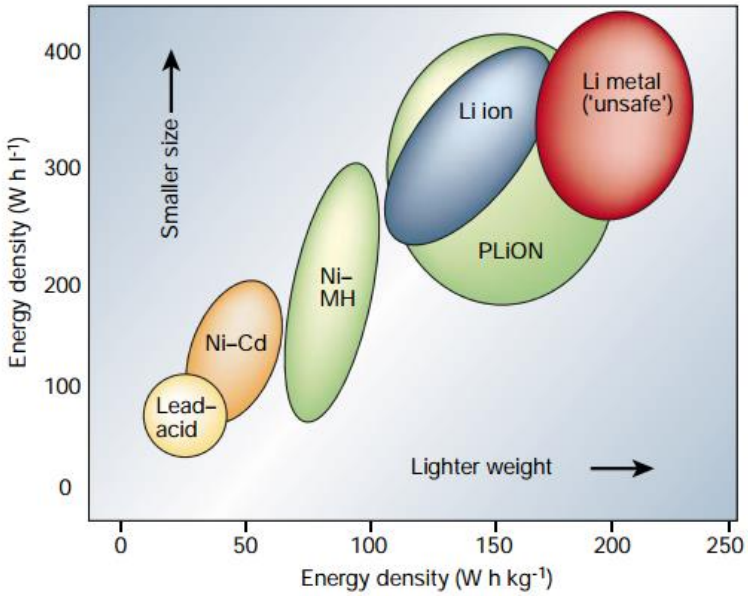

Figure 2.1: Comparison of different batteries in terms of volumetric and gravimetric energy density [17].

Li-ion batteries have several advantages more than common secondary batteries such as Nickel cadmium (Ni-Cd) and Nickel metal hydride (Ni-MH), not only higher energy density but also having no memory effects and environmental friendly structure [22, 23]. The most important advantages and disadvantages of Li-ion batteries are listed in Table 2.1.

Table 2.1: The advantages and disadvantages of Li-ion batteries [24].

Advantages	Disadvantages
High Energy/Power Density	High cost
Good cycle life	Ustable at high temperature
Coulombic efficiency	Unstable at overcharging
Low self-discharge rate	High internal resistance
No memory effect	Safety

For the amount of large batteries, high voltage is an advantage in order to reduce the number of cells needed to achieve the desired voltage for the electrical vehicle applications [25]. The commercial Li-ion batteries present a specific power and energy density at almost 200 W/l and 150 Wh/kg respectively. A Ragone plot (Figure 2.2) shows the performance of the Li-ion battery cells in comparison to other traditional batteries [26].

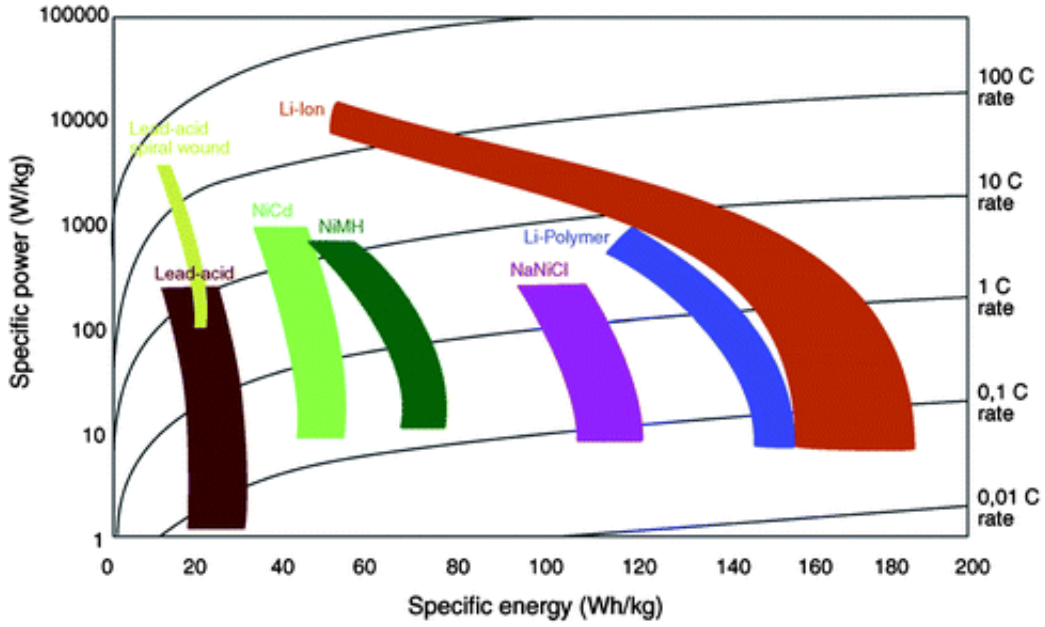

Figure 2.2: A ragone plot for commercial batteries [26].

Li-ion batteries have the best properties of environmental safety, high energy density, high power density, good cyclic stability and high cell voltage among the other rechargeable batteries [18]. The electrochemical performance parameters of Li-ion batteries are compared with other battery technologies in Table 2.2.

Table 2.2: The performance of rechargeable batteries [27].

	Energy Density (Wh/kg)	Power Density (W/kg)	Self Discharge (per month %)	Cycle Durability	Cell Voltage (V)
Li-ion	100-160	250-340	5-10	1200	3.6
Lead-acid	30-40	60-75	3-20	500-800	2.1
NiCD	40-60	150	10	2000	1.2
NiMH	30-80	250-1000	30	500-1000	1.2

2.1.1 Li-ion batteries

Lithium metal has been the most suitable and capable material for using as anode in secondary rechargeable batteries for the past few decades. Li-ion batteries have been attractive due to its low electronegativity of potential (-3.045 V), a very high specific capacity of 3860 mAh/g [28] that allows it to become a very light weight and superior power source among the other traditional batteries. Li-ion batteries can provide low self-discharge, good cyclability and high energy densities [24].

After the first usage of lithium metal as a negative electrode in commercial products for rechargeable batteries, resulted in safety and poor cycling performance problems. While charging/discharging process, lithium metal dissolved in electrolyte and dentrite formations occured [23] with a short circuit in the cell. Because of the fact that, cell become overheating and poor cycle performance. It has been also claimed that overcharging of these cells caused thermally unstable and a possible explosion, therefore serious injuries. Moreover, lithium metal is highly reactive with moisture, oxygen and nitrogen, needed to be handle with care and stored such glove boxes or clean rooms for production processes. Hence, researchers tried to solve these problems in the concept of Li-ion batteries [14].

After Sony Corp. (Japan) developed Li-ion secondary batteries in 1990, the usage of lithium metal as an anode material in rechargable batteries was given up. These cells are safer than lithium metal batteries and exhibit a better cycle life [24] which are made by a graphite carbon as anode electrode and a transitional metal oxide such as $LiCoO_2$ as cathode electrode. So Li^+ ions can be intercalate/deintercalate reversibly into the electrode material's crystalline structure resulting lithiated graphite compounds. This anode material has a great potential close to lithium metal and has a theoretical specific capacity of 372 mAh/g [22], also exhibits good cycling behaviour without dendrite formation during charge/discharge process [29].

A typical secondary rechargable Li-ion battery is illustrated in Figure 2.3. In the most common structure includes carbon graphite as a negative anode and a lithiated cobalt oxide (Li_xCoO_2) compound as a cathode material into which Li^+ ions inserted/extracted reversibly. Both structures of anode and cathode materials are just like the layered in order to provide a place for Li^+ ions. Inside the cell, organic solvent (EC) and lithium salt ($LiClO_4$) dissolved for electrolyte bath and a porous insulative separator put between electrodes [30, 31]. Organic electrolytes are superior

to aqueous electrolytes that provide a wider electrolyte window (Eg), which can obtain high cell voltages. In the liquid electrolytes, water tends to sustained reduction/oxidation reactions at high voltages [32].

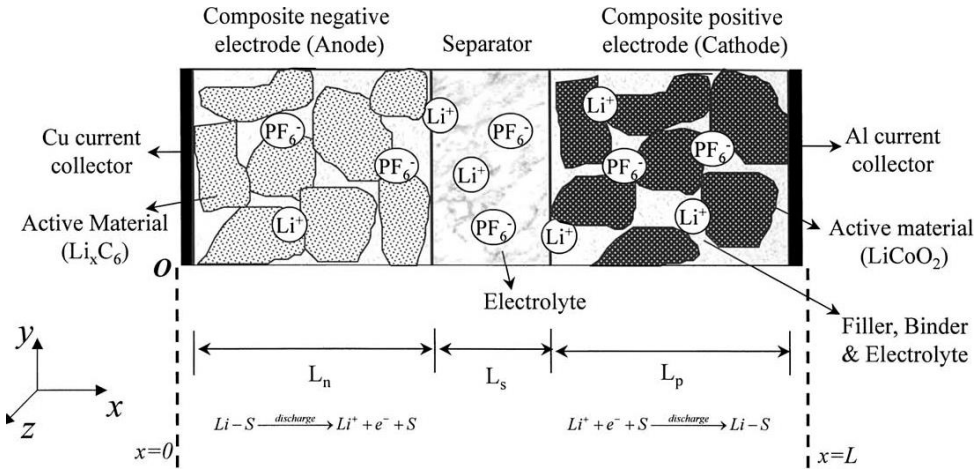

Figure 2.3: Li-ion battery structure illustration [33].

The movement of Li^+ ions insertion/extraction between anode and cathode material is called "intercalation" and "de-intercalation". If there is a space for other small ions such as Li^+ in the layered crystal structured electrode material, these kinds of reactions occur easily. Sometimes, solid solution reactions are resulted if there is a change in the chemical composition of material because of these reactions. Generally, these reactions are topotactic which means Li^+ ions move inside the electrode and stay inside the intersitial sites of the materials structure lattices [24]. These reactions occur around room temperature and with the help of large surface area to volume ratio. Nanomaterials such as nanopowders and nanowires can permit a short transportation path for Li^+ ions, so intercalation/de-intercalation process can be achieved more efficiently and faster [34]. Besides, a small volumetric change while insertion/extraction process occurs and make the structure of electodes more stable [35].

It is already been claimed in previous sections that in lithium-ion batteries the anode electrode is reactive with the electrolyte solutions and results in formation of dentrites and surface films. While charging/discharging process, because of the intercalation/deintercalation process of Li^+, these films compose a solid electrolyte interphase (SEI) layer on the electrode surface that allows Li^+ ions to intercalate/deintercalate in "*rocking chair*" or "swing battery" on the surface. This film also prevents no more dissolution of electrode surface in the electrolyte. These

SEI films are playing a very important role on the cell performance that are claimed to be ionically conductive but not electronically. SEI film continues to dissolve while charging/discharging reactions that cause an increment in impedance. As a result, the capacity and efficiency of cell performance continues to fading eventually [20].

In the Li-ion secondary batteries, Li^+ ions move reversibly between the anode and cathode through the electrolyte and results charge and discharge processes [36]. A charge/discharge process of Li-ion secondary battery is represented in Figure 2.4. In this cell, there most commonly used anode (Li_xC_6) and cathode ($Li_{1-x}CoO_2$) materials have been used and an electrolyte consisting lithium salt (e.g. $LiPF_6$) gives the system ionically conductive structure. During the discharge process negative electrode is lithiated and cathode has active cites to accept Li^+ ions. Therefore, the Li^+ ions are delithiated from the negative electrode to the electrolyte, meanwhile the same amount of Li^+ ions intercalate cathode from the electrolyte solution [19] and at the same time electrons travel from anode to the cathode material by an external circuit [37]. Because of the intercalation process, SEI is formed by different transport mechanisms such as migration and diffusion. The charging process is just the reversible reaction of discharge, applying an external voltage or current to the electrode materials, and electrons flow from the positive electrode to the negative electrode [38, 39]. The electrochemical reactions occurred while charge/discharge reactions are shown in equations [40].

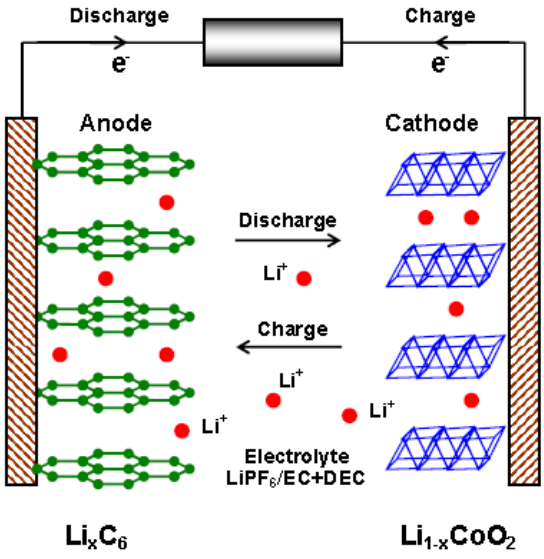

Figure 2.4: Li-ion secondary battery structure and charge/discharge process [41].

Anode reaction:

$$6\,C + xLi^{+} + e^{-} \xrightarrow{Charge} Li_xC_6 \quad \textbf{(2.1)}$$

Cathode reaction:

$$LiCoO_2 \xrightarrow{Charge} Li_{1-x}CoO_2 + xLi^{+} + xe \quad \textbf{(2.2)}$$

Total Reaction:

$$LiCoO_2 + C_6 \xrightarrow{Charge} Li_{x-1}CoO_2 + Li_xC_6 \quad \textbf{(2.3)}$$

Because of the fact that oil crisis and increment of the petroleum prices and extinction of the sources of fossil fuels, Li-ion batteries become the alternative source of energy in transportation sector, which is more efficient and environmental friendly. Therefore, Li-ion batteries are going to have more attention in power sources in the near future. It can be easily observed from the Figure 2.5 that sales of the rechargable batteries have been proliferated since 1990s, from the statics of Japan [20]. Commercial production of Li-ion batteries, dominated the market of secondary batteries, cell phones and power devices very fastly, that achieved from 30,000 units in 1995 to 200 millions of units in 2005.

Nowadays, there is an interest to use Li-ion batteries in highly powered and great energy density devices, electrical vehicles (EVs) and hybrid electric vehicles (HEVs), in industrial scale and aerospace applications. Nevertheless, Li-ion batteries needed to have higher energy densities, better cycle properties and long life rather than the power devices we use in daily life such as cell phones or laptops. For this reason, both researchers and industrial companies start to search for the most suitable electrode materials that can have higher specific capacity, higher energy densities, work in a wide range of thermal, stable when charging/discharging very fastly in the cyling and most importantly lower costs for the consumers [42].

The United States Advance Battery Consortium (USABC) have already established goals for the production of electric and hybrid electric vehicles performances with the contest with petroleum powered vehicles. The Li-ion batteries need to have a 10-15 years life time for the HEV and EV applications, and 4.2 V batteries are required [30]. Hence, it is obligated to product in large-scale batteries, increasing the stability,

efficiency and safety the cells in order to achieve the goal for the HEV and EV applications.

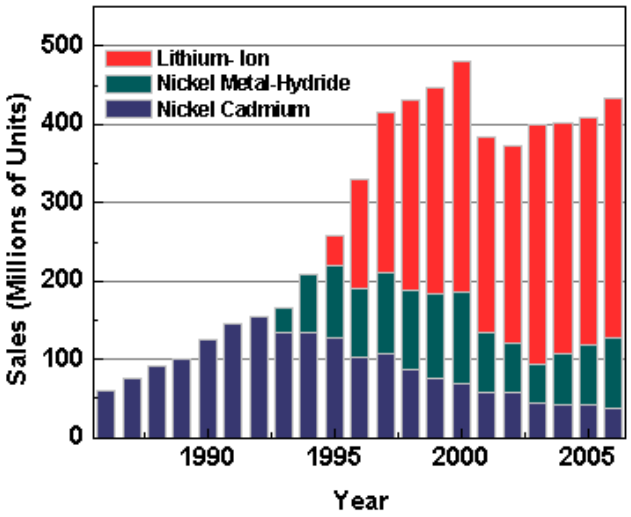

Figure 2.5: The sales statics of rechargeable batteries in Japan 1985 to 2005 [20].

Production of large-scale batteries can be just produced from the small cells such putting them together in a kind of packages for electric vehicles. Also, mass producted batteries, that are going to be used in EVs, cost fewer than such small batteries. Accordingly, researchers have been dedicated for reducing the cost of the cells, starting with the cathode electrode, so that the Li-ion batteries can possess the vehicle market comparing with the other power sources. For the producing large scale of Li-ion batteries, it is needed to reduce the prices of the electrode materials [24]. Consequently, cobalt material has been used since the first applications of the Li-ion batteries, that is going to be abandoned beacuse of the low efficient cycle life, and high costs. Producing the low cost and more efficient materials for the Li-ion batteries is going to be the most critical and important part of the mass fabrication of electrical vehicles.

In order to achieve the best suitable batteries for the electrical vehicle applications having the advantages of high energy densities, long cycle life and low cost, the researchers need to develop the material compounds that Li^+ is going to insertion and extraction, and satisfy many criterion in the Li-ion batteries [41]. There have been many attempts to find the best electrodes for the EV applications and Figure 2.6 shows potential materials that are under research. The properties to be achieved for the electrodes are summarized as below [43].

a) In order to maximize the cell voltage, both anode and cathode compounds should have appropriate chemical potential of lithium.
b) The work function of the cathode material (ΦC) must be as large and the work function of the anode material (ΦA) must be as low as possible, but not more than the limits of the electrolyte band gap (Eg). Work function of cathode material increases with the oxidation state of it increases and work function of anode material decreases with oxidation state of it decreases. So that if a transition metal is going to be used as a cathode such as Mn^{+} in the compound $Li_xM_yO_z$ must have a high oxidation state, but if it's going to be used as an anode in the compound, the oxidation state should be low.
c) The compound must allow a large amount of Li^{+} ions in the insertion/extraction process (x in $Li_xM_yO_z$ must be large) in order to maximize the cell capacity. Also, the valance sites and empty places in the crystal structure depend on the metal that Li^{+} ions can insert.
d) The compound should be stable and not to have chemical reaction with the electrolyte that is used in the cell to have a wide range of operating voltage.
e) In the charge/discharge process, there shouldn't be any change of the structure of the electrode material and these processes needed to be reversibly, while the Li^{+} ions insertion and extraction to achieve a good cycle life.
f) The compound that is used as an electrode must have both electronically and ionically conductive to prevent the polarization losses, to have a high current and power density.
g) It should be easy to achieve, cheap, light weight and environmentally friendly in the terms of commercial applications.

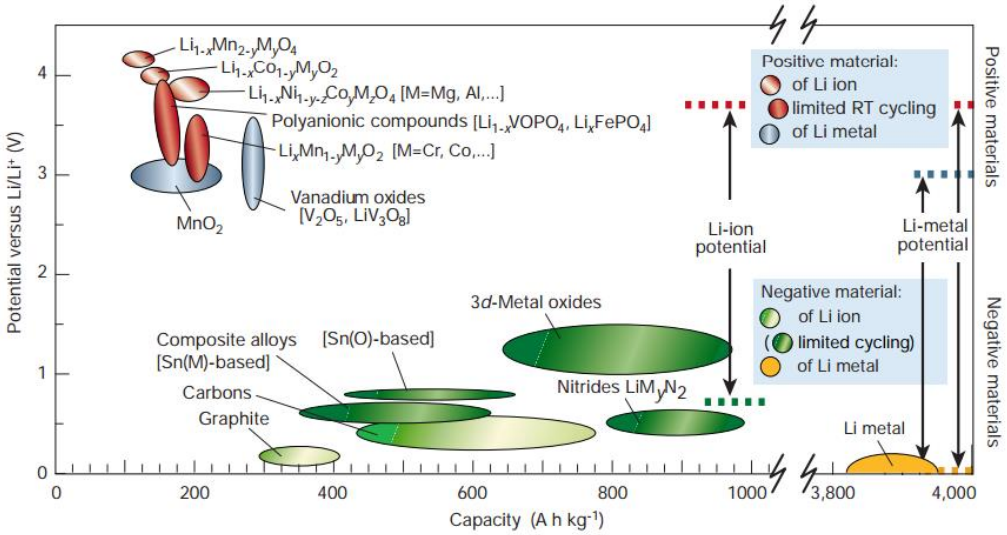

Figure 2.6: Potential and capacity of some electrode materials for future applications of Li-ion batteries [17].

2.1.1.1 Components of lithium-ion batteries

Batteries are made by four main components. First one is the anode that is the negative eletrode in the cell, which contains a metal, and donating electrons to the structure [44, 45]. Electrolyte is another important part of the batteries, which can be either in solid or aqueous form that allows the movement of Li^+ ions inside as an environment, helps transferring of charged molecules [46]. The other part of a cell is seperator that is an insulative material made from such a polymer having porous structure that admits of the charged ions migration. Also it prevents the direct contact between the anode and cathode material thus the short circuit of the cell [47]. The last and the most important part of the cell is cathode, that called positive material which contains the source of Li^+ ions, needed to be layered structure in order to easily intercalate/de-intercalate of ions [48, 49]. Anode and cathode materials' structure directly effects the charge-discharge cycles of the batteries and the working voltage of cell [37]. So it is obligated to understand the atomic structures and molecular properties of the electrode materials [38].

Anode materials

Lithium metal has been used as ideal negative electrode since the first invention of the Li-ion batteries till 1970, due to its high specific charge capacity (3860 mAh/g). The intercalation of lithium as anode material with cathode materials showed high potential, energy density and capacity [33]. Despite the fact that lithium metal is

higly reactive with electrolyte, difficulties of using litium as anode material occurred after cycling few times. Because of high reactivity, during the charge-discharge cycle, dentritic structures appear on the lithium metal which causes the shortcut of the cell. For having safety problems lithium metals can not be used as anode in secondary Li-ion batteries. Researchers tried to find out new anode materials from alloys and compounds instead of pure lithium metal. In order to achieve a good anode material, it should show a low voltage discharge and store Li^+ ions.

Anode materials can be divided two main categories in order the use as negative electrodes in Li-ion batteries which are called carbonaceous and noncarbonaceous. Because of the advantages of the carbons in graphitic structure such as excellent cyclable, low cost, non- toxicity, they have been widely used in the Li-ion batteries as negative electrodes [50, 51].

The commercial applications of secondary Li-ion batteries have been developed by Sony in 1990 using a carbon material as anode electrode. Since then Li-ion batteries still have been used graphite materials that can accept Li^+ ions in the structure within a significant amount (Li:C = 1:6) and lithium insert/extract without damaging the morphology and electronical properties inversibly [52]. Because of the high chemical potential of lithiated carbon materials that is so close to metalic lithium, they have been used wide range. The type of the carbon material affects in the first cycle, the energy and specific capacity, intercalation/de-intercalation process and cycling behaviour of Li-ion batteries [52]. Carbon has advantages such as low cost, high specific charge capacity, good clyclability, environmental safety, low Li^+ ion insertion potential. In the cell, when Li^+ ion intercalates into carbon called charge, and the de-intercalation of Li^+ ions from the structure is called discharge, reactions between lithium and carbon during the charge-discharge step are referred in the reaction (2.1).

In the applications of graphite accepts appreciate amount of Li^+ ions and forms LiC_6 that can deliver 372 mAh/g when de-lithiated at room temperature [49]. The electrochemical intercalation/de-intercalation of Li^+ ions is related to the structure and type of the carbon [53, 54]. Graphite anodes (sintering at 3000 °C) deliver a specific capacity 400 mAh/g while charging, but it can only deliver 290 mAh/g in discharge [55]. This difference is due to the solid electrolyte interface (SEI) formed on the graphite in the first charge [52].

Graphite is a type of carbon, having a layered structure and oriented such as ABAB as in Figure 2.7, that has sp^2 bonds between the C atoms, but each layer is only connected to other by a very weak Van Der Waals bonds. During charge/discharge process, Li^+ ions insertion towards the layers and make a little bit movement and change the morphology and leads to an AAA layered structure as show in Figure 2.8 [56, 57]. So that, graphite has the structure of layers that provide Li^+ ions insert/extract easily, flexible for reversibly intercalation process to serve an appropriate anode material for Li-ion batteries [58].

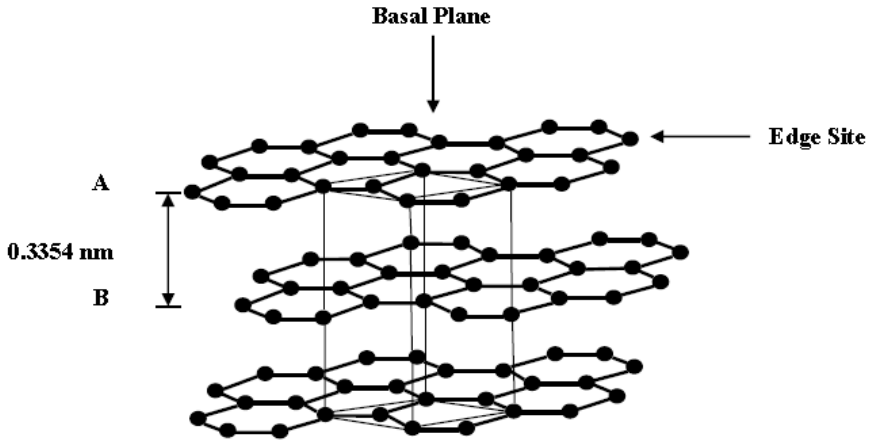

Figure 2.7: The layers and the structure of ABAB graphite **[20]**.

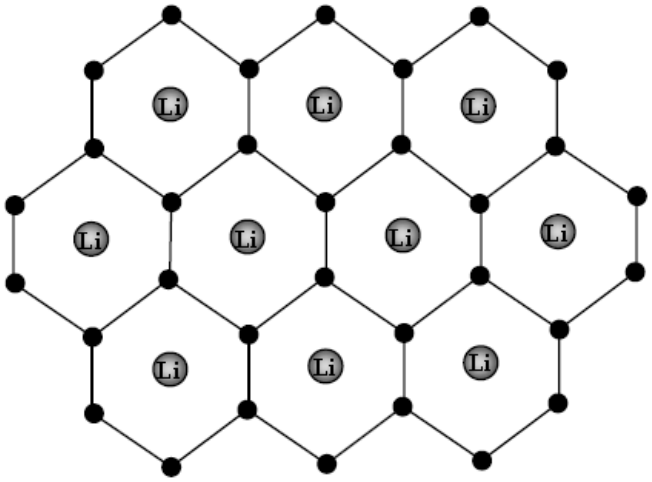

Figure 2.8: The structure of Li^+ ions between C atoms during insertion **[20]**.

There is another type of carbon material, called "hard carbon" that takes the Li^+ ions both layers and particles. Therefore hard carbon is a better host for the Li^+ ions as LiC_6 and has more specific capacity than the graphite [36]. In the first cycle of hard carbons, irreversible capacity loss is comparable with graphite anodes in the

intercalation process of Li^+ ions [38]. Hard carbon cells can be connected each other with a parallel connection and can be uniform voltage batteries [59, 48].

Although hard carbon has not high energy capacity, and because of the structure diffusion rate of Li^+ ions inside is slowly, it can be graphitized with the thermal processes and getting higher diffusion rate than the natural graphite [18].

In order to achieve a good anode material, researches are trying lithium alloys with different materials. These alloys exhibit high capacities and good cyclability than carbon with high voltage operation and stable structures as shown in Table 2.3. But some of them have very brittle structure and they show a great volume increase during cycling that causes stress on the surface and finally cracks. From these cracks, electrochemically inactive materials appear on surface causing the lower cycle stability. However due to their high energy density, high capacity and good cyclability, lithium alloys became the alternative anode material for the carbon.

Table 2.3: Volume changes and theoretical capacities of lithiated metals [60].

Material	Lithiated Phase	Capacity (mAh/g)	Capacity (mAh/ml)	Volume change (%)
C	LiC_6	372	833	12
Al	Li_9Al_{14}	2235	6035	238
Si	$Li_{22}Si_5$	4200	9800	400
Sn	$Li_{17}Sn_4$	994	7000	257
Bi	Li_3Bi	385	3773	115

There have been many attempts to find a suitable metal to alloy with lithium for the good anode materials. Among these materials silicon, tin, aluminum and titanium take great attention with their high capacity and energy densities [61, 62]. Among these materials silicon (Si) and tin (Sn) oxides have a high theoretical capacity when they are fully lithiated $Li_{22}Si_5$ (4200 mAh/g) and $Li_{22}Sn_5$ (994 mAh/g) [63, 64]. However, due to their high volume expansion (% 400 and % 676) [65] and loss of electronic contacts during cycling, they still couldn't be used commercially [66, 67].

Some researches showed that doping Si with carbon (C) and nickel (Ni) can solve some problems with volume expansion and maybe improve the electrochemical performance during cycling [68, 69]. With comparison of Al-Li alloys and Li-Sn alloys, Al-Li showed higher theoretical capacity (993 mAh/g) as the theoretic

capacity of fully lithiated $Li_{22}Sn_5$ alloys (994 mAh/g), with a less volume expansion of Al-Li (% 97) then Li-Sn alloys (% 676) [70]. Lately some researches focused on Li-Ti alloys such as $Li_4Ti_5O_{12}$ with high capacity and better cyclability and less volume changes, but still researches continue to improve the properties of anode materials in order to replace carbon [71, 72].

Cathode materials

Almost all cathode materials (positive electrode) have higher chemical potential than pure lithium metal. These compounds contain either lithium metal or Li^+ ions in order to move towards anode during the charge-discharge cycles [73].

Cathode materials are generally made from lithiated transition metals. These materials can be oxidated higher valances during the cycle when Li^+ ions are removed from the structure. Typically a cathode material has a layered structure with $LiMO_2$ formula, in which M refers to transition metal such as Ni, Mn or Co. In this structure Li^+ ions and metal ions are located in (111) planes and have octahedral sites, oxygen atoms are along the c-axis of the rock salt structure [74, 75].

Cathodes have lower specific capacity than anodes that limiting the performance of the Li-ion batteries. The capacity of cathodes should be improved to be used successfully in new generation rechargeable batteries. A cathode material should possess properties as follows [44]:

1- It should be a good conductor as a metal in order to achieve easy remove of electrons during cycle.
2- It should have the ability of intercalating with large amount of Li^+ ions.
3- It shouldn't react with electrolyte during the reaction.
4- Material should be stable and not change structure during charge/discharge.
5- It should be easily oxidized/reduced during reactions.
6- Material should react reversibly with Li^+ without any change of structure during intercalation.
7- Material should have a high free energy with reaction of lithium.
8- It should serve high specific capacity and working voltage.
9- It should be low cost and environmentally friendly.

For the usage in Li-ion batteries, $LiCoO_2$ was the first cathode material which was developed by Mizushima et al. in 1980 [6] and commercialized by Sony due to its

easy to reproducibly without any problems [76]. $LiNiO_2$ was developed later which has the same layered structure with $LiCoO_2$ but more stable and lower discharge rate. Working voltage is respectively 3.7 V for $LiCoO_2$ and 3.5 V for $LiNiO_2$ [77, 78]. Both of them are electrochemically unstable and having safety problems during reactions. As the removal of the Li^+ ions during the intercalation, structural changes cause exothermic reaction of $LiCoO_2$ with electrolyte [79, 80]. Lithium cobalt dioxide ($LiCoO_2$) is one of the most used cathode material in commercial applications of Li-ion batteries which has a layered α-$NaFeO_2$ structure that was invented by Mizushima et al. in 1980 [6]. It has a relative stability and 274 mAh/g theoretical capacity and higher energy capability with comparison to other cathode materials. The crystal structure of the $LiCoO_2$ is layered rhombohedral (space group R3m) shown as the Figure 2.9. In this structure oxygen atoms are ordered with Li and Co atoms in (111) planes that looks like distorted hexagonal struture. During the intercalation/deintercalation process, Li^+ ions move through the CoO_2 layers in the structure [81].

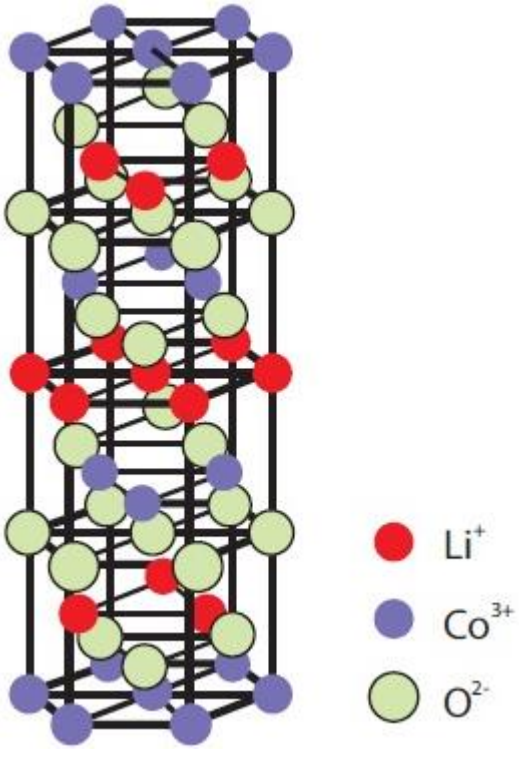

Figure 2.9: Crystal structure of layered $LiCoO_2$ [82].

$LiCoO_2$ has several phase transformations during charging to 4.2 V from hexagonal to monoclinic structure results decreasing cycle performance and capacity of cathode material. Moreover, dissolution of Co into electrolyte is observed when the battery is

charged over 4.2 V [17]. Consequently, $LiCoO_2$ was a good cathode material for the first applications of Li-ion batteries however it should be replaced due to its safety, cost and stability problems [83, 84]. Other alternative cathode materials are under research using transition materials such as Ni, Mn, Fe.

$LiNiO_2$ is one of the other cathode materials which has the hexagonal (R3m) crystal structure. It has 275 mAh/g theoretical capacity and 3.7 V working voltage [74]. $LiNiO_2$ is more promising cathode material comparing with $LiCoO_2$ and has many advantages such as higher capacity in reality (200 mAh/g), less cost and not harmful to environment however having the problems with synthesis and safety. Also phase transformations occur during cycle and cause the displacement of atoms in the structure which results with capacity fading [85].

The advantages of $LiNiO_2$ took some attention in order to be an alternative cathode material although some problems should be overcome before the use of commercially rather than $LiCoO_2$ [74]. During the electrochemically charging, Ni^{+2} ions can be oxidized to Ni^{+3} resulting structural changes and prevent intercalation of Li^+ ions [38]. Also, when the over potential applied, the loss of oxygen in exothermic reaction can cause explosion depending the flash point of electrolytes. The structural changes should be prevented in order not to have a capacity fading during the cycle.

Another alternative cathode material is Lithium Manganese Oxide ($LiMn_2O_4$) which has a cubic close pack spinel structure having a space group Fd3m as shown in the Figure 2.10. In this structure lithium atoms are occupied in the tetrahedral 8a sites, manganese atoms are sited in octahedral 16d and oxygen atoms are in center of the cubic faces. This spinel structured $LiMn_2O_4$ was developed by Thackeray et al in 1990s in order to lower the cost cathode materials [86]. Also it shows better stability and high voltage discharge and more environmentally safety. However it has lower theoretic capacity (148 mAh/g) and capacity loss in high temperatures with the comparison of layered cathode materials such as $LiCoO_2$ and $LiNiO_2$. There have been many studies to overcome of these problems such as coating the particle surfaces and using other type of electrolytes to prevent dissolving manganese [87].

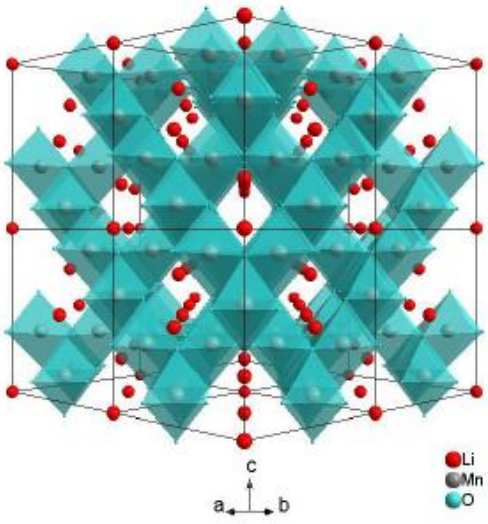

Figure 2.10: Crystal structure of spinel $LiMn_2O_4$ [32].

Nowadays many researchers are focused on producing more stable, high specific capacity cathode materials in order to displace the old type expensive and unstable cathodes. For this reason in some studies cobalt and nickel is being mixed with lithium to achieve a layered compositions such as $LiNi_{0.8}Co_{0.2}O_2$ which has not only lower cost and less harmful to environment but also higher capacity (180 mAh/g). There are still research for low cost and environmental friendly cathode materials having compounds of cobalt, nickel, phosphates, manganese and vanadium such as $LiMnPO_4$, $LiCoPO_4$ and $LiV_2(PO_4)_3$ [88].

Mixing nickel, cobalt and manganese in different rates gives better performance and lower cost than pure cathode materials such as $LiCoO_2$, $LiNiO_2$ or $LiMn_2O_4$. For this reason $LiNi_{1/3}Co_{1/3}Mn_{1/3}O_2$ systems are still under research to understand the optimum composition and the behaviours of the metals that are used in structure. This cathode shows 150 mAh/g capacity with 4.2 V working voltage with improved capacity retention and stabilized structure [89].

Also in recent years there have been many attempts to substitute nickel and cobalt atoms with other metals such as aluminium, gallium, manganese and titanium in order to have more stabilized structure and better electrochemical properties. Among these alternative cathode materials, $LiNi_{1-y-z}Co_yAl_zO_2$ has the better properties and started being used in commercially productions due to its high specific capacity (120-130 Wh/kg) without capacity fading during 1000 cycles [90].

In 1997 Goodenough and coworkers discovered a new cathode material called Lithium Iron Phosphate ($LiFePO_4$) which has gained more attention not only in researches but also industrial applications due to its great properties such as low cost and less toxicity with comparison other cathode materials made by Mn, Ni and Co. It has olivine type crystal structure with Pnma space group as shown in Figure 2.11. It has an orthorhombic symmetry where PO_4 tetrahedras, FeO_6 octahedras, Li^+ and Fe^+ ions are located in alternate planes (001) in the structure [91, 92]. $LiFePO_4$ has a working voltage 3.4 V which is lower than other layered cathode materials. But it has a high specific theoretic capacity (170 mAh/g) with better stable structure during cycle.

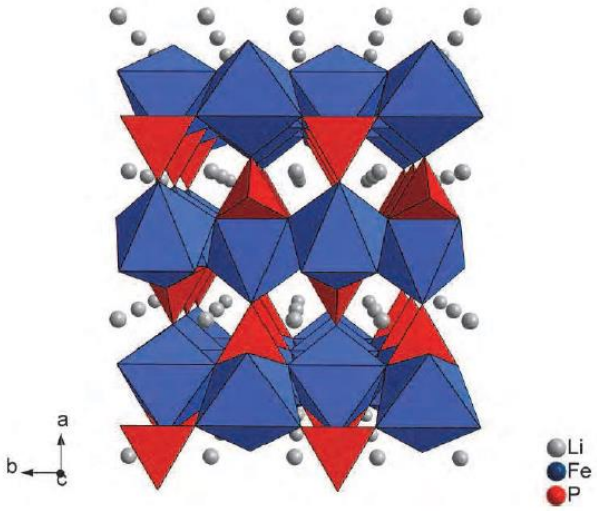

Figure 2.11: Crystal structure of olivine $LiFePO_4$ [93].

Although $LiFePO_4$ material has a low electronic conductivity around 10^{-9} S/cm because of the PO_4 groups and one dimensional diffusion pathway of Li^+ ions, many researches focused on achieving higher electronic conductivity of $LiFePO_4$ with carbon coating and producing the particles in nanometer sizes [94].

In a research, a graphite precursor was mixed with $LiFePO_4$ powders by Huang et al in order to improve the conductivitiy and electrochemical properties with controlling particle sizes in the nanometer ranges. In this work, $LiFePO_4$/C composites particles achieved a great cycling performance at C/2 with almost no capacity loss which showed that minimizing particles and adding carbon additives improve the performance of $LiFePO_4$ cathode materials [92]. In another article Franger and friends made $LiFePO_4$/C composites with mechanochemical method that particle sizes are between 0.5-2 μm having 125 mAh/g specific capacity at 1 C rate [95].

Yamada and friends produced 200-300 nm grain sized $LiFePO_4$ samples showing 160 mAh/g capacity [96] which is another proof of the lowering particle improves the performance and specific capacity of the samples.

$LiFePO_4$ cathode material is also took attention from industrial applications and Sony workers searched for the facts that effect the performance during the synthesis of the materials such as temperature. They realized that when the synthesis temperature decreases, it is possible to achieve smaller particles sizes, which is resulting better capacity and performance of the batteries [97].

$$LiFePO_4 \xrightarrow{Charge} (1-x)LiFePO_4 + xFePO_4 + xe^- + xLi^+ \qquad \textbf{(2.4)}$$

During the synthesis of $LiFePO_4$ powders, it is very important to prevent the formation of impurities such as Fe (III) because oxidation of unstable Fe (II). For this purpose, carbothermal reduction process gained a great interest nowadays due to its advantage of using directly Fe (III) precursors that are cheaper and more stable than Fe (II) precursors in order to produce $LiFePO_4$ powders. In an article, Liu and friends reported producing $LiFePO_4$/C powders at 750 °C with carbothermal reduction technique gives 133 mAh/g specific capacity at C/10 rate and almost no capacity decrease in 20 cycles [98].

In the carbothermal process, particle size distribution and crystallization degree is very important that can inhibit $LiFePO_4$ dissolution and result better performance during cycling. Zhi and friends reported the calcination temperature effect carbothermal reduction on crystallinity of $LiFePO_4$/C powders, which showed that low calcination temperatures results with nanosized particles, low crystallization degree. These powders had high initial capacities but poor electrochemical performance due to low stable structures during the cycling [99].

Microwave heating is another alternative method to produce $LiFePO_4$ powders with the help of easy controllable size and uniform particles, very short process times (2-20 mins), lower cost than other conventional techniques and not using any reductive gas during synthesis [100].

Higuschi and friends produced $LiFePO_4$ powders with microwave process showing 125 mAh/g capacity with a very low capacity decrease during cycling at 60 C [101]. In another study, it was found that the particle sizes of $LiFePO_4$ powders produced by microwave technique are smaller and uniform, having smooth surface and higher

capacity comparing to powders produced by other solid state techniques [102]. Another advantage of microwave heating technique is producing $LiFePO_4$ nanorods having 25-40 nm width and 0.1-1 μm length. These nanorods exhibit a great discharge capacity (161 mAh/g at C/10) and cycling performance when mixed with multi walled carbon nanotubes [103]. Also combined synthesize techniques can result smaller size particles. Parker and friends used combination of precipitation and microwave technique resulting smaller particles with a higher capacity (150 mAh/g at C/10 rate) [101].

Xu and friends produced $LiFePO_4$ powders with hydrothermal synthesis technique which is a cheap and simple way to produce pure and uniform powders. They covered powders with multi walled carbon nanotubes resulting a high specific capacity (160 mAh/g at 0.3 C rate) and good cycling with a low capacity fading in 50 cycles [104, 105].

Sol-gel is another way to produce powders with wet chemical synthesis technique in a low temperature having the advantages of low cost, high purity and uniform small particle sizes in nanometer ranges which takes very much attention for producing $LiFePO_4$ powders [106].

Dominko and friends studied to compare sol gel technique and solid state synthesis for the preparation of $LiFePO_4$, which has proved that the powders prepared by sol-gel technique has higher capacities around 150 mAh/g at C/10 and the others are 130 mAh/g in same rate [107]. $LiFePO_4$ powders have pore sizes in the range of 30-200 nm with the sol-gel synthesis. In a research of Dominko and friends analyzed pore sizes of $LiFePO_4$/C composite powders which are 60-90 nm having 160 mAh/g capacity in C/20 rate [108].

The pored structure have better influence on powders showing better electrochemical properties due to increasing surface area and making the path of Li^+ diffusion shorter [109]. In order to have better electronic conductivity and electrochemical performance, not only carbon but also other metals can be added to the $LiFePO_4$ structure such as Mg, Ti and Zr. Wang and friends found out that the samples doped with Ti metal has better capacity (160 mAh/g at C/8 rate) during cycling [110].

Myung and friends tried to achieve a composite of $LiFePO_4$/C powders by using aqueous emulsion drying method and having a capacity 140 mAh/g at 20 mA/g rate [111].

Nowadays microemulsion drying technique takes a great attention for producing nanosized $LiFePO_4$ powders. With the help of stabilizing agents it is easy to achieve thermodynamically stable solutions [112]. Myung and friends produced $LiFePO_4$/C powders using microemulsion drying technique, having particle sizes around 1μm and 125 mAh/g specific capacity at C/8.5 rate. It also increased conductivity in the range of 10^{-4} S/cm [113]. In order to have smaller particles in the synthesis of particles, stabilizers and surfactant materials can be added to microemulsion solutions. In an article 90 nm particle sized $LiFePO_4$/C are produced having 163 mAh/g initial discharge capacity at C/10 rate [114].

Although there are a lot of reports about improving the conductivity of $LiFePO_4$ cathode material, these kinds of carbon coatings can dissolve in electrolyte during cycling and result the formation of SEI layer. In order to prepare a high capacity cathode material it is difficult to produce the composite particles in nano size range due to high chemical reactivity [93].

For this purpose, Molenda et al. developed a unique technique to produce conductive carbon layers on nano sized particles. In this process nano sized particles are impregnated to the solutions of polymer compositions of pyromellitic acid (PMA) modified poly-N-vinylformamide (PNVF) in water [93]. After the mixture achieved, it is stirred till the evaporation of water and to prevent precipitation. After drying the powders in air furnace and pyrolysis around 500-700 °C under inert gas (Ar, N_2) atmosphere, conductive carbon layer (CCL) covered nanoparticles are achieved as an illustration in Figure 2.12 [93].

Figure 2.12: Producing CCL covered nanoparticles [93].

As a conclusion, $LiFePO_4$ is a good promising cathode material due to its high capacity, environmental friendly, good cycling and high stable structure. Although it has a low conductivity (10^{-10} S/cm at room temp.), it can be doped or covered with carbon additives, or producing uniform small particle sizes having large surface area in order to improve its electrochemical properties.

In this study, $LiFePO_4$ nanoparticles will be produced by the anaqueous solution technique and cover them by conductive carbon layers in order to improve the conductivity and electrochemical properties of powders.

Electrolyte

Inside of Li-ion batteries, water is not suitable solution using as an electrolyte due to its low stability in high working voltages. Even though nonaqueous organic solutions have lower ionic conductivities than water, they are used for higher electrochemical stability. Also, electrolytes should be suitable with the electrode materials [32]. An optimum electrolyte solution should have high ionic conductivity, large potential working range, thermally and chemically stable, low reactivity with electrodes and environmentally safe [115].

In order to produce liquid electrolytes, the solutions of esters such as ethylene carbonate (EC) for highly permittivity and dimethyl carbonate (DMC) for low viscosity are used for resulting good electrochemical performances with high conductivities.

In addition to the combination of EC and DMC, salt should be added to show better cycling properties and more stability up to 4.5 V. $LiPF_6$ is the most used salt in Li-ion batteries [116].

Although it is the most commercially used electrolyte solution, EC based electrolytes should not be used with the graphite anode electrodes causing the peeling of graphite [117].

Nevertheless, organic electrolyte solutions are highly combustible and easy to decompose because of the oxidizing effect of cathode materials. To overcome these problems, researchers tried to develop polymer based electrolytes to replace liquid electrolytes. In these polymer electrolytes, liquid electrolytes (EC-$LiPF_6$) are put into a polymer matrix of polycarbonate and polyvinylidene difluoride (PC, PVDF) having

the combination of a better mechanical properties and high conductivity at same time [118]. Although polymer electrolytes have the advantages of nonflammable structure and preventing the leak of liquid electrolyte, it has a very important disadvantage of low ionic conductivity (10^{-8} to 10^{-5} S/cm) compared with the liquid ones (10^{-3} to 10^{-2} S/cm). Also polymer electrolytes decrease the power densities of the batteries due to low Li^+ transfer number [119]. As a conclusion, polymer electrolytes promising have some advantages comparing with liquid electrolytes however some problems should be solved in order to be a replaced in for the next generation commercial Li-ion batteries.

Seperator

One of the main components of the Li-ion batteries are the seperators which prevents the direct contact of cathode and anode electrodes in order not to have a short circuit. Seperators should allow the ionic transfers between the electrodes [47].

Seperators must be selected for the best compatibility of each battery requirements. There are some important properties of separators that affect the performance and stability of the batteries such as:

- Mechanically stable
- Easily wetted by electrolyte
- Chemical resistance for other parts of battery
- Electronically insulating
- Prevent the particle transport
- Uniform surface structure and thickness
- Low resistance of electrolyte

Generally seperators are made from the polymeric electrolytes or porous plastic films such as polypropylene (PP) and polyethylene (PE). These are the most common used seperators in Li-ion batteries providing chemically stability, low cost and good mechanical properties. Additionally when the temperature of the cell rises more then the melting point of separator (130 °C), their pores are shut down in order to avoid of Li^+ transport and overcharging the battery [120].

3. MICROEMULSION

Emulsions are the mixture of two different liquids which are immiscible or partially miscible. Emulsion solutions are thermodynamically unstable and heterogeneous resulting one liquid is dispersed into another immiscible one. As a result, droplets achieved having diameter 1-100 μm. In these systems different phases occur, which are called "water" and "oil". The water phase is aqueous and oil phase is mostly hydrophobic materials (aliphatic, aromatic) such as toluene or n-decane [121]. There are two different kind of emulsions which are named from the dispersed phase: If "water" is the dispersed phase inside of continuous "oil" phase it is called "water in oil (W/O)" emulsions, and reversibly when the "oil" phase is dispersed in a continuous "water" phase, that are called "oil in water (O/W)" emulsions. In order to achieve a homogenous emulsion, surface active materials (surfactant) can be added to system. These surfactant materials control and adjust properties of the dispersed droplets and interphase between water and oil phase.

Emulsions can be classified by means of the dispersed phase and the diameter of droplets. The diameters of droplets affect their visual apperance resulted from the light scattering from droplets. "Macroemulsions" are the opaque-milky white solutions which have diameter of droplets larger then 0.3 μm that scatters the spectrum of visible light. When the droplet size decreases, the colour of the solution turns to gray translucent called "miniemulsion" which has a 0.1-0.3 μm droplet sizes that can only scatter some spectrum of the visible light. If the droplets have diameter less than 0.1 μm (1/4 of wavelength of visible length) the solutions becomes transparent and called "microemulsion" [121]. Because of the fact that macroemulsions had some problems with stability and flocculation, microemulsions had a great interest since the last few decades both from the academical and industrial applications.

In order to prepare a stable emulsion and achieve the properties as wanted, it is required to understand the parameters affecting the droplet sizes and the other forces between the dispersed and continuous phase. For this reason, researches have an

improving interest as it can be seen from the increment of the publications on microemulsion since 1990. In a research, from the database of scopus, for the "microemulsion" the published papers has a high rate of increase 1960-70s (112 papers), 1980s (974 papers), 1990s (2762 papers), 2000s (6933) [122]. Emulsions and microemulsions have some different structural properties such as physical and thermodynamic which effects their stability and droplet sizes. Emulsions are generally unstable, therefore droplets (1-100 μm) coalesence in time and grow larger. Finally phase seperation occurs in the emulsion systems because of the gravitational forces [123]. On the other hand, microemulsions are thermodynamically stable and isotropic transparent solutions which have droplet sizes in a range of 5-100 nm. Microemulsion properties are dependent on some parameters such as the concentration or type of the surfactants that are used to control the interfacial surface film between oil and water phases [124]. If the optimum conditions to produce microemulsions, the solution becomes stable spontaneously and stays from weeks to years [125].

There have been many researches about microemulsions since 1900s. In a publication of Hoar and Schulman in 1943 they mentioned that if oil and soap (cetyl trimethyl ammonium bromide) are mixed in a sufficient amount with the help of alcohol and water, it may result a transparent solution of continuous oil phase in which water droplets are dispersed [121]. They also tried to understand the forces on the surface of droplets. They found that interfacial tension has a very important influence which can be stabilized by an alcohol to prevent the repulsive electrostatic forces for water in oil microemulsion. Schulman described "microemulsion" in 1959 which can be also be water in oil (W/O) and oil in water (O/W) related the properties of the system and additives [126].

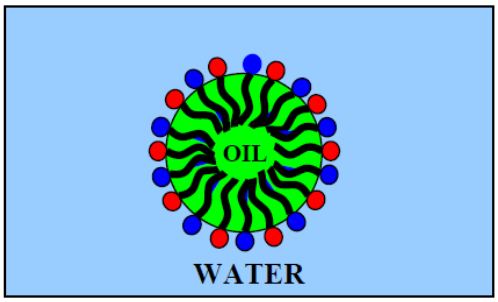

Figure 3.1: Schematic illustration of and oil-in-water (O/W) microemulsion system [126].

Determination of the type of microemulsion is more related to surfactant type rather than volume ratios of the phases in the system as referred to Bancroft rules. These rules are that in a microemulsion the contiuous phase will be in which the surfactant is more soluble [127].

Bowcott and Schulman published an article in 1955 and tried to explain the formation theory of microemulsions. This is related to molecular interactions at interface between oil and water phases. In this interphase, surfactant (potassium oleate) and cosurfactant (alcohol) dispersed between oil and water phase [121]. The structure of the microemulsions can vary from spherical to cylindrical which is separated from the continuous phase with an interphase [122].

In a microemulsion, there is a huge interfacial area created by droplets result the interfacial tension improvement. In Figure 3.2 there is a critical droplet size where the free energy is negative and makes the stable microemulsion [126].

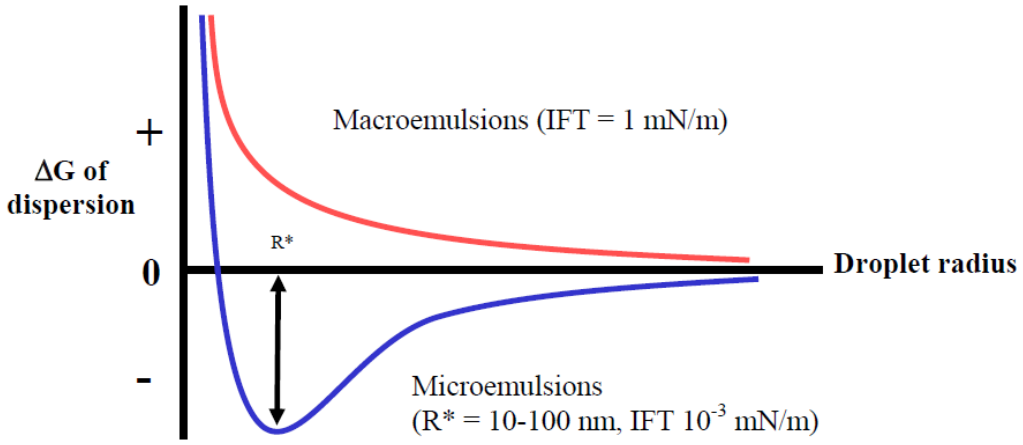

Figure 3.2: Thermodynamically stability of macroemulsions and microemulsions [126].

In the late years of 1970s, applications of microemulsions are improved in the oil industries after recovering the oil became an important issue. In some experiments, Schulaman and coworkers tried to understand and determine the properties such as droplet sizes of the microemulsion solutions using light scatter and X-ray diffraction, nuclear magnetic resonance (NMR), viscosimetry and ultra-centrifuge [126]. Although the sizes of particles in microemulsions don't refer the name of it (micro), it is an easy way to produce powders from nanometer to micrometer scale [122].

In microemulsion, nanoparticles can be produced in uniform sizes by controlling the parameters effecting the growth of micelle sizes. These parameters are mostly related to surfactant and the ratio of it which affect the interphase properties [128, 129].

There are several advantages of using microemulsion method for producing nanosized particles. It doesn't need any expensive devices or equipment as compared to other techniques. Uniform and homogenous nanoparties are obtained for the desired applications. Particle sizes and morphology can be adjusted by controlling the parameters [130, 131]. Also after the powders are produced, the temperature and the time of the annealing parameters can also effects the size and the crystallization of the product. In order to understand the properties of the microemulsions many researchers have been still investigating the phases and the relation between each other.

3.1. Applications of microemulsions

In daily life, microemulsions are widely used for productions in human life. In order to achieve the desired material, it is very crucial to understand and control the formation parameters during the process. In most cases microemulsions are used for the solubilisation of chemicals and removal of unwanted materials. For the industrial applications, the microemulsions should be low prices. There are many areas to use microemulsions for such desired applications of foams for fire fighting, cleaning stuff, decontamination of chemicals, microemulsion polymerization [132], food additives [133], medical and cosmetic applications [134]. In a report of using surfactants for such applications, it is indicated that 2 million m^3 surfactants are used in 2003 in the industrial scale which shows the importance of the microemulsion process and the products obtained [122].

Microemulsions have great advantage in using health applications due to their unique properties such as the ability of solubility of hydrophilic/hydrophobic particles and having stable for long times. For this reason, it is used for many health applications such as recovery of oil [135] and even delivering genes to cells in human body. Due to their unique physical and chemical properties, microemulsions are widely used in drug delivery processes such as proteins [136], transdermal [137], amphiphilic drugs [138]. There are many applications about gene delivery to cells [139], aim to cancer cells [140], biocatalyss [141] and for food products [142].

Since the first application of microemulsions for producing nanoparticles from 1990s, it became an important technique to produce polymeric nanomaterials [143], metal oxide nanoparticles [144], intermetallic and metallic nanoparticles [145] and magnetic nanoparticles [146].

As a conclusion, microemulsions are widely used in many industrial applications due to their advantages such as producing very small uniform particles and high surface area. It is very important to understand the interactions which occur on the interphases of droplets during microemulsion synthesis.

In order to produce stable and homogenous microemulsions, the formation of the system requires many conditions to be understood and controlled. Some of these conditions are [121];

a) In order to cover the surfaces of droplets there should be sufficient surfactant.
b) The interfacial layer should have solubility in oil and water phases
c) The surfactant should reduce the free energy at interphase.

4. EXPERIMENTAL PART

4.1 Producing $LiFePO_4$ Powders

In a novel anhydrous solution precipitation technique, olivine structured $LiFePO_4$ nano powders are prepared as precursor powders. For this purpose, lithium acetate dihydrate ($LiC_2H_3O_2.2H_2O$) from Sigma, ammonium dihydrogen phosphate [$(NH_4)H_2PO_4$] from POCH and iron(II) sulfate heptahydrate ($FeSO_4.7H_2O$) from ROTH are used as the raw powders as received without any further process. They are mixed in a stoichiometric ratio of Li:Fe:P (1.3:1:1). In order to prepare the solutions, each powder is dissolved in ethylene glycol ($C_2H_6O_2$) from POCH. They are stirred continuously seperated at room temperature and then mixed all together. Ammonium dihydrogen phosphate is dissolved in 200-250 ml ethylene glycol for 24 hours to achieve a pure, homogenous solution. Lithium acetate dihydrate is dissolved in 40-50 ml ethylene glycol for 1-2 hours and finally iron (II) sulfate heptahydrate is put into a sealed reactor and dissolved in 50-60 ml ethylene glycol for 1-2 hours under inert gas (Ar, N_2) atmosphere to prevent the formation of Fe (III) impurities caused by the oxidization of Fe (II) powders. After every solution achieved, first lithium solution and then phosphate solution added slowly onto the iron solution slowly in reactor, and left strirring continuously at room temperature for 24 hours under inert gas. During the mixing, solution turned to dark green. After the solution achieved, it is put into centrifuge at 3000-4000 rpm for 4-5 times (Heraeus Megafuge 40R) to sedimentation of powders from the ethylene glycol with the help of acetone. Finally, the powders are obtained in a slurry structure and put into air furnace (BMT-Venticell 55) at 80-90 °C for over a night in order to get rid of remaining liquid. After drying the powders, the $LiFePO_4$ raw powders are produced. Eventually, the precursor powders are calcinated in 550-750 °C for 6-24 hours in tube furnace under inert gas (Ar, N_2) atmosphere to have the crystalline phase.

In order to produce small nanoparticles and more stable structure of $LiFePO_4$ with the help of microemulsion technique, ammonium dihydrogen phosphate, lithium acetate dehydrate and iron (II) sulphate heptahydrate powders are prepared separated microemulsions and mixed as the same route of solution precipitation technique we used. For this reason, ethylene glycol (water phase) and toluene (oil phase) are used as solvents and sodium dodecyl sulfate (SDS) as surfactant and decanol as cosurfactant. For preparing the optimum stable solutions, precursor powders and other materials are mixed in different ratios to each other as referred by Friberg et al. [147].

4.2 Conductive Carbon Layer (CCL) Coating

In order to improve the conductivity of the $LiFePO_4$ powders, a novel process is developed by Moleda et al. [93]. Due to this reference, our particles are immersed in the solutions of polymer combinations. For this reason, first of all our $LiFePO_4$ powders are wetted by distilled water to have easy mixing with other solutions and mixed in ultrasonic mixer for 5-15 minutes. In the same time, pyromellitic acid (PMA) and poly-N-vinylformamide (PNVF) are dissolved in water around % 5-15 and mixed to each other and continue stirring around 30-40 minutes. Secondly the mixture of polymer solutions is added onto the $LiFePO_4$ powders. Final mixture is mixed by magnetic stirrer for 10-20 minutes, then ultrasonic mixer for 15-25 minutes and lastly 30-40 minutes on laboratory shaker until the homogenous mixture of the solutions are achieved.

Figure 4.1: CCL covering process of $LiFePO_4$ nanoparticles [93].

After this process, the solution is put into a plastic pot and stirring continuously at 50-60 °C on a temperature controlled magnetic stirrer till the loss of all water from the system. Mud-like powders are put into air furnace at 80-100 °C to be dried for 24 hours. Dried powders are glassy due to the polymeric cover over the particles. CCL covered $LiFePO_4$ powders (CCL/$LiFePO_4$) are put into tube furnace for controlled

pyrolysis around 550-700 °C for 6-24 hours on gold plates under inert atmosphere to prevent impurities during heat treatment. It can be seen the illustration of the CCL covering of the particles in Figure 4.1.

In this study, $LiFePO_4$ nanoparticles are covered with CCL in the ratio of 5-20 %. The amount of covered CCL on the nanoparticles of CCL/$LiFePO_4$ is calculated from TGA curves. To compare the performance of CCL/ $LiFePO_4$ nanocomposites with commercial carbon black (CB), $LiFePO_4$ nano powders are mixed CB in the same ratios of CCL.

4.3 Characterization of Powders

4.3.1 TGA

In order to estimate the calcination temperature of $LiFePO_4$ precursor powders, thermogravimetric analysis (TGA) with single differential thermal analysis (SDTA) are performed in Mettler-Toledo 851^e thermo analyzer coupled to Thermostar GSD 300 T Balzers using open aluminium oxide crucibles as reference material. Quadruple mass spectrometer (QMS) is also joined online to determine the mass and type of the gases during analysis. In TGA, it is analysed that the mass change of sample with temperature, thermal stability and decomposition temperature of material. During SDTA anaylsis, empty inert reference crucible is heated and measured as the same of sample material and calculate the difference between them, so physical and chemical transitions such as melting of sample can be determined. In the QMS analysis, the mass lines are referred to OH (17), H_2O (18) and CO_2 (44) species. With the DTG (derivative thermogravimetric) analysis, it is observed more clearly and detailed in the mass changes with temperature. The samples are put into 150 µl aluminium oxide crucibles and heat treated under air atmosphere (80 ml/min) within temperature range 25–1000 °C heating rate of 10 °C/min.

4.3.2 XRD

As-prepared $LiFePO_4$ powders are examined before and after covering with CCL by XRD analyser (Bruker D2 Phaser, CuK_α=1.5418 Å) scanning in the range of 2Θ=10-80° in order to determine the phases and crystal structure. Particles sizes are calculated from the full width at half maximum (FWHM) diffraction peaks using the Scherrer equation as:

$$d_{\mathrm{XRD}} = \frac{\mathrm{K}\lambda}{\beta\cos\theta} \quad \textbf{(4.1)}$$

where d is the crystallite size, λ is the diffraction wavelength (1.5418 Å), β is full width half maximum intensity from the strongest peaks, Θ is the diffraction angle of the peak and K is Scherrer constant (0.89) value depending on particle shape [148].

4.3.3 BET

Specific surface areas and pore diameters of $LiFePO_4$ and CCL/$LiFePO_4$ nanocomposites are measured by N_2-BET isotherm method in analyzer (Micrometrics ASAP 2010). In order to charactarize surface properties of the samples, average pore sizes and distribution of them are determined during the adsorption/desorption of N_2. Particle sizes of the samples are calculated assuming spherical shapes and narrow size distributed and relating the surface areas as the formula [149]:

$$d_{BET} = \frac{6000}{A_{ss}\rho} \quad \textbf{(4.2)}$$

where A_{ss} is referred to the specific surface area (m^2/g) measured from BET results and ρ is attributed the theoretical density (g/cm^3) of $LiFePO_4$ as 3.6 g/cm^3 [150].

4.3.4 Conductivity

For comparison of the electrical conductivities of nanocomposites CCL/$LiFePO_4$ and mixture of CB/$LiFePO_4$ was measured by AC (33Hz) 4-probe technique (Sigma 1 in AC) within the range of temperature (-20) °C and (+40) °C. The samples are so elastic structured after CCL cover, so they are put into a glass tube and squeezed with screw between gold electrode discs (∅=5 mm) until no change in resistance in order to make the pellets.

Electrical conductivity results of the samples CCL/$LiFePO_4$ and CB/$LiFePO_4$ are shown as a function of temperature and activation energies are calculated by the Arrhenius law based on the formula [151]:

$$\sigma = \sigma_0 \exp(-\frac{E_a}{K_B \mathrm{T}}) \quad \textbf{(4.3)}$$

where K_B is the Boltzmann constant, σ is the conductivity of material, σ_0 is pre-exponential factor and Ea is the activation energy.

4.3.5 Electrochemical Characterization

The electrochemical tests of $LiFePO_4$ are measured using CR 2032 coin cells assembled in a glove box under argon atmosphere as shown in Figure 4.2. For this reason, $LiFePO_4$ powders are used as active material and mixed with acetylene black to improve conductivity and polyvinylidene fluoride (PVDF) as binder in different ratios (% wt 80:10:10 and 75:15:10) to compare results. The mixture is dissolved in 1-methyl-2-pyrrolidinone (NMP) and coated as a thin film on Al foil for current collector. The films are dried at 100-120 °C for 2 hours in vacuum oven and then pressed at 10 MPa for 5 minutes. Finally films are cut to form a disk electrode having 1.5 cm^2 area. Finally batteries are assembled using these $LiFePO_4$ films as cathode electrode, lithium metal is used as negative (counter) electrode and separator is used polypropylene membranes (Celgard). The electrolyte was 1 M LiPF6 (lithium hexafluorophosphate) dissolved in mixture solution of EC (ethylene carbonate) and DMC (dimethyl carbonate) having volume ratio of 1:1 which is obtained as LP 30 from Merck.

Figure 4.2: An illustration of assembling a coin cell.

4.3.5.1 Cyclic voltammetry

Cyclic voltammetry (CV) is an electrochemical technique to measure a cell behaviour. The datas can be obtained from the redox reactions thermodynamically and also kinetics of electron transfer during the reactions. The shapes and the characteristic position of voltammetric analysis are special for electrochemical properties from a redox reaction [14, 167].

With the help of CV technique, it can be investigated all types of potential dependent interface processes, double layer capacitances and charge transfer reactions [167].

In order to the cyclic voltammetry measurement of a cell (working electrode versus counter electrode), voltage is applied to working electrode linearly vs time. In a typical experiment of CV a solution is placed in contact with electrodes and reduced or oxidized. When the positive/negative voltage is applied to system, electrode is forced to transfer electrons from surface. The response of cell is measured by current (*i*) vs potential (*U*) in electrode circuit reversibly and plotted as cyclic voltammogram (CV). For example, $LiMn_2O_4$ is a well known cathode as working electrode versus lithium metal as counter electrode. The cell is cycled between 3.4 and 4.3 V at 0.1 mV/s rate. The resulting CV plot is shown as Figure 4.3 [14].

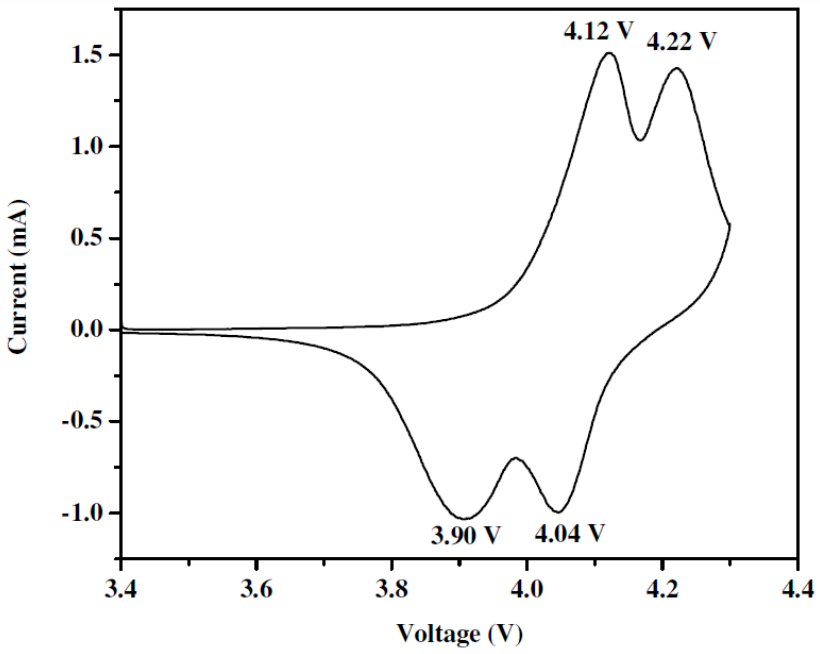

Figure 4.3: CV plot of $LiMn_2O_4$ electrode [14].

During the cycling of electrode, anodic and cathodic peaks are observed due to resersible oxidation and reduction reactions from lithium insertion/extraction. These voltammetric waves are indicating that electrode material changes phase during intercalation of Li^+ ions. The anodic peaks around 4.12 and 4.22 V are attributed to oxidation reactions due to deintercalation (removal) of Li^+ ions from tetrahedral sites of cathode electrode during charge process. When the material is synthesized in high crystallinity, peaks will be observed sharper and splitted from each other [14].

Sometimes, peaks are not located exactly at the thermodynamic potentials because of overpotentials which are caused by charge transfer resistance, diffusion process, resistance between current collector and active material, electrolyte resistance. High scan rate would increase the overpotentials, however low scan rate may result the peaks as expected thermodynamic potentials [167].

4.3.5.2 Electrochemical impedance spectroscopy (EIS)

Electrochemical impedance spectroscopy (EIS) is a very useful technique to analyse electrical and electroctrochemical properties of materials and energy storage systems such as fuel cells and batteries. Ionic and electronic conductivities of electrodes can be investigated with the help of this technique. Also, electrochemical diffusion coefficient can be charazterized by impedance analysis [164]. EIS applies a sinusoidal electrochemical potential or current to material in a wide range of frequency which shows the reactions take place in different rates and allows to measure the capacitance of electrode [14].

When there is a voltage (potential) applied on electrochemical cell that will result a electric current flow over the cell. The ions will move through the electrolyte because of the potential difference and form new chemical species as a result of some reactions [24].

During the measurements of EIS, generally a sinusoidal AC voltage signal $U(t)$ is used and sinusoid of same frequency gives us an AC current response $I(t)$ but in a different phase. The combination of the formulas of applied AC voltage and response signal gives us the impedance formula as complex function [167]:

$$Z = Z_0 \frac{\sin(\omega t)}{\sin(\omega t + \varphi)} = Z_0 \exp(j\varphi) = Z_0 (\cos(\varphi) + \sin(j\varphi)) \qquad \textbf{(4.4)}$$

where ω is the radial frequency and φ is the phase shift. Impedance has a real part that is plotted on x-axis and and an imaginary part (negative of imaginary) is plotted on y-axis in a Nyquist plot. As an example of a circuit that a resistor is parallel to a capacitive part then we obtain a plot as in Figure 4.4 [167].

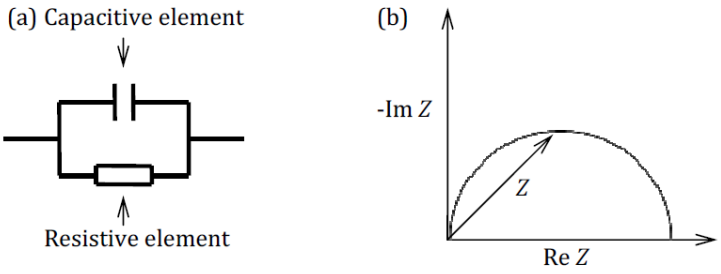

Figure 4.4: An example of circuit and Nyquist plot [167].

The resistance of Li-ions diffusion in the electrolyte can be calculated from the distance between y-axis and first point of real component of first semi circle. The charge transfer of the ions from electrode through electrolyte is shown as a semi circle, which can ocur in a wide range of frequency related to electrode material and electrolyte properties. The movement of ions and interaction with organic solvents in Li-ion batteries is represented in Figure 4.5. When the AC signal frequency is higher than 10^5 Hz then the reaction takes less than 10 µs. As a result, in this sample only a real part appear for impedance in Nyquist plot which means no capacitive behaviour of material. While the middle range frequency applied between 10^0 and 10^5 Hz, ion charge transfer happens in 10 µs and 1 s. When the low frequency applied less than 10^0 Hz, a 45° angle plot appears in Nyquist which refers to solid state diffusion in material. In that low frequency ranges impedance is totally capacitive and Li-ions can not diffuse into material [167].

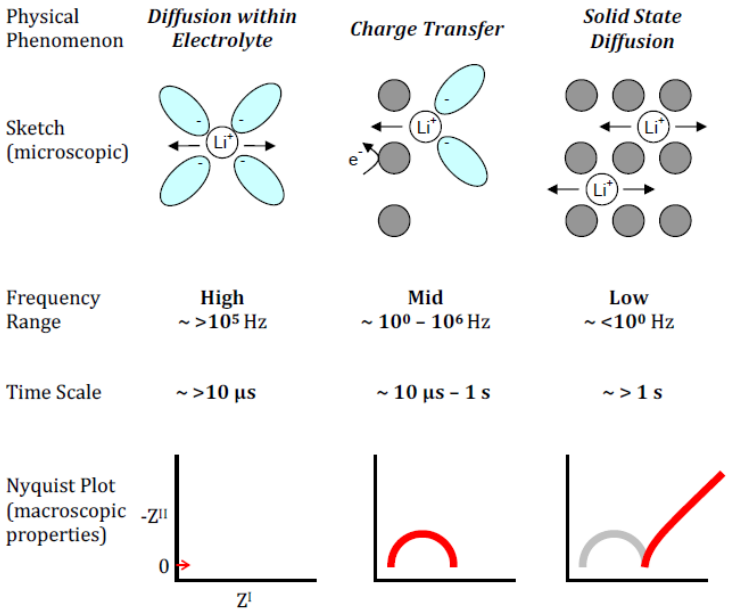

Figure 4.5: Li-ion transfer and Nquist plots appear in Li-ion batteries [167].

Electrochemical cells are assumed as the combination of capacitors and resistors in an equivalent circuit. In the impedance analysis (from real and imaginary parts), we can decide the circuit and different components properties. The electroactive parts of an equivalent ciruit are shown in Figure 4.6 which is offered by Randles et al. In this model, R_I or R_e represents the ohmic resistance of electrode and electrolyte in the cell, C_{DL} or CPE (constant phase element) is the capacitance of double layer in the interface between electrode and electrolyte. In the cell, the electrodes have charged electrons on surface and they are balanced with the oppositely charged ions in electrolyte. Θ is also represented by R_{ct} which is charge transfer resistance of Li^+ ions through electrolyte determined by reaction rate. Lastly, Z_w is called as Wargburg impedance which means the complex impedance coming from the diffusion of electroactive species in the cell [24].

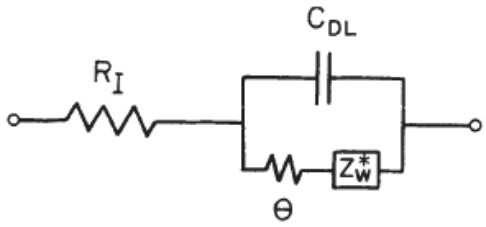

Figure 4.6: An instance for the equivalent circuit of AC impedance system [24].

5. RESULTS AND DISCUSSIONS

5.1 Preparation of Powders by Solution Precipitation

During the preparation of powders, raw materials are weighted on analytical balances and dissolved in ethylene glycol. In this process, it is observed that ammonium dihydrogen phosphate is dissolved in ethylene glycol very slowly at room temperatures. To make dissolving of phosphate rate faster, water is added to ethylene glycol solution resulting very fast dissolving. But some impurities occurred in the further characterization of samples by XRD due to the oxidization of the materials in the solution. For this reason, ethylene glycol was used as the only solvent to dissolve raw materials.

After the solution of powders achieved, they are put into centrifuge for precipitation by the help of acetone. Solutions are centrifuged in 4000 rpm by 30-40 minutes. In this step it was seen that the faster centrifuge speed and longer time resulting better precipitation of the powders. For better results, centrifuge was repeated several times. Later the powders are dried in air furnace as-produced powders are obtained. These powders are analyzed in TGA in order to determine optimum calcination temperature for $LiFePO_4$.

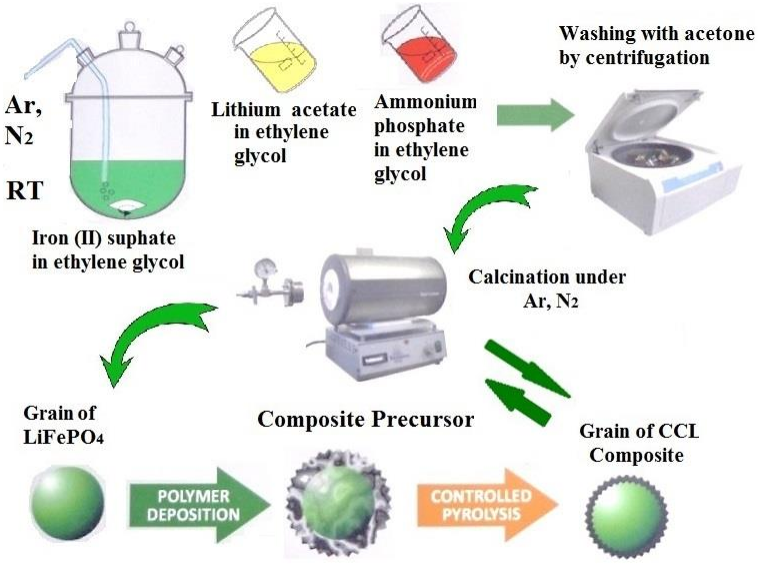

Figure 5.1: Syhmetically representation of powder production.

From the TGA results it is decided that the optimum calcination temperature will be around 600 °C. For this reason powders are calcinated at 600 °C for 12 hours in tube furnace with 5 °C/min heating rate on golden crucibles. Meanwhile, another pot has active carbon and copper foil in order to prevent the oxidization of powders and impurities under inert gas atmosphere (Ar). After the calcination powders are characterized by XRD in order to see the crystal structure and particle sizes. From the XRD results, the samples which have best pure structure and phases without any impurities are covered with CCL. Finally covered CCL/$LiFePO_4$ nanocomposite powders are characterized by XRD for structural, phase properties and particle sizes, TGA for measuring the carbon amount, BET for surface properties, lastly analyzed for conductivity and electrochemical measurements.

5.2 Preparation of Powders by Microemulsion

Achieving stable nanoparticles and improvement the efficiency of the particles with reducing sizes as desired by controllable parameters are some of the advantages of microemulsions. For this reason surfact and cosurfactant materials are used to stabilize the system. In this study, in order to produce anequous microemulsion, the components (ethylene glycol, decanol, toluene, SDS) are mixed to each other with different weight ratios. Solubilization ratio of surfactant material (SDS) and other parameters affecting the properties of homogenous solution are investigated by adding the materials seperatedly. In accordance to the reference article, ethylene glycol can be dissolved in decanol with % 33 wt. ratio, SDS dissolves in ethylene glycol till % 5 wt. Also it is claimed that additional toluene helps with dissolving of SDS in ethylene glycol however over a critical point of toluene/decanol ratio, solubility of ethylene glycol in system decreases [147]. All of the results are observed during the preparation of the microemulsions and the key points are noted such as adding SDS and decanol results more homogenous and stable solutions.

According to the experimental results of producing a homogenous nonaqueous microemulsion with different surfactant and cosurfactant ratios are mixed from 1-10 gr as shown in Table 5.1. Finally, homogenous stable microemulsion solution achieved and used to produce nanoparticle powders.

Table 5.1: Microemulsion experiments by different weight ratios of components.

Material	**Amount (min-max) gr**		**Stability**
Ethylene Glycole	1	10	No
Cyclohexane	5	8	No
Triton x-100/n-hexanol (2:1)	2	8	No
Main components			
Toluene	1	10	No
SDS	1	10	No
Ethylene Glycole	1	10	No
Decanol	1	10	No
Optimum homogenous solution			
Toluene	5		**YES**
SDS	0,5		
Ethylene Glycole	5		
Decanol	8		

After achieving the microemulsion solution with components, the precursor powders (lithium acetate dihydrat, ammonium dihydrogen phosphate and iron (II) sulfate heptahydrate) are prepared to dissolve in microemulsions seperatedly. For preparing 1 gr of $LiFePO_4$ powders by microemulsion, ammonium dihydrogen phosphate is dissolved in 50 ml ethylene glycol, lithium acetate dihydrat and iron(II) sulfate heptahydrate are dissolved 10 ml ethylene glycole (as other components are added by the ratios of calculation of optimum microemulsion solution). However, it was impossible to achieve homogenous microemulsion with precursor powders which can be attributed to changing ions in the solution. It is predicted that the powder ratio of precursors in microemulsions are relatively high to be dissolved. As a result, powder ratios are decreased (from % 15 to % 1) and tried to be dissolved again. Even then, it is observed particulates and phase separation in the solution that the surfactant/cosurfactant ratios are not optimum to produce microemulsion. The ratios of components changed and tried to achieve microemulsion with precursor powders again and finally homogenous solutions are achieved and mixed under inert gas (Ar) atmosphere in reactor as the same procedure mentioned before followed with solution precipitation process.

5.3 TGA Results

In order to determine the calcination temperature, precursor $LiFePO_4$ powders are heated between 25-1000 °C with 10 °C/min rate. During the heat treatment QMS and SDTA of the samples are also measured for the comparison of the weight loss from sample. The TGA and QMS graphs are collected from the data and plot as shown in Figure 5.2 and Figure 5.3.

It can be seen the TGA results of weight loss during heating of precursor $LiFePO_4$ Figure 5.2 which illustrates the decomposition temperature is close to the phase transformation of $LiFePO_4$. All organic substances show a weight loss around a temperature range due to the decomposition and pyrolysis of material till 450-500 °C. In the same time of TGA measurement, quadruple mass spectrometer (QMS) results are also collected as representing the as OH (17), H_2O (18) and CO_2 (44) respectively. Although there is a small amount of weight loss till 600 °C, it is estimated for the pyrolysis of remaining organic materials.

In the TGA results of precursor powders the weight loss around % 30 from room temperature till 170-180 °C (endothermic peak) is related to the release of physically adsorbed moisture or water molecules. There is another endothermic peak from 170-380 °C related to the weight loss around % 20-25 from decomposition and pyrolysis of acetates and other organic compounds in the system. Around 380-420 °C the exothermic peak can be attributed to the formation of Fe^{+3} from the oxidation of Fe^{+2} and resulting Fe_2O_3 during the heat treatment**.** In the temperature range of 450-480 °C, the exothermic peak represents the crystallization of $LiFePO_4$. These results are also confirmed by the QMS results. Decomposition of all organic materials is completed around 600 °C and there was no weight loss after this temperature. As a result, it is reasonable to set calcination temperature and synthesize powders around 600-750 °C.

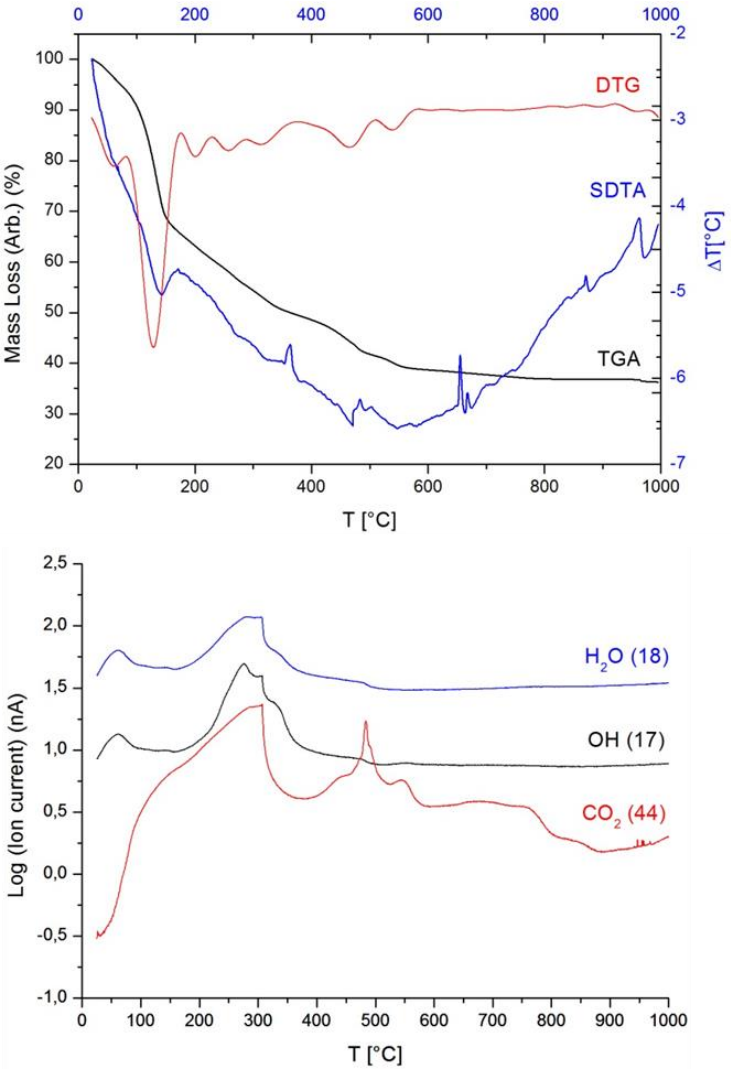

Figure 5.2: TGA and QMS results of precursor $LiFePO_4$ powders.

For the nanocomposites of CCL/$LiFePO_4$ the TGA and QMS results (for 15 CCL/$LiFePO_4$) are shown in Figure 5.3. The mass loss between room temperature and 250 °C is attributed to the evaporation of the water molecules and decomposition of organic materials. Between 300 °C till 500 °C the endothermic weight loss is resulted from the pyrolysis of pyromellitic acid (PMA) and poly-N-vinylformamide (PNVF) and formation of conductive carbon layers as confirmed from the QMS results determined as CO_2 species. Around 500 °C the exhothermic peak can be resulted from the combustion of carbon or oxidation of Fe (II) in the structure of $LiFePO_4$ as the reaction:

$$LiFePO_4 + (1/4)\ O_2 \rightarrow (1/3)\ Li_3Fe_2(PO_4)_3 + (1/6)\ Fe_2O_3 \qquad \textbf{(5.1)}$$

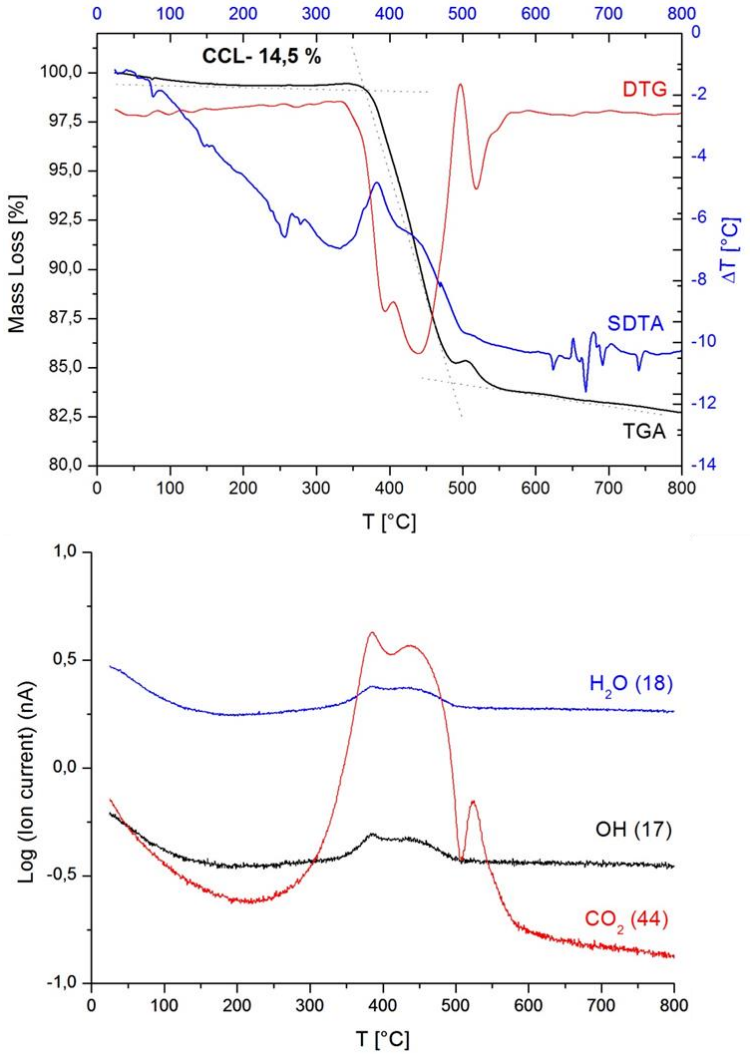

Figure 5.3: TGA and QMS results of 15 CCL/$LiFePO_4$ powders

Carbon amounts are calculated from the TGA graphs and shown in Table 5.2 which proved that the CCL amounts of the nanocomposites are homogenously covered as predicted ratios during covering process. The rest of the graphs of CCL/$LiFePO_4$ nanocomposites are shown in the appendix.

Table 5.2: CCL amounts of powders as predicted and calculated from TGA results.

Sample	Predicted CCL (%)	Calculated CCL (%)
5 CCL/$LiFePO_4$	5	2.5
10 CCL/$LiFePO_4$	10	7.4
15 CCL/$LiFePO_4$	15	14.5
20 CCL/$LiFePO_4$	20	14.7

5.4 XRD Results

Precursor $LiFePO_4$ powders are calcined between 600-700 °C. Many experiments are done to find the homogenous and best crystalline structure without any impurities. Also trying with other temperatures, it was detected that the samples produced by nonaquaeous solution precipitation that is calcined at 600 °C for 12 hours shows the best crystalline structure and smaller particle sizes in the range of 30-40 nm.

Also the powders are produced by microemulsion technique and calcined at the same temperature at 600 °C for 12 hours. However, there have been many impurities observed in XRD results. For this reason, microemulsion is decided to be a time and money consuming technique for producing homogenous and pure $LiFePO_4$ nanoparticles. Further researches and experiments should be done to achieve better results of preparation of fine $LiFePO_4$ particles with microemulsion technique.

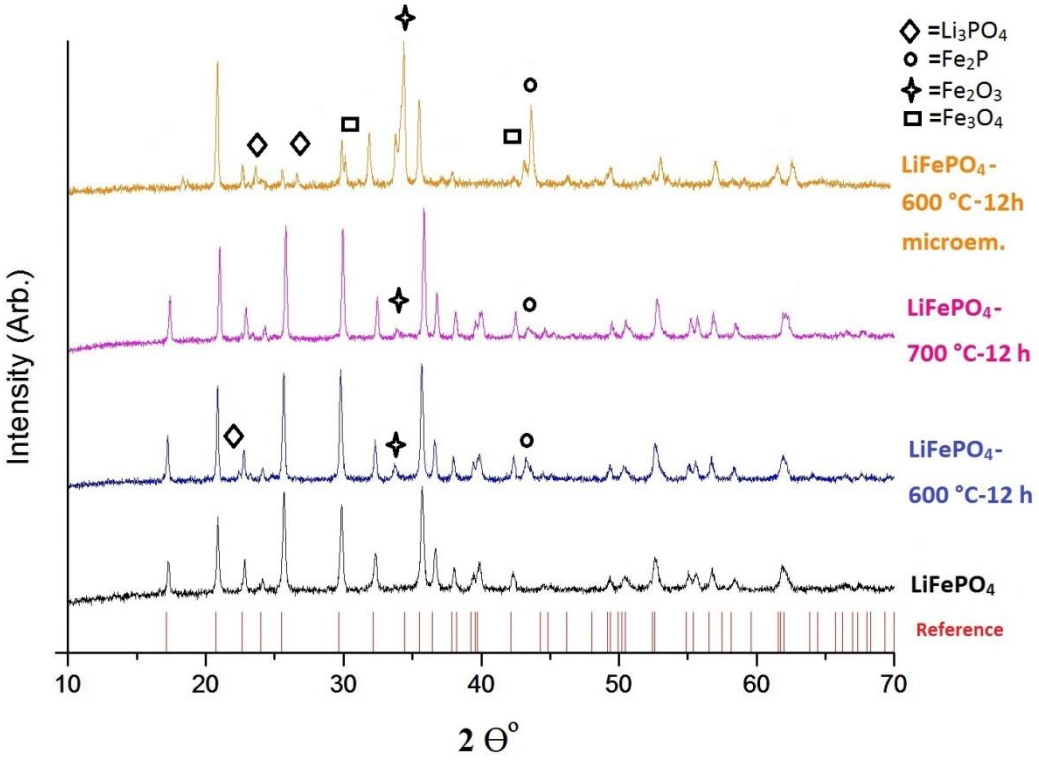

Figure 5.4: XRD results of the $LiFePO_4$ powders synthesized in different temperatures.

However, other samples calcined at 600 °C and 700 °C have impurities detected due to difference source of Fe (II) powders possibly had oxidized Fe (II) particles. The powder produced with water addition has also impurities shown in XRD results, which is calcined at 600 °C for 12 hours.

As it can be seen in the XRD results, most of the impurities are caused by the degradation of Fe (II) to Fe (III) particles and formation Fe_2O_3, Fe_3O_4 and Li_3PO_4 phases according to Seung-Ah et al [152]. These impurities have lower conductivities which result lower rate capable batteries, low conductivities and shorter cycle life with lower capacities and also they cause the degradation of the cathode material during the cycling.

The impurities in $LiFePO_4$ powders that are made by water assisted solutions (calcined at 600 °C and 700 °C) which are around $2\Theta=44°$ are attributed to Fe_2P phases which has a good effect of improving conductivity of $LiFePO_4$/C materials due to its high electronic conductivity (1.5 S/cm). This impurity gives the material better properties such as high reversible capacity and better rate capability [153]. The best powders are made by anhydrous solution precipitation that is calcined at 600 °C for 12 hours, and all further experiments will be done on these $LiFePO_4$ samples.

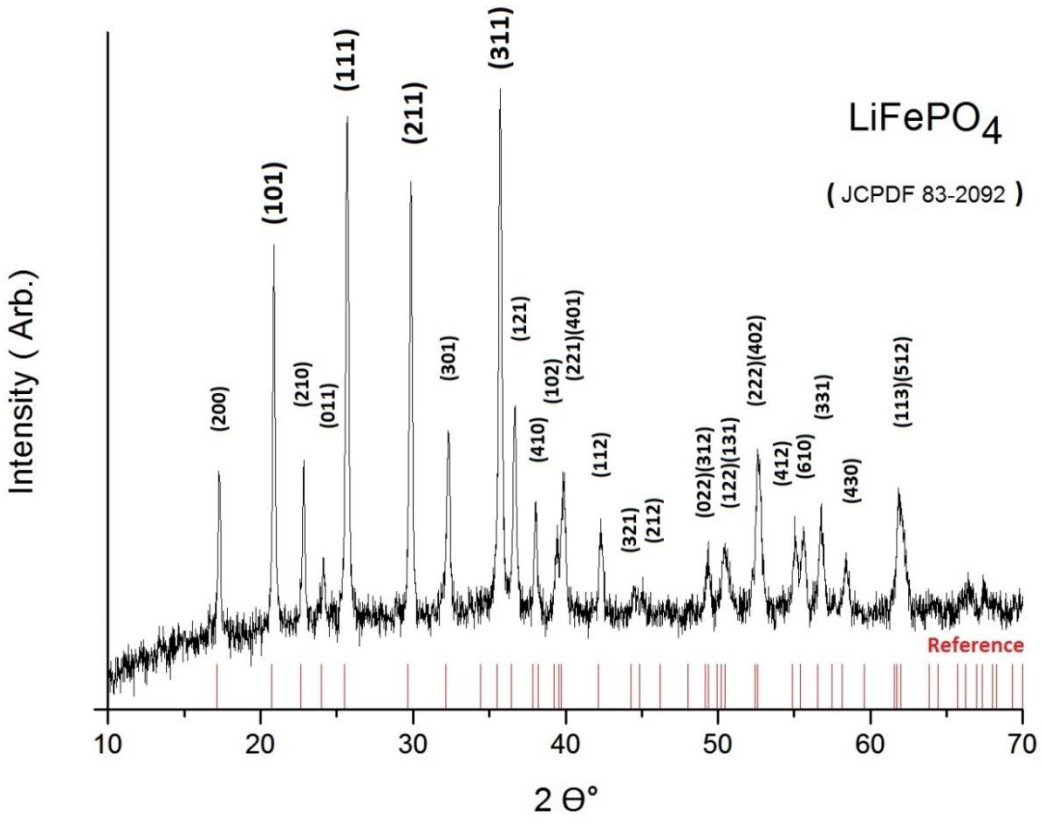

Figure 5.5: XRD result of $LiFePO_4$ powders.

As shown in Figure 5.5 all the diffraction peaks obtained from $LiFePO_4$ powders that are obtained from anhydrous solution precipitation, can be attributed as the orthorhombic olivine phase with space group *Pnmb*, referred to the standard pattern of JCPDS-83-2092 respectively. The XRD results indicate that the as-prepared (dissolved in ethylene glycol only) $LiFePO_4$ powders at 600 °C for 12 hours are well-crystallized with olivine-structure and there are no detectable impurity phases.

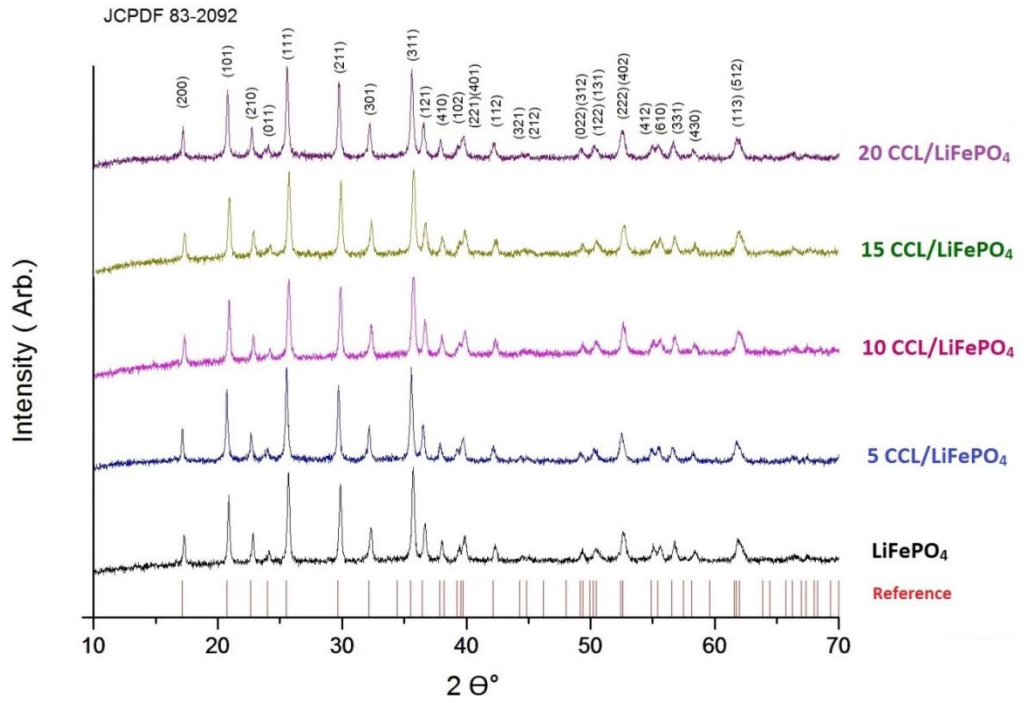

Figure 5.6: Crystal structure and phases of CCL/$LiFePO_4$ nanocomposites.

In order to compare the XRD result of nanocomposites with pure $LiFePO_4$ powders, all of the plots are shown in Figure 5.6. In this figure, it can be easily seen that with the additional CCL covering there is not any differences in crystal structure as predicted and all peaks are represent the standard pattern of JCPDS-83-2092.

Table 5.3: Crystallite sizes of the pure $LiFePO_4$ and CCL/$LiFePO_4$ nanocomposites.

Sample	Crystal sizes (nm)
$LiFePO_4$	35.5
5CCL/ $LiFePO_4$	36.3
10 CCL/ $LiFePO_4$	31.4
15 CCL/ $LiFePO_4$	30.2
20 CCL/ $LiFePO_4$	34.5

It can be seen from Table 5.3 as all the CCL/$LiFePO_4$ nanocomposite powders are produced in the sizes range of 30-40 nm. For the Li-ion batteries, small particle production is very important to improve the conductivity of cathode materials. When the particle sizes are smaller, Li^+ ions have to diffuse shorter distances between boundary and the center of crystalline grains resulting better conductivites [154]. Therefore nanosized CCL/$LiFePO_4$ composites promise better conductivities.

5.5 Raman Spectroscopy

Raman spectroscopy is another technique to investigate the chemical and physical structures from characteristic patterns such as XRD. When the light beam (made by photons) interacts with material, it can pass through directly, scattered or absorbed. If the energy of photons are between the valance band and conduction band, that can be absorbed by the molecule. This interaction is measured by the energy loss of radiation from light beam. If the light interacts and scatter from material, it can be observed by collecting the light beam at an angle (24). Radiation is characterized from the interaction with material and shown in energy in terms of wavenumber (ω).

$LiFePO_4$ powders are analyzed by Raman Spectroscopy in order to see the interaction with light beam. The Raman spectra of $LiFePO_4$ powders are shown in Figure 5.7. In the spectrum, it can be observed small band around 430, 950 cm^{-1} and two broad lines at 1350, 1585 cm^{-1} are corresponding peaks from orthorhombic symmetry of $LiFePO_4$ [163].

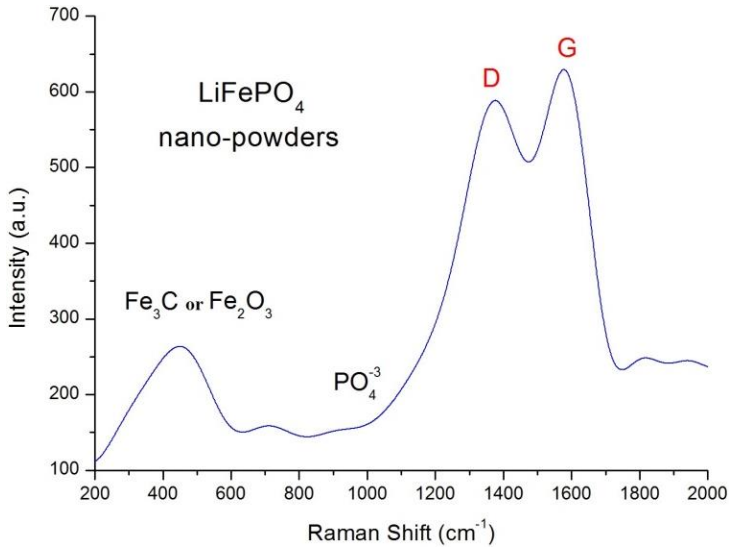

Figure 5.7: Raman spectra of $LiFePO_4$ powders.

In the Raman spectra, the small band at 950 cm^{-1} is related to symmetric PO_4 stretch vibration in the olivine $LiFePO_4$. The broad line in 1350 cm^{-1} is obtained from the structure of disorder allowed zone edge modes of graphite which is called D (disordered) line, the broad line in 1585 cm^{-1} corresponds from optically allowed E_{2g} zone center mode of crystalline graphite which is called G (graphite) line of carbon. The ratio of D/G intensities shows the bonding between disordered/graphite. The high D/G ratio means low graphite but high disordered carbon amount, that results low electronic conductivity. For this reason, it is important to achieve lower D/G ratios to improve conductivity and better electrode performances [164].

Although, it is not common to observe D and G bonds in pristine $LiFePO_4$ powders, it can be attributed to residual carbon from the decomposition of acetates as will be seen in EDAX analysis. However, the ratio of D/G is lower than 1, which means that material contains crystal graphite more than disordered disordered carbon. As a result, $LiFePO_4$ powders are expected to show better conductivity results.

Additionally, some peaks are observed in Raman spectrum at low wave numbers around 450 cm^{-1} can be referred to Fe_3C particles comparing with the reports before. This material is probably produced during the thermal decomposition of products, and the diffusion of carbon through nanoparticles. Due to its metallic structure, the presence of Fe_3C particles may influence and improve electronic conductivity [165].

Furthermore, exposing Raman laser beam onto the surface of $LiFePO_4$ olivine cathode materials leading decomposition of structure according to equation [166]:

$$12LiFePO_4 + 3O_2 \rightarrow 4Li_3Fe_2(PO_4)_3 + 2Fe_2O_3 \qquad \textbf{(5.2)}$$

Additional of decomposition of $LiFePO_4$ powders, also carbon gasification occurs in the structure and leading changes in G and D bands of carbon. The more laser power applied on material, the more decomposition continues even without any oxygen atmosphere. The oxygen will be relased from the decomposition of PO_4 molecules in structure of $LiFePO_4$ [166].

As a result, the power of the Raman laser beam may resulted the decomposition of our $LiFePO_4$ powders and lead to the D and G bands which is referred to carbon, also Fe_3C/Fe_2O_3 particles are occured which are not seen in the XRD results.

5.6 SEM Results

Morphological and surface properties of $LiFePO_4$ powders are observed by SEM. In Figure 5.8 and 5.9, it can be seen that as prepared particles are almost similar sized around 50-100 nm individually, however after calcination particles are agglomerated to each other and resulted irregular shaped larger particles.

The particle sizes are higher than calculated from XRD results due to agglomerations. However, size differences causes to porous network surface resulting high surface area.

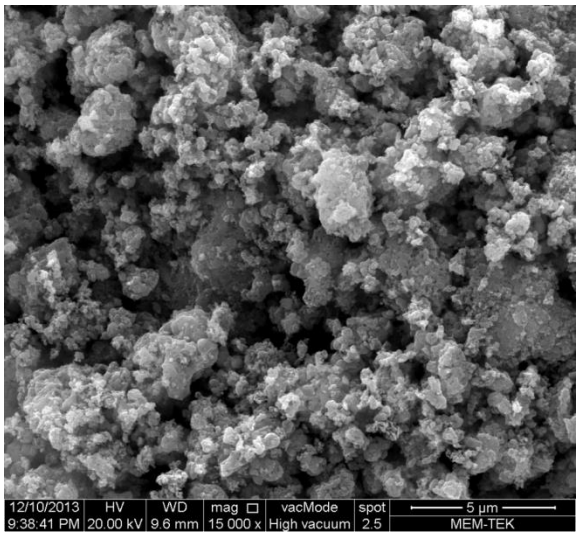

Figure 5.8: SEM image of $LiFePO_4$ powders (15 kX).

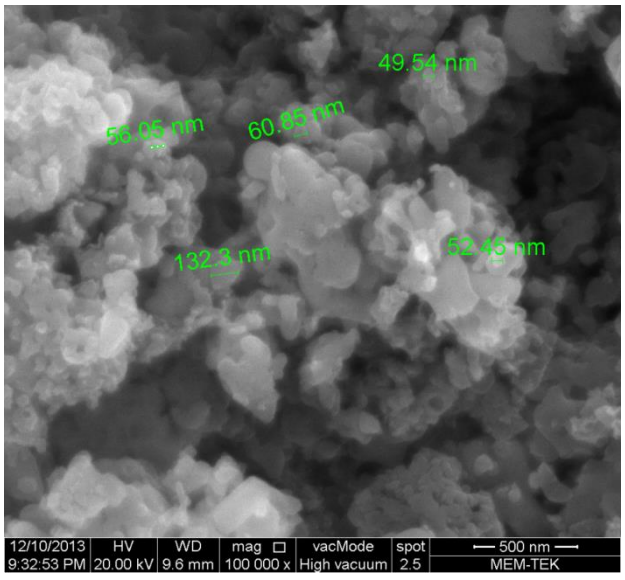

Figure 5.9: SEM image of $LiFePO_4$ powders (100 kX).

The smaller and homogenous particle sizes of $LiFePO_4$ are very important to decrease lithium-ion diffusion distance and improve electrochemical behaviour. Due to its surface properties, $LiFePO_4$ powders are expected to have good cycle performances.

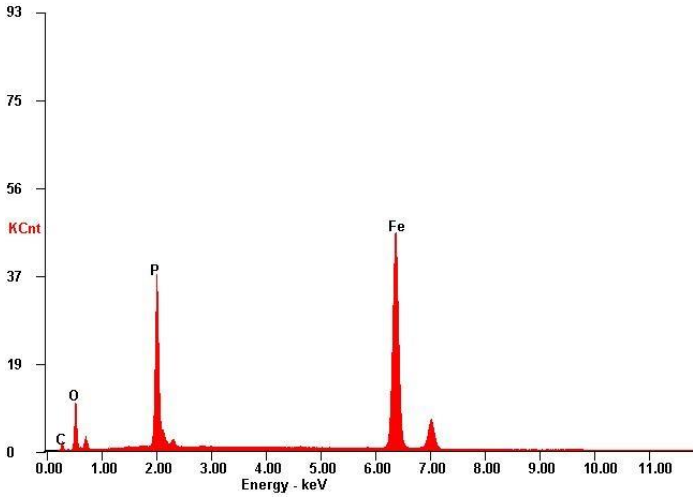

Figure 5.10: EDAX analysis of $LiFePO_4$ powders.

Elemental analysis of $LiFePO_4$ powders are shown as Figure 5.10. However the device parameters are not able to show Li metal amount. We can see that our powders contain wt. % 9.42 C element which is a proof of some of residual particles. Although that is something looks like impurity, when we compare with Raman results we can see that the carbon particles are observed as the graphite form of the carbon. So it can be considered as the carbon coated $LiFePO_4$ powders naturally, that many researchers trying to do. As a consequent, powders will be used as the form with C residuals and expected to have higher conductive and better cycle properties.

Table 5.4: Elemental analysis of elements from powders.

Element	% Wt.	% At.
C	09.42	22.52
O	16.80	30.14
P	22.79	21.12
Fe	50.99	26.21

5.7 BET Results

In order to measure specific surface area, average pore sizes of the $LiFePO_4$ and CCL/$LiFePO_4$ samples are analyzed under N_2 adsorption/desorption with BET (Brunauer-Emmett-Teller) technique. According to these results, isotherms of samples are presented as Figure 5.11 and Figure 5.12 which corresponds to IV type isotherm with a H3 hysteresis loop. That loops indicate a porous surface characteristics referring plate shaped particles having slit like pores [155]. Pore sizes and distributions are calculated by Barret–Joyner–Halenda (BJH) model.

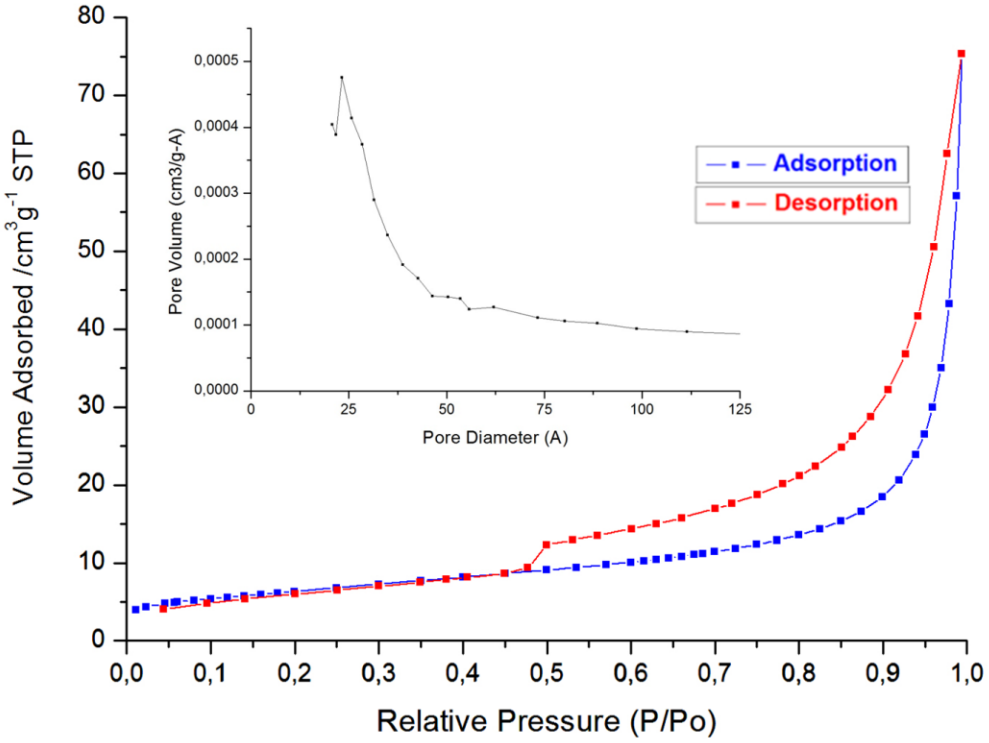

Figure 5.11: BET graph of precursor $LiFePO_4$ powders after calcination.

The specific surface area of the $LiFePO_4$ sample is 22.2 m^2/g, and the average pore diameter is 21.5 nm and pore volume is 0.11 cm^3/g respectively. Moreover, it can be seen from the results that the pore sizes range from 7 to 20 nm, indicating the mesoporosity of $LiFePO_4$ particles according to IUPAC [156].

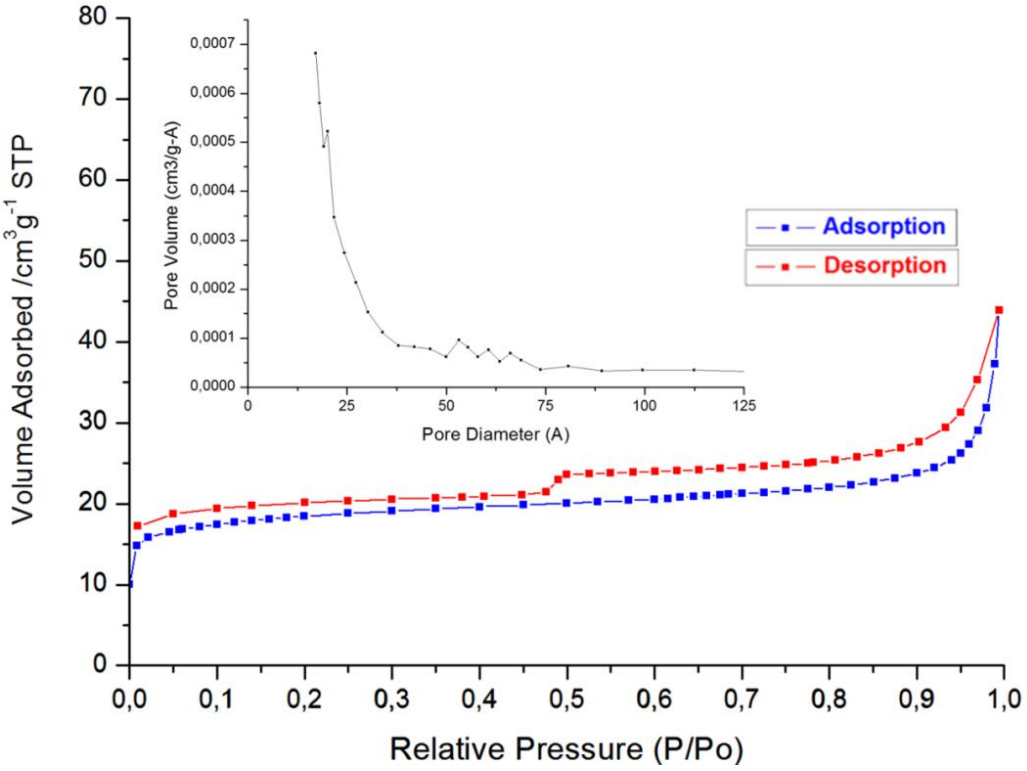

Figure 5.12: BET graph of 15 CCL/ $LiFePO_4$ powders after pyrolysis.

However, average particle sizes of $LiFePO_4$ powders are calculated around 75.0 nm that are larger than the ones from XRD results (30-40 nm) which can be attributed to agglomeration of particles as it can be seen from SEM results.

Table 5.5: Surface areas and pore diameters of $LiFePO_4$ samples.

Sample	Surface Area (m^2/g)	Volume of pores (cm^3/g)	Average pore diameter (Å)	Average Particle Sizes (nm)
$LiFePO_4$	22.2	0.1165	215.1	75.0
5 CCL/$LiFePO_4$	27.9	0.1007	151.5	
10 CCL/$LiFePO_4$	36.6	0.0720	77.0	
15 CCL/$LiFePO_4$	58.2	0.0679	71.6	
20 CCL/$LiFePO_4$	59.2	0.0785	100.3	

The specific surface areas are increasing with the CCL amount, as it can be seen from Table 5.5. Sample 20 CCL/$LiFePO_4$ exhibits the highest specific surface area of 59.2 m^2/g which is nearly 3 times greater than bare $LiFePO_4$. This can be mainly attributed the small particle sizes and porous network structure on surface which can

provide shorter distance between the boundary and center of crystalline grains for Li^+ diffusion. These porous surfaces also have the advantages of reduced resistance of Li^+ insertion/extraction due to multi dimension channels resulting better electrochemical properties during the cycle [157].

5.8 Conductivity Results

Electrical conductivities of the nanocomposite CCL/$LiFePO_4$ and CB/$LiFePO_4$ samples are measured between (-20 °C) and (+40 °C) and plots are shown as Figure 5.13 and Figure 5.14. The conductivities of CCL/$LiFePO_4$ composites are much higher than bare $LiFePO_4$ (10^{-9} S/cm) [158] and getting higher with increasing CCL amount.

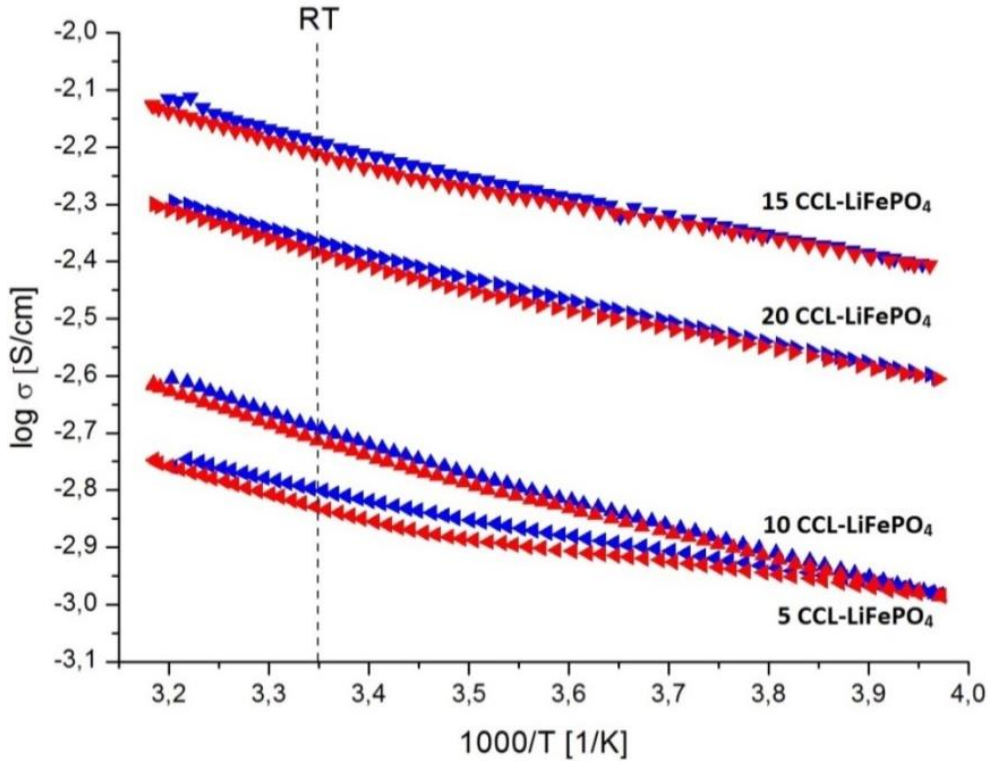

Figure 5.13: Conductivity plots of CCL/$LiFePO_4$ powders.

It can be seen from the plots that 20 CCL/$LiFePO_4$ has lower conductivity than 15 CCL/$LiFePO_4$. Once the particle surfaces covered with optimum CCL amount homogenously and reached the limit, they are not capable to accept CCL anymore. Excess amount of CCLs are possibly agglomerate on the surface, making the cover layers thicker and less porous surface.

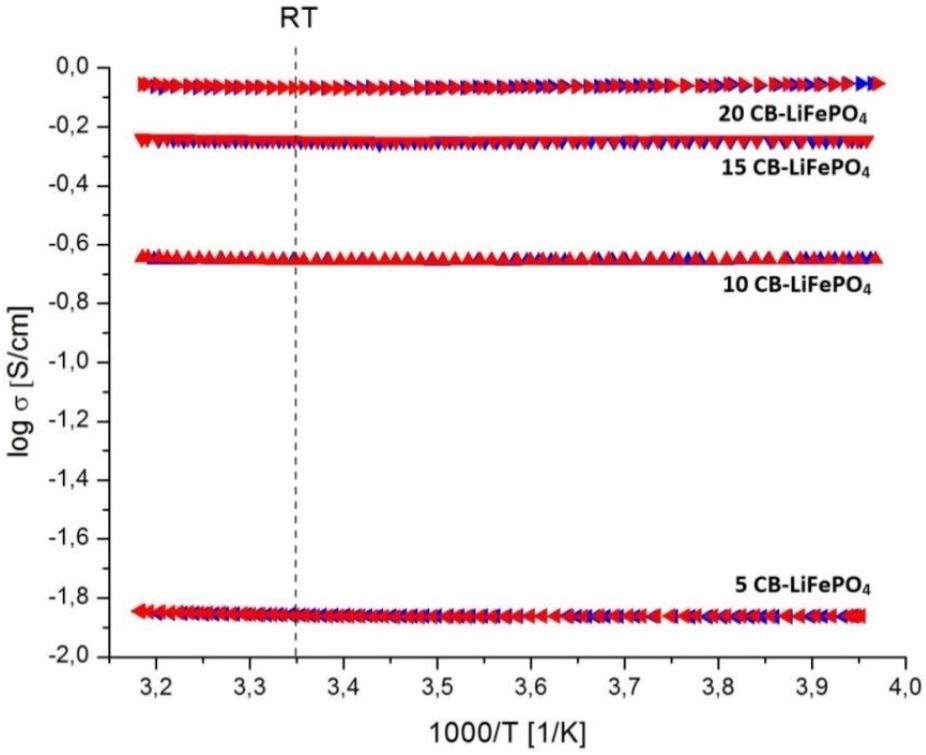

Figure 5.14: Conductivity plots of CB/$LiFePO_4$ powders.

The pathway for the transportation from boundary to center of crystals becomes longer which resulting lower conductivity results [154].

Table 5.6: Conductivity results of CCL/$LiFePO_4$ and CB/$LiFePO_4$ samples.

Sample	**Conductivity (+ 25 °C) σ (S/cm)**
5 CB/$LiFePO_4$	$1.38*10^{-2}$
10 CB/$LiFePO_4$	$2.22*10^{-1}$
15 CB/$LiFePO_4$	$5.64*10^{-1}$
20 CB/$LiFePO_4$	$8.57*10^{-1}$
5 CCL/$LiFePO_4$	$1.58*10^{-3}$
10 CCL/$LiFePO_4$	$2.02*10^{-3}$
15 CCL/$LiFePO_4$	$6.40*10^{-3}$
20 CCL/$LiFePO_4$	$4.29*10^{-3}$

From the conductivity results from Table 5.6, high electrical conductivities of CCL/$LiFePO_4$ are achieved in room temperature comparing with bare $LiFePO_4$. When the datas are compared, CB/$LiFePO_4$ powders show much higher conductivity results than CCL/$LiFePO_4$. Nano sized particles and highly porous surface areas of CCL/$LiFePO_4$ are promising electrochemical properties for Li-ion cathode materials.

In order to calculate the activation energies (E_a) of the samples, Arrhenius equation is used from the conductivity versus temperature (ln σ-1000/T) graphs as shown in Figure 5.15 and Figure 5.16. From the the slope of these graphs, it is easy to determie the activation energy. For this reason, data from the cooling of samples during conductivity measurements are used for calculation and activation energies for samples are shown in Table 5.7.

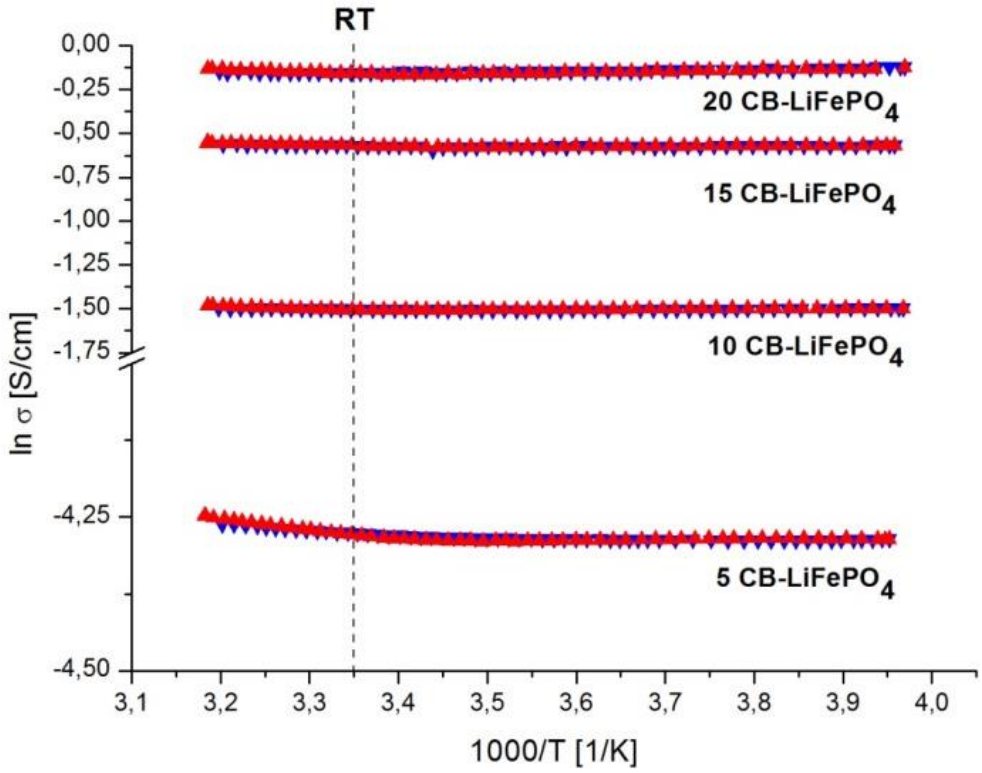

Figure 5.15: Conductivity plots (ln σ-1000/T) of CB/$LiFePO_4$ samples.

The activation energy of conductivity is directly affected by temperature difference which is the minimum potential energy barrier to achieve mobility for ions [159].

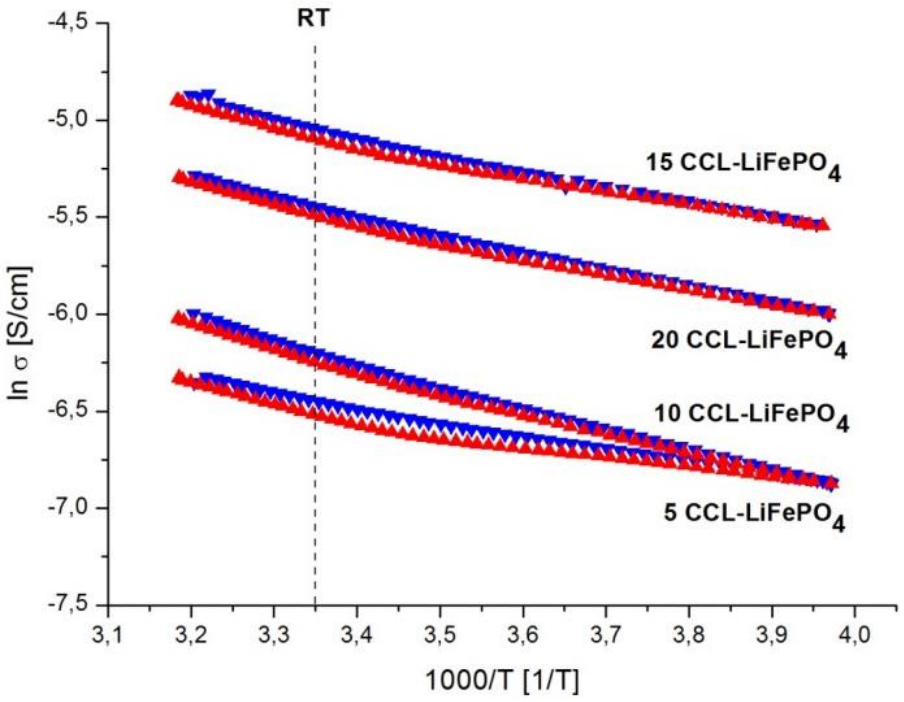

Figure 5.16: Conductivity plots (ln σ-1000/T) of CCL/$LiFePO_4$ samples.

As it can be seen from the plots, the conductivity of materials increase with temperature referred as Arrhenius law. The high increasing of conductivity between 300-310 °K is related to heat absorption of samples hence electrons move from valance band to the conduction band resulting higher conductivities comparing to lower temperatures [160].

Table 5.7: Activation energies of CB/$LiFePO_4$ and CCL/$LiFePO_4$ samples.

Sample	**Activation Energy E_a (eV)**
5 CB/$LiFePO_4$	$8.53*10^{-3}$
10 CB/$LiFePO_4$	$3.70*10^{-3}$
15 CB/$LiFePO_4$	$5.34*10^{-3}$
20 CB/$LiFePO_4$	$4.32*10^{-4}$
5 CCL/$LiFePO_4$	$7.37*10^{-2}$
10 CCL/$LiFePO_4$	$1.17*10^{-1}$
15 CCL/$LiFePO_4$	$9.96*10^{-2}$
20 CCL/$LiFePO_4$	$9.49*10^{-2}$

From the results which are shown in Table 5.7, the activation energies for CB/$LiFePO_4$ samples are between $4.32*10^{-4}$ eV and $8.53*10^{-3}$ eV for the CCL/$LiFePO_4$ samples it ranges between $9.96*10^{-2}$ eV and $1.17*10^{-1}$ eV. These results show us that our CCL/$LiFePO_4$ nanocomposite materials have smaller activation energies which is easier for electron mobility resulting better conductivities comparing to the pure $LiFePO_4$ that having 10^{-9} S/cm conductivity at room temperature with 0.65 eV activation energy [161, 162].

5.9 Electrochemical Results

5.9.1 Cyclic Voltammogram

The assembled batteries are cycled galvanostatically using a potentiostat (Parstat) between a potential range of 2.5 V and 4.5 V (vs. Li/Li^+) for cyclic voltammogram analysis at a scan rate of 1 mV/s and 5 mV/s. Within these tests, it is observed the rate capability and cycle performances of the cells.

The cyclic voltammogram of CB/$LiFePO_4$ is shown as the Figure 5.17 and Figure 5.18 are obtained from the mixture of active material ($LiFePO_4$), carbon additive (acetylene black) and binder (PVDF) in the ratio of % wt. 75:15:10 and 80:10:10 respectively.

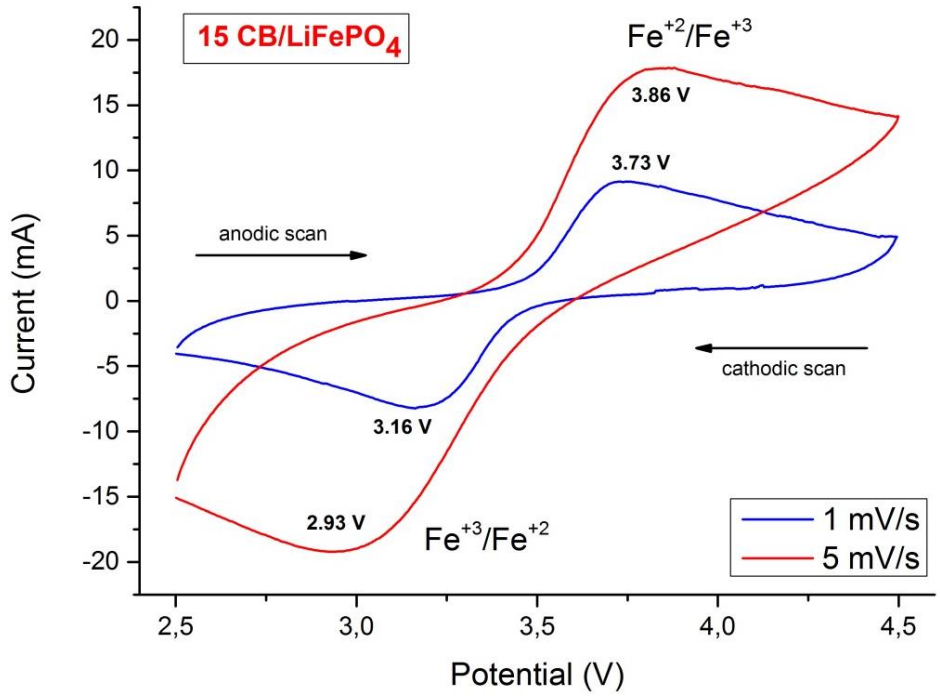

Figure 5.17: CV polts of CB/$LiFePO_4$ (% wt. 15:75) powders (vs Li^+/Li).

In the cyclic voltammetry graphs for both samples (15 CB/$LiFePO_4$ and 10 CB/$LiFePO_4$) exhibit one anodic (charge) and one cathodic (discharge) peak. These peaks are attributed to the redox reactions of Fe^{+2}/Fe^{+3} during the lithium intercalation/deinterecalation. The anodic peak around 3.7 V is corresponded to oxidation of Fe^{+2} to Fe^{+3} and extraction (removal) of Li^+ ions from crystal structure of $LiFePO_4$ cathode material during charging. Reversibly, the cathodic peak around 3.0 V is attributed from the reduction of Fe^{+3} to Fe^{+2} and insertion of Li^+ ions to the structure of $LiFePO_4$ cathode during the discharge.

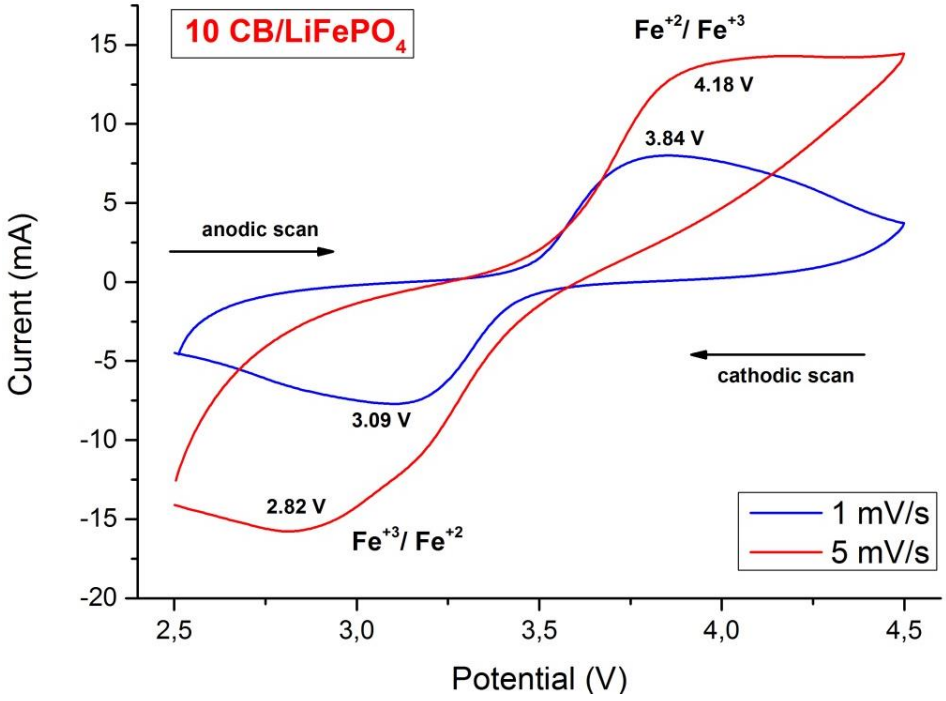

Figure 5.18: CV polts of CB/$LiFePO_4$ (% wt. 10:80) powders (vs Li^+/Li).

The intensity and shape of the peaks in CV measurements change by the type and amount of the carbon additives. Carbon coated $LiFePO_4$ cathode electrodes show higher peaks than bare $LiFePO_4$ as mentioned in published articles lately [169, 170]. Carbon additive effect is also proved in CV plots of 15 CB/ $LiFePO_4$ and 10 CB/ $LiFePO_4$ powders.

The separation between redox peaks (ΔV) of 15 CB/ $LiFePO_4$ is 0.57 V for the 1 mV/s scan rate and increased to 0.93 V for the 5 mV/s scan rate. The big separation between redox reaction peaks indicates that the electrochemical behavior is controlled by the diffusion step.

The intensities and separation between the anodic and cathodic peaks are increased with the increasing scan rate as also mentinoed in literature before [170].

The peak intensities are shown in Table 5.8. The anodic peak intensity of 15 CB/ $LiFePO_4$ is observed as 9.151 mA for 1 mV/s scan rate, however the anodic peak intensity for the same sample is increased to 17.855 mA for the 5 mV/s scan rate. Also the anodic peak for 15 CB/ $LiFePO_4$ appears at 3.73 V for the 1 mV/s scan rate, but the same anodic peak is shifted to 3.86 V for the 5 mV/s scan rate.

Table 5.8: Redox peak intensities of 10CB/$LiFePO_4$ and 15CB/$LiFePO_4$.

	Anodic peak intensity (I_p)-mA		**Cathodic Peak intensity (I_p)-mA**	
Rate	1 mV/s	5 mV/s	1 mV/s	5 mV/s
10 CB/$LiFePO_4$	8.003	14.296	7.712	15.773
15 CB/$LiFePO_4$	9.151	17.855	8.221	19.208

Due to results, 15 CB/ $LiFePO_4$ shows higher peaks than 10 CB/$LiFePO_4$ that indicate Li^+ ions and electrons are contributed to oxidation/reduction reactions due to carbon additive. The CV plots are almost the same after 3 cycles which indicates that the kinetic reactions for both samples are very good reversible. As a conclusion, due to high conductivity depending on carbon additive, 15 CB/ $LiFePO_4$ exhibit better cyclability and higher than 10 CB/$LiFePO_4$ even at great scan rates (5 mV/s).

5.9.2 Electrochemical Impedance Spectroscopy

To understand the effect of different carbon additive intensively, electrochemical impedance spectroscopy (EIS) measurements are carried out with CR-2032 coin cells using potentiostat (Parstat 2263). During the analysis, AC voltage is applied to cells of frequency ranges between 10 mHz and 100 kHz at a scan rate of 5 mV at room temperature. All samples are cycled galvanostatically for five times before EIS measurements in order to be sure of electrode is permeated by electrolyte and have the stable SEI film formation. Measurements are done when the cells are fully lithiated (discharge) state and having 3.429 V for 15 CB/ $LiFePO_4$ and 3.436 V for 10 CB/ $LiFePO_4$ respectively.

The Nyquist plots of EIS measurements of both samples show a straight line at low frequency regions, a semi-circle in the middle frequency ranges and finally intercepts at high frequency ranges. In the high frequency, sometimes another semicircle occur due to the migration of Li^+ ions at electrode and electrolyte interface through solid electrolyte interphase (SEI) film formed during the first few charge/discharge cycles.

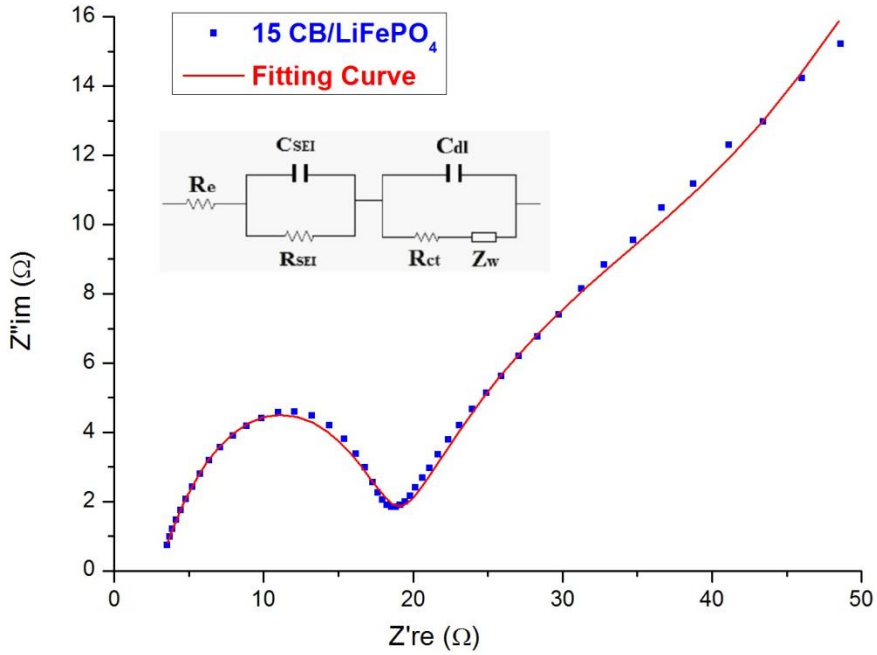

Figure 5.19: EIS analysis of CB/$LiFePO_4$ powders (15:75).

The electrochemical impedance analysis of CB/$LiFePO_4$ is shown as the Figure 5.19 and Figure 5.20 are obtained from the mixture of active material ($LiFePO_4$), carbon additive (acetylene black) and binder (PVDF) in the ratios of % wt. 75:15:10 and 80:10:10 respectively.

When compared the plots of samples for the cells assembled with %wt. 10 and 15 carbon black (CB) additives, it is observed that the semicircle of 15 CB/ $LiFePO_4$ is smaller than the one for 10 CB/ $LiFePO_4$. That shows the decrease of charge transfer resistance with increase of additive CB amount due to increased conductivity. Charge transfer resistances are calculated around 20 Ω and 30 Ω for the 15 CB/ $LiFePO_4$ and 10 CB/ $LiFePO_4$ respectively. The small semicircle (R_{ct}) represents the improved electrochemical performance of the electrode. Due to higher conducitivity of 15/ $LiFePO_4$ powders, it is expected to show high rate capability during cycle as also proved by CV results.

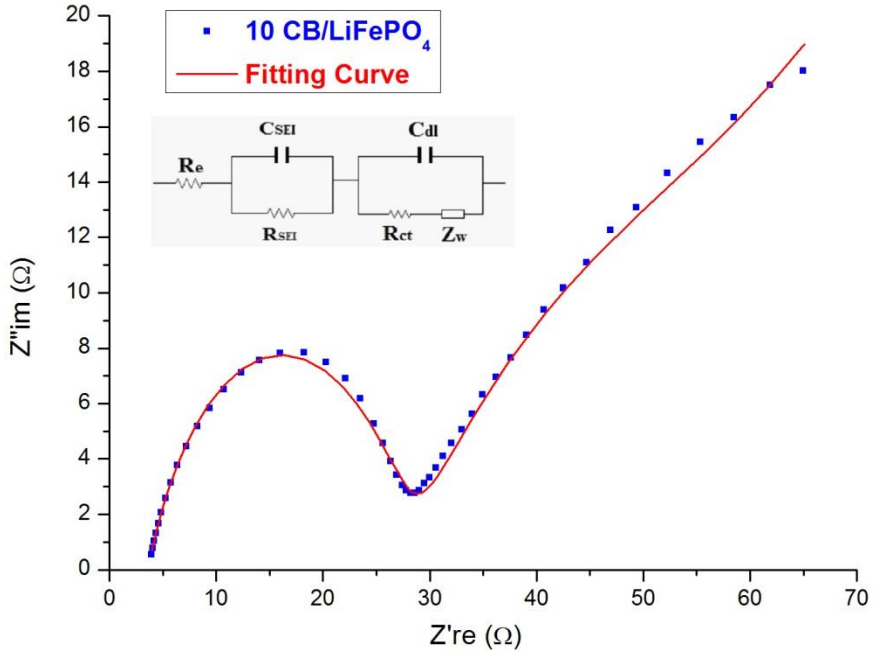

Figure 5.20: EIS analysis of CB/$LiFePO_4$ powders (10:80).

These EIS plots are fitted by the equivalent circuit model of Randles by the ZSimp Win software as shown in the insert of Figure 5.19 and Figure 5.20. In this circuit model, R_e is the ohmic resistance of electrolyte which corresponds the interception in the high frequency region. Also, R_{SEI} is the resistance and C_{SEI} is the capacitance of the solid electrolyte interphase layer formed on surface of electrode in the high frequency region. The semicircle at medium frequency is related to the charge transfer resistance (R_{ct}) of particles between electrode/electrolyte interface and double layer capacitance (C_{dl}) between electrode/electrolyte during the electrochemical reaction.The sloping line in the low frequency range is attributed to Li^+ ions diffusion in bulk electrode material ($LiFePO_4$) which is also called as Wargburg (Z_w) diffusion impedance.

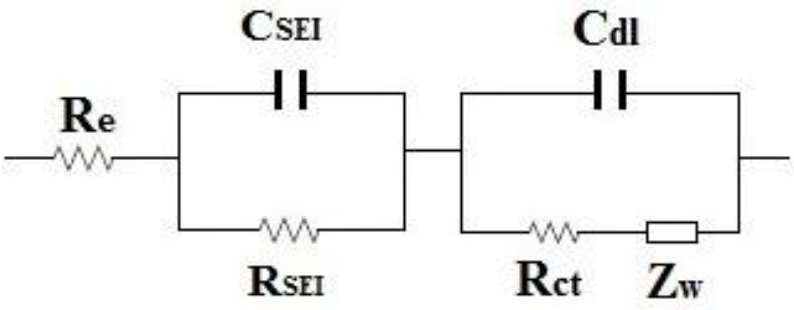

Figure 5.21: The equivalent circuit model of Randles.

The ohmic resistances (Re) of the samples are almost same in the high frequency range due to the same preparation route of adding conductive carbon black and using same type of electrolyte. Both samples show better EIS results than $LiFePO_4$ samples comparing literature reviews [168, 169], which is a proof of improved electrical conductivity on particle surface and higher Li^+ ion diffusion rate from electrolyte. These improved results are attributed the small particle sizes and high surface area of our $LiFePO_4$ powders, which also enhances the short diffusion path way for Li^+ ion diffusion. As a conclusion, small particle sized powders exhibit reduced resistances during the cycling and they are expected to achieve higher capacity, fast charge/discharge capability rates and better electrochemical properties.

Table 5.9: Equivalent circuit fitting datas for EIS plots of $LiFePO_4$.

	10 CB/$LiFePO_4$	**15 CB/$LiFePO_4$**
R_e (Ω/cm^2)	3.598	3.037
R_{SEI} (Ω/cm^2)	24.33	15.67
C_{SEI} (Ss^n/cm^2)x10^{-4}	1.023	1.699
n	0.71	0.65
R_{ct} (Ω/cm^2)	47.462	29.563
C_{DL} (Ss^n/cm^2)x10^{-4}	439	468
n	0.52	0.54
Z_W ($Ss^{1/2}/cm^2$)	0.1815	0.1882
Chi-square (x10^{-4})	1.68	1.32

The EIS datas are fitted by the equivalent circuit model of Randles as shown in Figure 5.21 and the values of resistance and capacitances of system is calculated and written as Table 5.9. During the fitting process, Chi-squared values are tried to be as low as possible between 10^{-4} and 10^{-5} ranges to have better fitting results. In the table we can also see the "n" values that is coming from the reaction rates on surface and influencing the capacity of SEI and double layer exponentionally. If the value of n=0 means the material is a very conductive material without any resistance, if n=1 means that the material is totally capacitive. As a result, with the increasing value of "n" between $0<n<1$ the resistance increases and the semicircle gets larger. It is proved that the value of "n" is smaller for 15 CB/$LiFePO_4$ due to its higher conductivity it showed a smaller semi-circle in EIS plots than 10 CB/$LiFePO_4$.

It can be seen that the charge transfer resistances are almost 30 Ω/cm^2 for 15 CB/$LiFePO_4$ and 50 Ω/cm^2 for 10 CB/$LiFePO_4$ which are much lower than the ones in literature [169].

The electrolyte and electrode resistance (R_e) is almost the same for both 15 CB/$LiFePO_4$ and 10 CB/$LiFePO_4$ samples around 3.0-3.5 Ω/cm^2. It is also observed that the charge transfer resistance (R_{ct}) and electrode/electrolyte interphase layer (SEI) resistance (R_{SEI}) are lower for 15 CB/$LiFePO_4$ due to its high conductivity. Total resistance of impedance from 10 CB/$LiFePO_4$ sample is 2 times larger than 15 CB/$LiFePO_4$ sample which is a proof of improving conductivity with CB additive results better conductivity that is expected to show better electrochemical performances.

The resistance for solid electrolyte interphase (R_{SEI}) is also smaller than charge transfer resistance (R_{ct}) for both samples indicate that electrochemical performance of the cells are mainly influenced by charge transfer resistance.

6. CONCLUSIONS AND RECOMMENDATIONS

Anhydrous solution precipitation technique is a convenient and simple technique to produce nano $LiFePO_4$ particles. Dissolving of raw powders without water based solvents (ethylene glycol) resulted homogenous and pure powders and no impurities can be detected. During the producing solutions and calcination of $LiFePO_4$ powders, system should be under controlled atmosphere (Ar) in order to prevent impurities due to oxidation and degradation of powders.

Microemulsion technique is challenging to understand and control the forces due to changing ion concentrations of raw powders in the solution. Also, larger particles and impurities occurred in the structure during analysis. For this reason, it is decided to be money and time consuming technique to produce homogenous nano particles. For using microemulsion technique of producing $LiFePO_4$ nano powders, many researches should be done and understand to controlling parameters for further applications.

From TGA results, it is seen that decomposition of all components are completed around 550-600 °C and no weight loss can be seen after 600 °C. For this reason, it is reasonable to set the optimum calcination temperature to 600 °C. All the TGA results and weight loss of materials are confirmed by QMS results. Also, it is proved that the CCL covered the surface of particles homogenously and as predicted amounts.

Homogenous and pure nano $LiFePO_4$ precursor powders are achieved by solution precipitation technique without any detectable impurities. All of the diffraction peaks are related to orthorhombic olivine crystal structure of $LiFePO_4$ as reference patterns JCPDS-83-2092. It is observed that from the XRD results of the powders produced using water based solutions and microemulsion, many impurities are caused by the oxidation and degradation of Fe (II) to Fe (III) particles and forming other phases such as Fe_2O_3, Fe_3O_4 and Li_3PO_4. These impurities lower the electronic conductivities of materials for batteries which can lead low rate capability and lower lifetime with low capacities. For the CCL covered particles, it is seen that additive

CCL layers don't have any influence on crystal structure or particle sizes as predicted. All of the particle sizes of the samples are calculated between 30-40 nm. Small particle sizes improve conductivity and cycling performances of cathode materials due to shorter diffuse distances for Li^+ ions. As a result, the powders are promising for better conductivity and electrochemical performances.

Precursor $LiFePO_4$ powders are covered with conductive carbon layers (CCL) with different amounts (% 5-20) succesfully. Carbon amounts are calculated from TGA plots and proved of the same ratios as predicted which shows that powders are covered homogenously. However, 20 CCL/$LiFePO_4$ doesn't show a cover as predicted, that can be related to the agglomeration of excess CCLs over the optimum limit.

It is seen from EDAX results that $LiFePO_4$ powders contain almost % wt. 10 C due to residual particles from the calcination. These C atoms resulted as Fe_3C particles in the Raman spectroscopy wavelength at 450 cm^{-1}. Also, the carbon atoms are observed as crystal graphite form in Raman wavelength at 1600 cm^{-1}. As a result, $LiFePO_4$ powders are expected to show high conductivity and better electrochemical properties due to the metallic structure of Fe_3C and crystal graphite.

Surface areas and porosities are measured under nitrogen atmosphere by Brunauer-Emmett-Teller (N_2-BET) technique and pore sizes are calculated by Barret–Joyner–Halenda (BJH) model. From these results, CCL/$LiFePO_4$ nanoparticles represent IV type isotherms with H3 hysteresis loops related to porous surfaces and plate shaped particles. Surface areas are between 20-60 m^2/g and increasing by CCL amount, and pore sizes are around 5-20 nm which is mesoporous surface according to IUPAC.

Porous surface provides shorter diffusion distance and multi dimension channels resulting better electrochemical properties. Despite, average particle sizes are larger (75.0 nm) than BET results than the particle sizes calculated from XRD results (30-40 nm) that can be resulted from agglomeration of particles. Also it can be seen that the sample 20 CCL/$LiFePO_4$ has a very high specific surface area (59.2 m^2/g) that indicates of porous network structure of the surface. These porous surfaces can contribute multi dimensional channels for Li^+ trasportation resulting better electrochemical properties.

The powders are obtained around 50-100 nm separated, however the particles are agglomerated and achieved larger particles during heat treatment as it can be seen from SEM results. The size difference between the particles shows the high surface areas due to porous structure result the decrease of distance for lithium-ion diffusion which improves the electrochemical behavior of $LiFePO_4$.

Electrical conductivities of CCL/$LiFePO_4$ powders are measured between (-20 °C) and (+40 °C) that they show much higher conductivities (10^{-2} to 10^{-3} S/cm) than pure $LiFePO_4$ powders (10^{-9} S/cm) and increased with CCL amount. However 20 CCL/$LiFePO_4$ shows lower conductivity at room temperature ($8.57*10^{-1}$ S/cm) than 15 CCL/$LiFePO_4$ ($5.64*10^{-1}$ S/cm) due to the agglomeration of excess CCL covered on surface. These agglomerations resulting the thicker and less pores on the surface which preventing the transportation of ions and resulting lower conductivities. The powders with CB added show much higher conductivity than the CCL covered particles.

Moreover, conductivities of samples are increasing with temperature due to lower activation energies as reffered by Arrhenius law. Activation energies of CCL/$LiFePO_4$ are also calculated from conductivity plots and shown lower values ($9.96*10^{-2}$ eV and $1.17*10^{-1}$ eV) than bare $LiFePO_4$ (0.65 eV) which means easier electron mobility and better electronic conductivities.

The cycling performance of $LiFePO_4$ cathode powders are analyzed from CV experiments. The oxidation/reduction reactions of Fe^{+2}/Fe^{+3} are observed around 3.7 V and 3.0 V during the charging and recharging reversibly. The peak intensities are directly affected from C additives and gets higher with increasing C amount. The peak intensities and separation between anodic/cathodic peaks are influenced from the scan rate of CV analysis and getting higher and more separated with increasing scan rates. As a conclusion, due to the higher conductivity of 15 CB/ $LiFePO_4$ more than 10 CB/$LiFePO_4$ powders, it showed better cycle performance and high rate capability.

The impedance and resistance values for 15 CB/$LiFePO_4$ are much lower than 10 CB/$LiFePO_4$ due to its higher conductive structure. Both samples show better EIS performances compared to literature results which is attributed to low particle sizes and high surface areas enhancing short path way for Li^+ ion diffusion. As a conclusion, powders are expected to show high rate capabilities and better electrochemical performances during cycling.

As a result, pure and homogenous $LiFePO_4$ powders are prepared by solution precipitation technique and covered with CCL in order to achieve better conductivity successfully. For further applications, doping the powders with other metal ions and improving other electrochemical properties can be investigated for new generation alternative cathode materials.

REFERENCES

[1] **Meyer, W.H**. (1998). Adv. Mater., 10, 439.

[2] **Flipsen, S.F.J.** (2006). J. Power Sources, 162, 927.

[3] **Mader, J.** (1996). IEEE AES Systems magazine, 11, 17.

[4] **Erikkson, T.** (2001). $LiMn_2O_4$ as a Li-ion battery cathode from bulk to electrolyte interface. PhD Dissertion, Uppsala University, Sweden.

[5] **Hwang, B.J., Santhanam, R. and Chen, C.H.** (2003). Effect of synthesis conditions on electrochemical properties of $LiNi_{1-y}Co_yO_2$ cathode for lithium rechargeable batteries. Journal of Power Sources, 114, (2), 244-252.

[6] **Mizushima, K., Jones, P.C., Wiseman, P.J. and Goodenough, J.B.** (1980). Li_xCoO_2: A new cathode material for batteries of high energy density. Materials Research Bulletin 15, (6), 783-789.

[7] **Simonis, D.A. and Hertzenberg, C.** (1999). Lives & Legacies. Orxy Press, Phoenix, 256.

[8] **McNeil, I.** (2002). An Encyclopaedia of the History of Technology. London: New York Routledge, 1033.

[9] **Daintith, J.** (1999). A Dictionary of Scientist. Oxford, New York: Oxford University Press (UK), 463.

[10] **Jensen, K.M.Ø., Christensen, M., Tyrsted, C., Bremholm, M. and Iversen, B.B**. (2011). Structure, Size, and Morphology Control of Nano crystalline Lithium Cobalt Oxide. Crystal Growth & Design, 11, (3), 753-758.

[11] **Li, D., Sasaki, Y., Kobayakawa, K. and Sato, Y.** (2006). Morphological, structural, and electrochemical characteristics of $LiNi_{0.5}Mn_{0.4}M_{0.1}O_2$. Journal of Power Sources, 157, (1), 488-493.

[12] **Sivaprakash, S., Majumder, S.B., Nieto, S. and Katiyar, R.S.** (2007). Crystal chemistry modification of lithium nickel cobalt oxide cathodes for lithium ion rechargeable batteries. Journal of Power Sources, 170, (2), 433-440.

[13] **Ellis, B.L., Lee, K.T. and Nazar, L.F.** (2010). Positive Electrode Materials for Li-ion and Li-Batteries. Chemistry of Materials, 22, (3), 691-714.

[14] **Katiyar, R.K.** (2009). Synthesis and Characterization of Cathode Materials For High Energy Density and High Rate Capability Lithium-ion Rechargeable Batteries. M.Sc. Theis, University Of Puerto Rico, Puerto Rico.

[15] **Gao, Y., Yakovleva, M.V. and Ebner, W.B.** (1998). Novel $LiNi_{1-x}Ti_{x/2}Mg_{x/2}O_2$ Compounds as Cathode Materials for Safer Lithium-ion Batteries. Electrochemical and Solid-State Letters, 1, (3), 117-119.

[16] **Majumder, S.B., Nieto, S. and Katiyar, R.S.** (2006). Synthesis and Electrochemical Properties of $LiNi_{0.80}(Co_{0.20-x}Al_x)O_2$ (x=0.0 and 0.05) Cathodes for Li ion Rechargeable Batteries. Journal of Power Sources, 154, 262-267.

[17] **Tarascon, J.M. and Armand, M.** (2001). Issues and challenges facing rechargeable lithium batteries. Nature, 414, (6861), 359-367.

[18] **Wakihara, M.** (2001). Materials Science and Engineering, R33, 109.

[19] **Wang, S.** (2009). Iron Phosphates as Cathodes For Lithium-ion Batteries. PhD Dissertion, Binghamton University State University of New York, USA.

[20] **Moss, P.L.** (2008). Study of Capacity Fade of Lithium-ion Polymer Battery With Continuous Cycling & Power Performance Modeling Of Energy Storage Devices. PhD Thesis, The Florida State University, USA.

[21] **Ma, M.** (2005). Layered $LiMn_{0.4}Ni_{0.4}Co_{0.2}O_2$ As Cathode For Lithium Batteries. PhD Thesis, Binghamton University State University of New York, USA.

[22] **Fu, L.J., Liu, H., Li, C., Wu, Y.P., Rahm, E., Holze, R. and Wu, H.Q.** (2006). Surface modifications of electrode materials for lithium ion batteries. Solid State Sciences, 8, (2),113-128.

[23] **Endo, M., Kim, C., Nishimura, K., Fujino, T. and Miyashita, K.** (2000). Recent development of carbon materials for Li ion batteries. Carbon, 38, (2), 183-197.

[24] **Trevey, J.E.** (2011). Advances And Development of All-Solid-State Lithium-ion Batteries. PhD thesis, Graduate School of The University of Colorado, USA.

[25] **Scrosati, B.** (1995). Battery technology-Challenge of portable power. Nature, 375, 557-558.

[26] **Bossche, V.P., Vergels, F., Van Mierlo, J., Matheys, J. and Van Autenboer, W.** (2006). An assessment of sustainable battery technology. Journal of Power Sources, 162, 913-916.

[27] **Liu, D.** (2010). Engineering Nanostructures and Surface Chemistry of Efficient Lithium-ion Intercalation Electrodes. PhD thesis, University of Washington, USA.

[28] **Chang, R.** (1994). Chemistry. 5th ed, McGraw Hill Companies, USA, 543.

[29] **Rydh, C.J. and Svard, B.** (2003). Impact on global metal flows arising from the use of portable rechargeable batteries. Science of the Total Environment, 302, (1-3), 167-184.

[30] **Kim, H.S., Periasamy, P. and Moon, S.I.** (2005). Electrochemical properties of the Li-ion polymer batteries with P(VdF-co-HFP)-based gel polymer electrolyte. Journal of Power Sources, 141, (2), 293-297.

[31] **Choi, N.S., Lee, Y.G. and Park, J.K.** (2002). Effect of cathode binder on electrochemical properties of lithium rechargeable polymer batteries. Journal of Power Sources, 112, (1), 61-66.

[32] **Annamalai, A.K.T.** (2007). Chemical, Structural, And Electrochemical Characterization of 5 V Spinel And Complex Layered Oxide Cathodes Of Lithium Ion Batteries. PhD Thesis, The University Of Texas At Austin, USA.

[33] **Arora, P., White, R.E. and Doyle, M.** (1998). Capacity fade mechanisms and side reactions in lithium-ion batteries. Journal of the Electrochemical Society, 145, (10), 3647-3667.

[34] **Sakamoto, J.S. and Dunn, B.** (2002). J. Electrochem. Soc. A26, 149.

[35] **Liu, D.W., Garcia, B.B., Zhang, Q.F., Guo, Q., Zhang, Y.H. Sepehri, S. and Cao, G.Z.** (2009). Adv. Funct. Materi., 19, 1015.

[36] **Yamada, Y., Koyama, Y., Abe, T. and Ogumi, Z.** (2009). Correlation between Charge−Discharge Behavior of Graphite and Solvation Structure of the Lithium Ion in Propylene Carbonate-Containing Electrolytes. The Journal of Physical Chemistry C, 113, (20), 8948-8953.

[37] **Ménétrier, M., Delmas, C. and Levasseur, A.** (1992). On the behavior of interactlation compounds in solid state batteries. Materials Science and Engineering: B, 15, (1), 101-104.

[38] **Peres, J.P., Delmas, C., Rougier, A., Broussely, M., Perton, F., Biensan, P. and Willmann, P.** (1996). The relationship between the composition of lithium nickel oxide and the loss of reversibility during the first cycle. Journal of Physics and Chemistry of Solids, 57, (6-8), 1057-1060.

[39] **Wicker, S.A.** (2011). Development of a Green Soft Chemical Method for the Synthesis of Cathode Materials Utilized in Lithium-ion Energy Storage Technologies. PhD thesis, Southern University and A & M College, Louisiana, USA.

[40] **Vetter, J., Novak, P., Wagner, M.R., Veit, C., Möller, K.-C., Besenhard, J.O., Winter, M., Wohlfahrt-Mehrens, M., Vogler, C. and Hammouche, A.** (2005). Ageing mechanisms in lithium-ion batteries. Journal of Power Sources, 147, (1-2), 269-281.

[41] **Manthiram, A. and Kim, J.** (1999). Recent Res. Devel. Electrochem., 2, 31.

[42] **Heitner, K.L.** (2000). The search for the better polymer electrolyte. Journal of Power Sources, 89, (2), 128-131.

[43] **Ahn, D.** (2010). Electrochemical Insertion of Lithium into Polymer Derived Silicon Oxycarbide and Oxycarbonitride Ceramics. PhD Thesis, Graduate School of the University of Colorado, USA.

[44] **Whittingham, M.S.** (2004). Lithium Batteries and Cathode Materials. Chemical Reviews, 104, (10), 4271-4302.

[45] **Long, J.W., Dunn, B., Rolison, D.R. and White, H.S.** (2004). Three-Dimensional Battery Architectures. Chemical Reviews, 104, (10), 4463-4492.

[46] **Reisch, M.S.** (2010). Betting On Lithium. Chemical & Engineering News, 88, (36), 44-45.

[47] **Arora, P. and Zhang, Z.** (2004). Battery Separators. Chemical Reviews, 104, (10), 4419- 4462.

[48] **Bard, A.J. and Faulkner, L.R.** (2001). Electrochemical Methods Fundamentals and Applications. 2nd ed,; John Wiley & Sons, Inc, Hoboken, 833.

[49] **Fergus, J.W.** (2009). Recent Developments in Cathode Materials for Lithium-ion Batteries. Journal of Power Sources, 195, (4), 939-954.

[50] **Bruce, P.G.** (1995). Solid State Electrochemistry, P.G. Bruce, Ed., Cambridge University Press, Cambridge.

[51] **Vashista, P., Mundy, J.N. and Shenoy, G.K.** (1979). Fast Ion Transport in Solids. Elsevier North Holland, New York, 131.

[52] **Dahn, J.R., Sleigh, A.K., Shi, H., Reimers, J.N., Zhong, Q. and Way, B.M.** (1993). Dependence of the electrochemical intercalation of lithium in carbons on the crystal structure of the carbon. Electrochimica Acta, 38, (9), 1179-1191.

[53] **Linden, D. and Reddy, T.B.** (2002). Handbook of Batteries. 3rd ed., McGraw-Hill Companies, Inc., New York, USA.

[54] **Kuzmu, M.D., Menden, A., Makovec, D., Bele, M., Jamnik, J. and Gaberscek, M.** (2009). Electrochemical activity of Li_2FeTiO_4 and Li_2MnTiO_4 as potential active materials for Li ion Batteries: A comparison with Li_2NiTiO_4. Journal of Power Sources, 189, 81-88.

[55] **Zhang, H.-L., Sun, C.-H., Li, F., Liu, C., Tan, J. and Cheng, H.-M.** (2007). New Insight into the Interaction between Propylene Carbonate-Based Electrolytes and Graphite Anode Material for Lithium Ion Batteries. The Journal of Physical Chemistry C, 111, (12), 4740-4748.

[56] **Denholm, P., Ela, E., Kirby, B. and Milligan, M.** (2010). The Role of Energy Storage with Renewable Electricity Generation. Laborator, N.R.E., Ed. U.S. Department of Commerce, Golden, 1-61.

[57] **Patoux, S.D., Bourbon, C., Liginier, H., Pagano, C., Jouanneau, S. and Martinet, S.** (2009). High Voltage spinel oxide for Li-ion batteries: From the material research to application. Journal of Power Sources, 189, 344-352.

[58] **Pecharsky, V.K. and Zavalij, P.Y.** (2009). Fundamentals of Powder Diffraction and Structural Characterization of Materials. Second Edition ed., Springer Science, Business Media, LLC, New York, USA.

[59] **Bockris, J.O.M. and Reddy, A.K.N.** (1998). Modern Electrochemistry 1. 2 ed.; Plenum Publishing Corporation, New York, Vol. 1, 769.

[60] **Kasavajjula, U., Wang, C. and Appleby, A.** (2007). Nano- and bulk-silicon-based insertion anodes for lithium-ion secondary cells. Journal of Power Sources, 163, 1003.

[61] **Zhu, J., Lu, Z., Aruna, S.T., Aurbach, D. and Gedanken, A.** (2000). Chem. Mater., 12, 2557.

[62] **Nam, S.C., Kim, Y.H., Cho, W.I., Cho, B.W., Chun, H.S. and Yun, K.S.** (1999). Electrochem. Solid-State Lett. 2, 9.

[63] **Park, M.-S., Kang, Y.-M., Rajendran, S., Kwon, H.-S. and Lee, J.-Y.** (2006). Si–Ni–Carbon composite synthesized using high energy mechanical milling for use as an anode in lithium ion batteries. Materials Chemistry and physics, 100, (2-3), 496-502.

[64] **Aurbach, D., Levi, M.D., Levi, E. and Schechter, A.** (1997). J. Phys. Chem. B, 101, 2195.

[65] **Soga, K., Hosada, S., Tazuke, Y. and Ikeda, S.** (1976). J. Polym. Sci., Poly. Lett., 14, 161.

[66] **Liu, W.-R., Yang, M.-H., Wu, H.-C., Chiao, S.M. and Wu, N.-L.** (2005). Enhanced cycle life of Si anode for Li-ion batteries by using modified elastomeric binder. Electrochemical and Solid State Letters, 8, (2), A100-A103.

[67] **Krause, L.J., Lamanna, W.L., Summerfield, J., Engle, M., Korba, G., Loch, R. and Atanasoski, R.** (1997). J. Power Sources, 68, 320.

[68] **Dimov, N., Kugino, S. and Yoshio, M.** (2003). Carbon-coated silicon as anode material for lithium ion batteries: advantages and limitations. Electrochimica Acta, 48, (11), 1579-1587.

[69] **Pasquier, A.D., Blyr, A., Courjal, P., Larcher, D., Amatucci, G., Gérand, B. and Tarascon, J.-M.** (1999). J. Electrochem. Soc., 146, 428.

[70] **Kim, C., Noh, M., Choi, M., Cho, J. and Park, B.** (2005). Chem. Mater., 17, 3297.

[71] **Winter, M., Besenhard, J.O., Spahr, M.E.and Novak, P.** (1998). Adv. Mater., 10, 725.

[72] **Arico, A.S., Bruce, P.G., Scrosati, B., Tarascon, J.M. and Van Schalkwijk, W.** (2005). Nat. Mater., 4, 366.

[73] **Xiao, J.** (2008). Layered Lithium Nickel Manganese Cobalt Dioxide As A Cathode Material For Li-ion Batteries. PhD Thesis, Binghamton University State University Of New York, USA.

[74] **Ohzuku, T., Ueda, A. and Nagayama, M.** (1993). Electrochemistry and Structural Chemistry of $LiNiO_2$ (R3m) for 4 Volt Secondary Lithium Cells. Journal of Electrochemical Society, 140, (7), 1862-1870.

[75] **Pouillerie, C., Suard, E. and Delmas, C.** (2001). Structural Characterization of $Li_{1-z-x}Ni_{1+z}O_2$ by Neutron Diffraction. Journal of Solid State Chemistry, 158, (2), 187-197.

[76] **Shao-Horn, Y., Levasseur, S., Weill, F. and Delmas, C.** (2003). Probing Lithium and Vacancy Ordering in O_3 Layered Li_xCoO_2 ($x \approx 0.5$). Journal of The Electrochemical Society, 150, (3), A366-A373.

[77] **Ermete, A.** (1998). Preparation and properties of Li-Co-O compounds. Journal of the European Ceramic Society, 18, (10), 1405-1411.

[78] **Delmas, C., Saadoune, I. and Rougier, A.** (1993). The cycling properties of the $Li_xNi_{1-y}Co_yO_2$ electrode. Journal of Power Sources, 44, (1-3), 595-602.

[79] **Aurbach, D., Gamolsky, K., Markovsky, B., Salitra, G., Gofer, Y., Heider, U., Oesten, R. and Schmidt, M.** (2000). J. Electrochem. Soc., 147, 1322.

[80] **Chebiam, R.V., Prado, F. and Manthiram, A.** (2001). Chem. Mater., 13, 2951.

[81] **Osaka, T. and Datta, M.** (2000). Energy Storage Systems for Electronics. New Trends in Electrochemical Technology, Taylor & Francis, Vol. 1.

[82] **Huggins, R.A.** (2008). Handbook of Batteries. Materials Science Aspects, Springer.

[83] **Abrahamson, J.T. and Strano, M.S.** (2010). Analytical Solution to Coupled Chemical Reaction and Thermally Diffusing Systems: Applicability to Self-Propagating Thermopower Waves. The Journal of Physical Chemistry Letters, 1, (24), 3514-3519.

[84] **Carthey, N.A. and Kerridge, D.H.** (1987). Molten lithium carbonate-sodium carbonate potassium carbonate eutectic: electronic spectroscopy of first-row transition metal compounds. Journal of the Chemical Society, Dalton Transactions, (10), 2329-2331.

[85] **Delmas, C., Pérès, J. P., Rougier, A., Demourgues, A., Weill, F., Chadwick, A., Broussely, M., Perton, F., Biensan, P. and Willmann, P.** (1997). On the behavior of the Li_xNiO_2 system: an electrochemical and structural overview. Journal of Power Sources, 68, (1), 120-125.

[86] **Thackeray, M., Mansuetto, M. and Bates, J.** (1997). Structural stability of $LiMn_2O_4$ electrodes for lithium batteries. Journal of Power Sources, 68, 153-158.

[87] **Shin, Y. and Manthiram, A.** (2002). Microstrain and capacity fade in spinel manganese oxides. Electrochemical and Solid State Letters, 5, A55-A58.

[88] **Saidi, M.Y., Huang, H., Swoyer, J.L. and Baker, J.** (2002). Proceedings of the 20th International Seminar and Exhibit on Primary and Secondary Batteries, Fort Lauderdale, Florida.

[89] **Yabuuchi, N. and Ohzuku, T.** (2003). J. Power Sources, 171, 119-121.

[90] **Nytén A.** (2006). Low-Cost Iron-Based Cathode Materials For Large-Scale Battery Applications. PhD Dissertion, Acta Universitatis Upsaliensis Uppsala, 179, 54, Sweden.

[91] **Padhi, A.K., Nanjundaswamy, K.S., Masquelier, C., Okada, S. and Goodenough, J.B.** (1997). J. Electrochem. Soc., 144, 1609.

[92] **Huang, H., Yin, S.C. and Nazar, L.F.** (2001). Approaching theoretical capacity of $LiFePO_4$ at room temperature at high rates. Electrochemical and Solid State Letters, 4, (10), A170-A172.

[93] **Molenda, M. and Molenda, J.** (2011). Composite Cathode Material for Li-ion Batteries Based on $LiFePO_4$ System: Metal, Ceramic and Polymeric Composites for Various Uses, John Cuppoletti.

[94] **Ravet, N., Goodenough, J.B., Besner, S., Simoneau, M., Hovington, P. and Armand, M.** (1999). Electrochem. Soc. Abstr., 127.

[95] **Franger, S., Cras, L.F., Bourbon, C. and Rouault, H.** (2002). $LiFePO_4$ synthesis routes for enhanced electrochemical performance. Electrochemical and Solid State Letters, 5, (10), A231-A233.

[96] **Yamada, A., Chung, S.C. and Hinokuma, K.** (2001). Optimized $LiFePO_4$ for lithium battery cathodes. Journal of the Electrochemical Society, 148, (3), A224-A229.

[97] **Takahashi, M., Tobishima, S., Takei, K. and Sakurai, Y.** (2001). Characterization of $LiFePO_4$ as the cathode material for rechargeable lithium batteries. Journal of Power Sources, 97, 8, 508-511.

[98] **Liu, H., Zhang, P., Li, G.C., Wu, Q. and Wu, Y.P.** (2008). $LiFePO_4$/C composites from carbothermal reduction method. Journal of Solid State Electrochemistry, 12, 1011-1015.

[99] **Zhi, X., Liang, G., Wang, L., Ou, X., Zhang, J. and Cui, J.** (2008). The cycling performance of $LiFePO_4$/C cathode materials. Journal of Power Sources, 189, (1), 779-782.

[100] **Wang, L., Huang, Y., Jiang R. and Jia, D.** (2007). Preparation and characterization of nanosized $LiFePO_4$ by low heating solidstate coordination method and microwave heating. Electrochimica Acta, 52, 6778-6783.

[101] **Higuchi, M., Katayama, K., Azuma, Y., Yukawa, M. and Suhara, M.** (2003). Synthesis of $LiFePO_4$ cathode material by microwave processing. Journal of Power Sources, 119121, 258-261.

[102] **Guo, X.F., Zhan, H. and Zhou, Y.H.** (2009). Rapid synthesis of $LiFePO_4$/C composite by microwave method. Solid State Ionics, 180, 386-391.

[103] **Muraliganth, T., Murugan, A.V. and Manthiram, A.** (2008). Nanoscale networking of $LiFePO_4$ nanorods synthesized by a microwave solvothermal route with carbon nanotubes for lithium-ion batteries. Journal of Materials Chemistry, 18, (46), 5661-5668.

[104] **Somiya, S. and Roy, R.** (2000). Hydrothermal synthesis of fine oxide powders. Bulletin of Materials Science, 23, (6), 453-460.

[105] **Yang, S., Zavalij, P.Y. and Whittingham, M.S.** (2001). Hydrothermal synthesis of lithium iron phosphate cathodes. Electrochemistry Communications, 3, 505-508.

[106] **Arumugam, D., Kalaignan, G.P. and Manisankar, P.** (2009). Synthesis and electrochemical characterizations of nanocrystalline $LiFePO_4$ and Mg doped $LiFePO_4$ cathode materials for rechargeable lithium ion batteries. Journal of Solid State Electrochemistry, 13, 301-307.

[107] **Dominko, R., Goupil, J.M., Bele, M., Gaberscek, M., Remskar, M., Hanzel, D. and Jamnik, J.** (2005). Impact of $LiFePO_4$/C Composites Porosity on Their Electrochemical Performance. Journal of The Electrochemical Society, 152, (5), A858-A863.

[108] **Dominko, R., Bele, M., Gaberscek, M., Remskar, M., Hanzel, D., Goupil, J. M., Pejovnik, S. and Jamnik, J.** (2006). Porous olivine composites synthesized by sol-gel technique. Journal of Power Sources, 153, 274-280.

[109] **Choi, D. and Kumta, P.N.** (2007). Surfactant based sol gel approach to nanostructured $LiFePO_4$ for high rate Li-ion batteries. Journal of Power Sources, 163, 1064-1069.

[110] **Wang, G.X., Bewlay, S., Yao, J., Ahn, J.H., Dou, S.X. and Liu, H.K.** (2004). Characterization of $LiM_xFe_{1-x}PO_4$ (M=Mg, Zr, Ti) Cathode Materials Prepared by the Sol Gel Method. Electrochemical and Solid State Letters, 7, (12), A503-A506.

[111] **Myung, S.T., Komaba, S., Takagai, R., Kumagai, N. and Lee, Y.S.** (2003). Emulsion drying preparation of $LiFePO_4$/C composite and its enhanced high-rate performance at 50 °C. Chemistry Letters, 32, (7), 566-567.

[112] **Myung, S.T. and Chung, H.T.** (1999). Preparation and characterization of $LiMn_2O_4$ powders by the emulsion drying method. Journal of Power Sources, 84, 32-38.

[113] **Myung, S.T., Komaba, Sh., Hirosaki, N., Yashiro, H. and Kumagai, N.** (2004). Emulsion drying synthesis of olivine $LiFePO_4$/C composite and its electrochemical properties as lithium intercalation material. Electrochimica Acta, 49, 4213-4222.

[114] **Xu, Z., Xu, L., Lai, Q. and Ji, X.** (2007). Microemulsion synthesis of $LiFePO_4$/C and its electrochemical properties as cathode materials for lithium-ion cells. Materials Chemistry and Physics, 105, 80-85.

[115] **Wakihara, M. and Yamamoto, O.** (1998). Lithium Ion Batteries Fundamentals And Performance. Wiley-Vch, Weinheim, Germany.

[116] **Wu, Y.** (2008). Structural And Electrochemical Characterization and Surface Modification of Layered Solid Solution Oxide Cathodes Of Lithium Ion Batteries. PhD Thesis, The University Of Texas At Austin.

[117] **Tarascon, J.M.** (1994). Guyomard, D., Solid State Ionics, 69, 293.

[118] **Appetecchi, G.B., Croce, F., Romagnoli, P., Scrosati, B., Heider, U. and Oesten, R.** (1999). Electrochem. Commun., 1, 83.

[119] **Song, J.Y., Wang, Y.Y. and Wan, C.C.** (1999). Review of gel-type polymer electrolytes for lithium-ion batteries. Journal of Power Sources, 77, (2), 183-197.

[120] **Laman, R.C., Gee, M.A. and Denovan, J.** (1993). Journal of Electrochem. Soc., 140, L51.

[121] **Naouli, N.** (2005). Non-Ionic Microemulsion Mechanism and Theory of Formation. PhD Thesis, The City University of New York.

[122] **Najjar, R.** (2012). Microemulsions – A Brief Introduction, Microemulsions - An Introduction To Properties And Applications. Intech, Tabriz, Iran.

[123] **Maitra, A.N.** (1984). Determination Of Size Parameters Of Water-Aerosol Ot-Oil Reverse Micelles From Their Nuclear Magnetic Resonance Data. Journal Phys. Chem., 88, 5122–5125.

[124] **Lindman, B. and Friberg, S.E.** (1999). Microemulsions—A Historical Overview. In Handbook Of Microemulsion Science And Technology. Kumar, P.; Mittal, K., Eds. Marcel Dekker, Inc: New York, P 1.

[125] **Moulik, S.P. and Paul, B.K.** (1998). Adv. Colloid Interface Sci., 78, 99.

[126] **James-Smith, M.A.** (2006). Molecular Interactions In Surfactant Solutions: From Micelles To Microemulsions. PhD Thesis, University of Florida, USA.

[127] **Ruckenstein, E.** (1999). Thermodynamic insights on macroemulsion stability. Adv. Colloid Interface Sci., 79, (1), 59-76.

[128] **Ganguli, A.K., Ganguly, A. and Vaidya, S.** (2010). Microemulsion-based synthesis of nanocrystalline materials. Chemical Society Reviews, 39, 474-485.

[129] **Xu, Z., Xu, L., Lai, Q. and Ji, X.** (2007). Microemulsion Synthesis of $LiFePO_4$/C and its electrochemical properties as cathode materials for lithium-ion cells. Materials Science and Chemistry, 105, 80-85.

[130] **Lu, C.-H. and Wang, H.-C.** (2004). Reverse microemulsion preparation and characterization of ultrafine orthorhombic $LiMnO_2$ powders for lithium-ion secondary batteries. Journal of the European Ceramic Society, 24, 717-723.

[131] **Althues, H., and Kaskel. S.** (2002). Sulfated zirconia nanoparticles synthesized in reverse microemulsions: preparation and catalytic properties. Langmuir, 18, 7428-7435.

[132] **Xu, X.-J. and Gan L.M.** (2005). Recent advances in the synthesis of nanoparticles of polymer latexes with high polymer-to-surfactant ratios by microemulsion polymerization. Current Opinion in Colloid & Interface Science, 10, 5–6, 239-244.

[133] **Engström, S. and Larsson, K.** (1999). Microemulsions in Foods. In Handbook of Microemulsion Science and Technology, Kumar, P.; Mittal, K., Dekker, M., Inc.: New York, 789-796.

[134] **Valenta, C. and Schultz, K.** (2004). Influence of carrageenan on the rheology and skin permeation of microemulsion formulations. J. Controlled Release, 95, 2, 257-265.

[135] **Pillai, V., Kanicky, J.R. and Shah, D.O.** (1999). Applications of Microemulsions in Enhanced Oil Recovery. In Handbook of Microemulsion Science and Technology, Kumar, P.; Mittal, K. L., Dekker, M., Inc., New York, 743-754.

[136] **Kim, S.K., Lee, E.H., Vaishali, B., Lee, S., Lee, Y.-K., Kim, Ch.-Y., Moon, H.T. and Byun, Y.** (2005). Tricaprylin microemulsion for oral delivery of low molecular weight heparin conjugates. J. Controlled Release, 105, 1–2, 32-42.

[137] **Kantaria, Sh., Rees, G.D. and Lawrence, M.J.** (1999). Gelatin-stabilised microemulsion based organogels: rheology and application in iontophoretic transdermal drug delivery. J. Controlled Release, 60, 2–3, 355-365.

[138] **Djordjevic, L., Primorac, M., Stupar, M. and Krajisnik, D.** (2004). Characterization of caprylocaproyl macrogolglycerides based microemulsion drug delivery vehicles for an amphiphilic drug. Inter. J. Pharm., 271, 1–2, 11-19.

[139] **Gupta, A.K., Gupta, M., Yarwood, S.J. and Curtis, A.S.G.** (2004). Effect of cellular uptake of gelatin nanoparticles on adhesion, morphology and cytoskeleton organisation of human fibroblasts. J. Controlled Release, 95, 2, 197-207.

[140] **Tao, G.-P., Chen, Q.-Y., Yang, X., Zhao, K.-D. and Gao, J.** (2011). Targeting cancer cells through iron (III) complexes of di(picolyl)amine modified silica core–shell nanospheres. Colloids Surf. B: Biointerfaces, 86, 1, 106-110.

[141] **Stamatis, H. and Xenakis, A.** (1999). Biocatalysis using microemulsion-based polymer gels containing lipase. J. Molecular Cat. B: Enzymatic, 6, 4, 399-406.

[142] **Rao, J. and McClements, D.J.** (2012). Lemon oil solubilization in mixed surfactant solutions: Rationalizing microemulsion & nanoemulsion formation. Food Hydrocolloids, 26, 1, 268-276.

[143] **Ma, Y., Liang, J., Sun, H., Wu, L., Dang, Y. and Wu, Y.** (2012). Honeycomb micropatterning of proteins on polymer films through the inverse microemulsion approach. Chem. Eur. J., 18, 2, 526-531.

[144] **Lin, J.-C., Lee, C.-P. and Ho, K.-C.** (2012). Zinc oxide synthesis via a microemulsion technique: Morphology control with application to dye-sensitized solar cells. J. Mater. Chem., 22, 4, 1270-1273.

[145] **Shokri, M., Hosseini, M.G., Khosravi, M., Najjar, R. and Sheikhy, S.** (2011). The preparation of Pt-modified TiO_2 nanoparticles via microemulsions, and their application in photocatalytic removal of an azo dye (C.I. Acid Red 27). Fresenius Environmental Bulletin, 20, 4 A, 1063-1068.

[146] **Jing, L., Li, Y., Ding, K., Qiao, R., Rogach, A.L. and Gao, M.** (2011). Surface-Biofunctionalized Multicore/Shell CdTe@SiO_2 Composite Particles For Immunofluorescence Assay. Nanotech., 22, 50, 505104.

[147] **Friberg, S.E. and Sun, W.M.** (1990). A Non-Aqueous Microemulsion System of Ethylene Glycol, Sodium Dodecyl Sulfate, Toluene, And Decanol. Colloid Polym Sci, 268, 755-759.

[148] **Akbari, B., Tavandashti, M.P. and Zandrahimi, M.** (2011). Particle Size Characterization of Nanoparticles – A Practical Approach. Iranian Journal Of Materials Science & Engineering, 8, 2.

[149] **Bowen, P.** (2002). Particle Size Distribution Measurement From Millimeters to Nanometers and From Rods to Platelets. Journal of Dispersion Science and Technology, 13, 631-662.

[150] **Chen, Z. and Dahn, J.R.** (2002). Reducing Carbon in $LiFePO_4$ /C Composite Electrodes to Maximize Specific Energy, Volumetric Energy, And Tap Density. Journal of the Electrochemical Society, 149, (9), A1184-A1189.

[151] **Jentjens, L., Raeth, N.L., Peithmann, K. and Maier, K.** (2011). Electrical Conductivity and Asymmetric Material Changes Upon Irradiation of Mg-Doped Lithium Niobate Crystals With Low-Mass, High-Energy Ions. Journal of Applied Physics, 109, 12, 124104.

[152] **Hong, S.-A., Kim, S.J., Kim, J., Lee, B.G., Chung, K.Y. and Lee, Y.-W.** (2012). Carbon Coating On Lithium Iron Phosphate ($LiFePO_4$): Comparison Between Continuous Supercritical Hydrothermal Method And Solid-State Method. Chemical Engineering Journal, 198–199, 318–326.

[153] **Xu,Y., Lu, Y., Yan, L., Yang, Z. and Yang, R.** (2006). J. Power Sources, 160, 570-576.

[154] **Han, C., Wen-Zhi, Y., Shao-Chang, H. and Zhong-Yu, X.** (2007). Preparation And Electrochemical Properties of $LiFePO_4$/C Composite With Network Structure for Lithium-ion Batteries. Trans. Nonferrous Met. Soc. China, 17, 951-956.

[155] **Sing, K.S.W., Everett, D.H., Haul, R.A.W., Moscou, L., Pierotti, R.A., Rouquerol, J. and Siemieniewska, T.** (1985). Reporting Physisorption Data For Gas/Solid Systems With Special Reference To The Determination of Surface Area And Porosity. Pure & Appl. Chem., 57, 4, 603-619.

[156] **Li, X.L., Zhang, Y.L., Song, H.F., Du, K., Wang, H., Li, H.Y. and Huang, J.M.** (2012). The Comparison of Carbon Conductive Additives With Different Dimensions on The Electrochemical Performance of $LiFePO_4$ Cathode. Int. J. Electrochem. Sci., 7, 7111-7120.

[157] **Chen, H., Han, S.-C., Yu, W.-Z., Bo, H.-Z., Fan, C.-L. and Xu, Z.-Y.** (2006). Preparation and Electrochemical Properties of $LiFePO_4$/C Composite Cathodes for Lithium-ion Batteries. Bull. Mater. Sci., 29, 7, 689–692.

[158] **Wang, C. and Hong, J.** (2007). Ionic/Electronic Conducting Characteristics of $LiFePO_4$ Cathode Materials. Electrochemical and Solid-State Letters, 10, 3, A65-A69.

[159] **Harun, M.H., Saion, E., Kassim, A., Hussain, M.Y., Mustafa, I.S. and Omer, M.A.A.** (2008). Temperature Dependence of Ac Electrical Conductivity of PVA-PPy-$FeCl_3$ Composite Polymer Films. Malaysian Polymer Jounal, 3, 2, 24-31.

[160] **Tominaga, Y., Asai, S., Sumita, M., Panero, S. and Scrosati, B.** (2005). A Novel Composite Polymer Electrolyte: Effect of Mesoporous SiO_2 on Ionic Conduction in Poly(Ethylene Oxide)–$LiCF_3SO_3$ Complex. Power Source, 146, 402-406.

[161] **Zaghib, K., Mauger, A., Goodenough, J.B., Gendron, F. and Julien, C.M.** (2007). Electronic, Optical, And Magnetic Properties of $LiFePO_4$: Small Magnetic Polaron Effects. Chem. Mater., 19, 3740–3747.

[162] **Molenda, J., Ojczyk, W., Świerczek, K., Zając, W., Krok, F., Dygas, J. and Liu, R.-S.** (2006). Diffusional Mechanism of Deintercalation in $LiFe_{1-y}Mn_yPO_4$ Cathode Material. Solid State Ionics, 177, 2617–2624.

[163] **Yang, J., Wang, J., Li, X., Wang,D., Liu, J., Liang, G., Gauthier, M., Li, Y., Geng, D., Li, R. and Sun, X.** (2012). Hierarchically porous $LiFePO_4$/nitrogen-doped carbon nanotubes composite as a cathode for lithium ion batteries. J. Mater. Chem., 22, 7537.

[164] **Hong, J.** (2009). Synthesis and Characterization of High Performance Electrode Materials for Lithium Ion Batteries, PhD Thesis, State University of New York, USA.

[165] **Wilcox, J.D., Doeff, M.M., Marcinek, M. and Kostecki, R.** (2007). Factors Influencing the Quality of Carbon Coatings on $LiFePO_4$. Journal of Electrochemical Society, 154, 5, A389-A395.

[166] **Salehi, A.** (2013). Performance Qualification and Raman Investigation on Cell Behaviour and Aging of $LiFePO_4$ Cathodes in Lithium-Ion Batteries. MSc. Thesis, The University of Texas at Arlington, USA.

[167] **Patey, J.T.** (2009). Oxide Nanoparticles for Electrodes in Lithium-Ion Batteries. PhD Thesis, ETH Zurich, Switzerland.

[168] **Fang, H., Liang, G., Zhao, L., Wallace, T., Arava, H., Zhang, L.-L., Ignatov, A. and Croft, M. C.** (2013). Electrochemical Properties of Cathode Material $LiFePO_4$ with Ti Substitution. Journal of The Electrochemical Society, 160, 5, A3148-A3152.

[169] **Sun, X., Sun, K., Wang, Y., Bai, X., Chen, C. and Cui, B.** (2013). Scale-up synthesis, Structure Characterization and Electrochemical Characteristics of C-$LiFePO_4$ Nanocomposites for Lithium Ion Rechargeable Batteries. Int. J. Electrochem. Sci., 8, 12816 – 12836.

[170] **Park, C.K., Park, S.B., Oh, S.H., Jang, H. and Cho, W.II.** (2011). Li-ion Diffusivity and Improved Electrochemical Performances of the Carbon Coated $LiFePO_4$, Bull. Korean Chem. Soc., 32, 3, 836.

APPENDICES

APPENDIX A: TGA Plots of CCL/$LiFePO_4$ samples

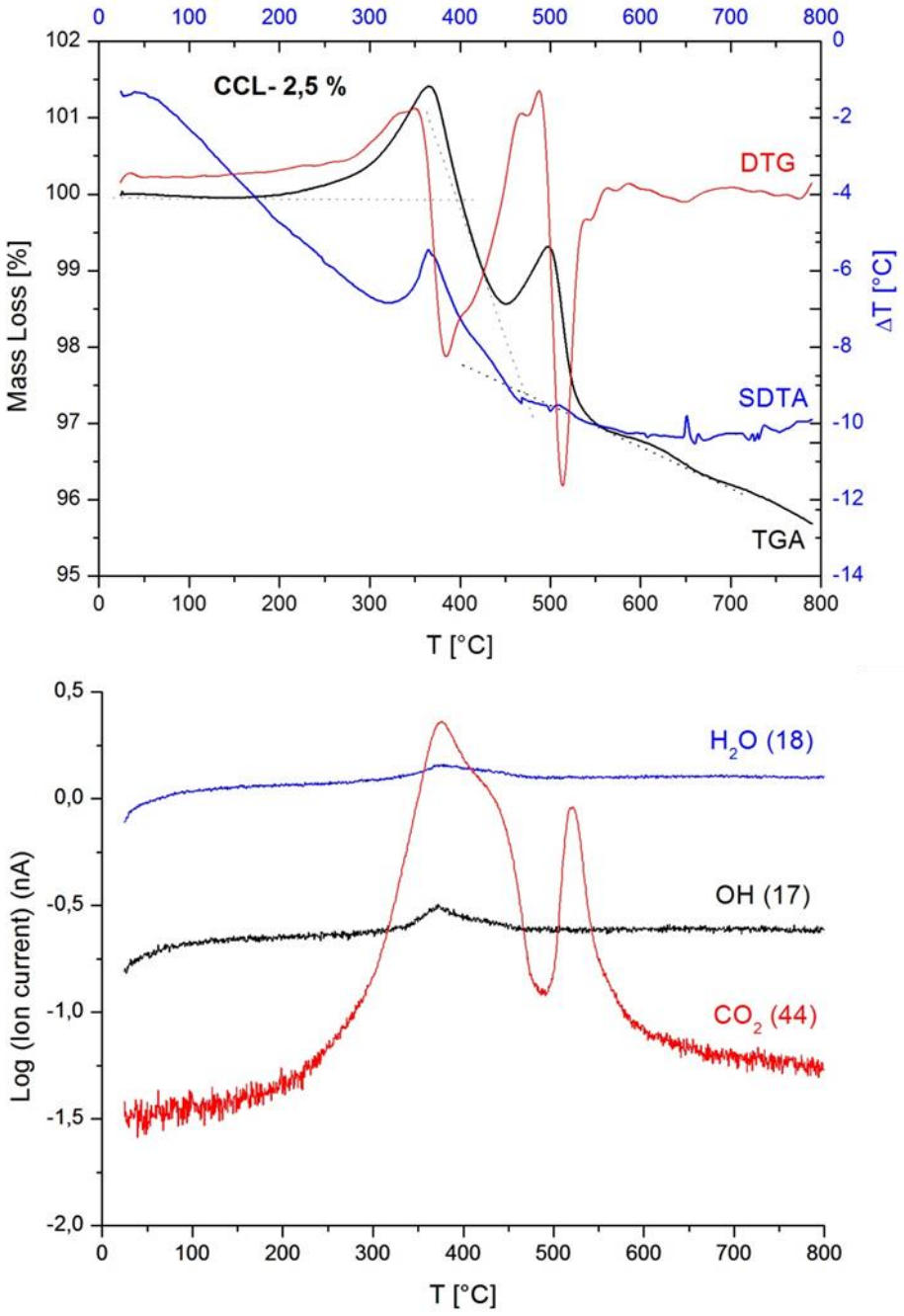

Figure A.1: TGA and QMS results of 5 CCL/$LiFePO_4$ powders.

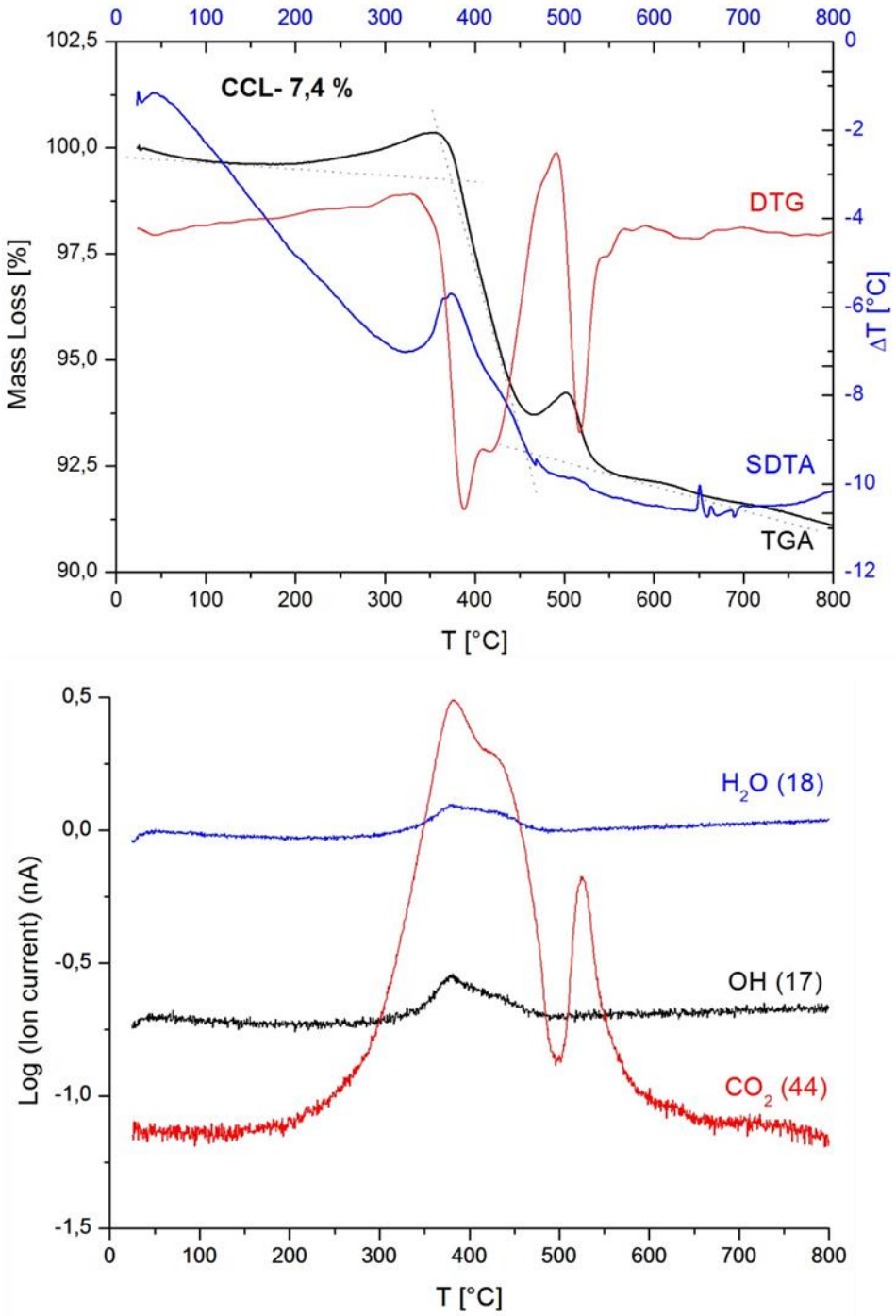

Figure A.2: TGA and QMS results of 10 CCL/$LiFePO_4$ powders.

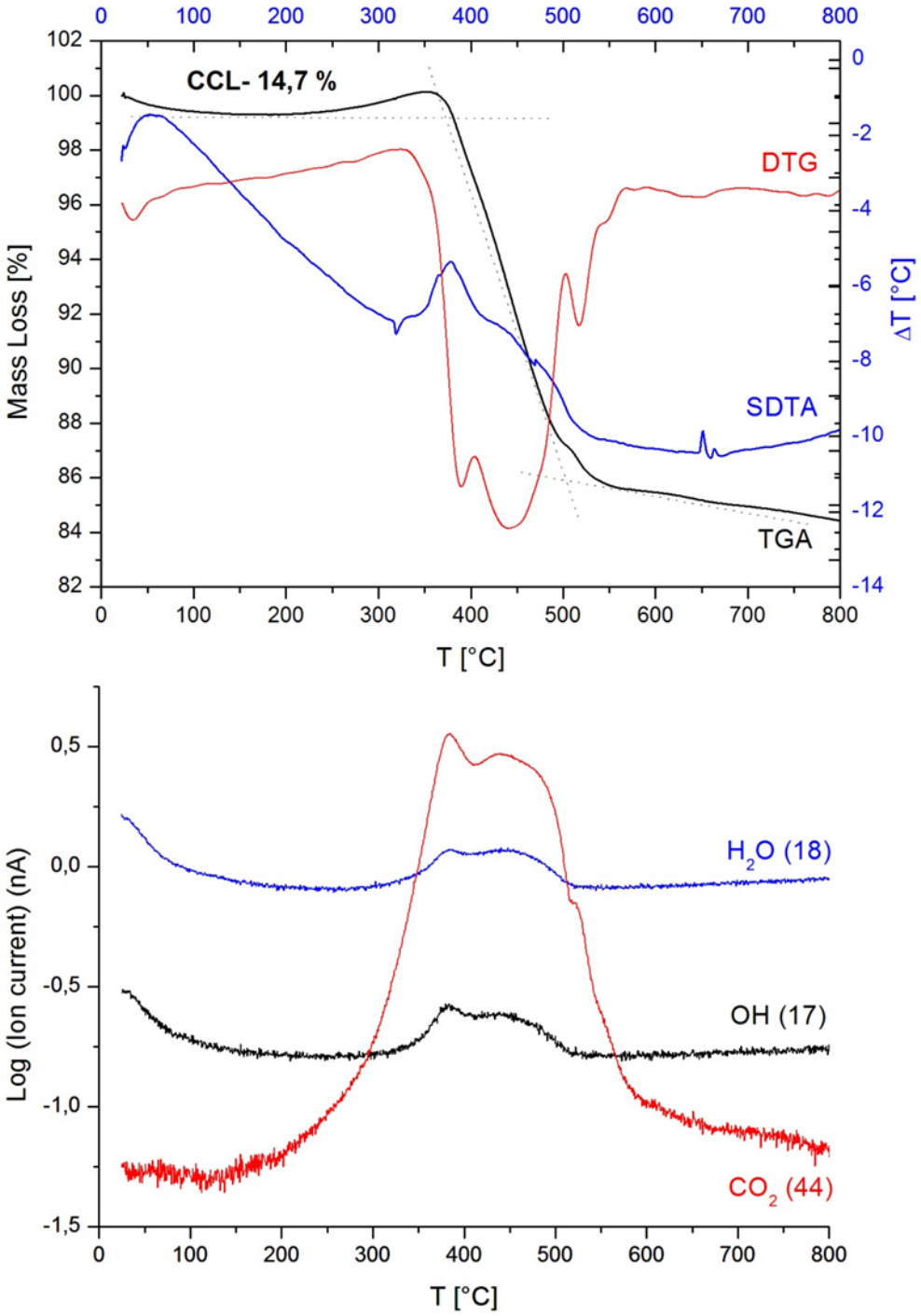

Figure A.3: TGA and QMS results of 20 CCL/$LiFePO_4$ powders.

APPENDIX B: BET Plots of CCL/ $LiFePO_4$ samples

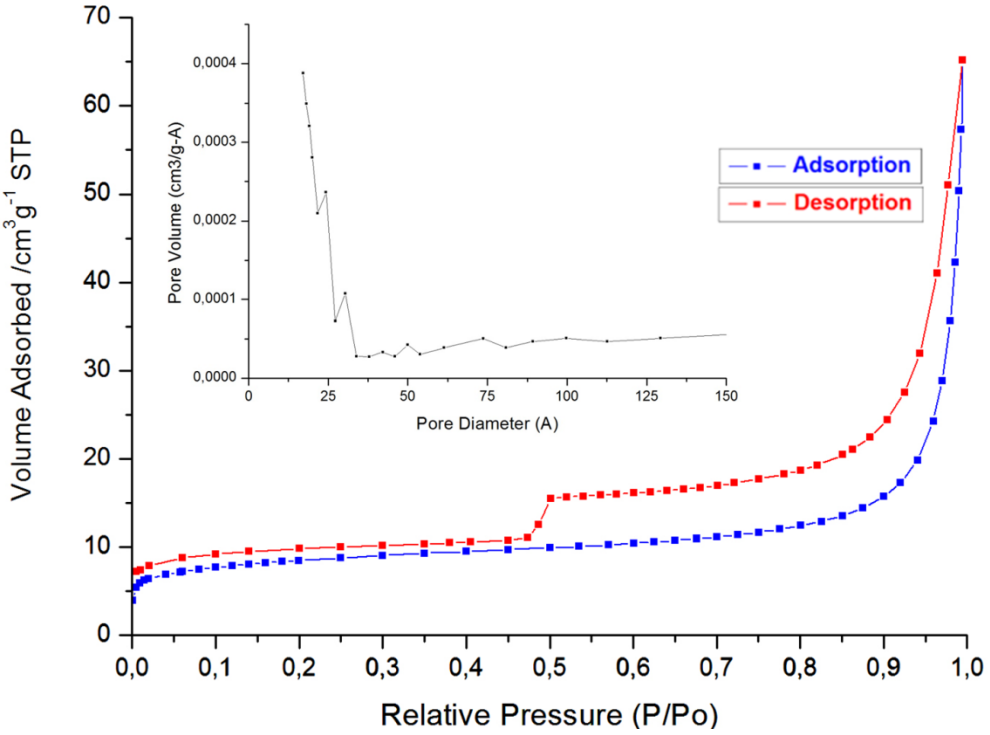

Figure B.1: BET graph of 5 CCL/ $LiFePO_4$ powders after pyrolysis.

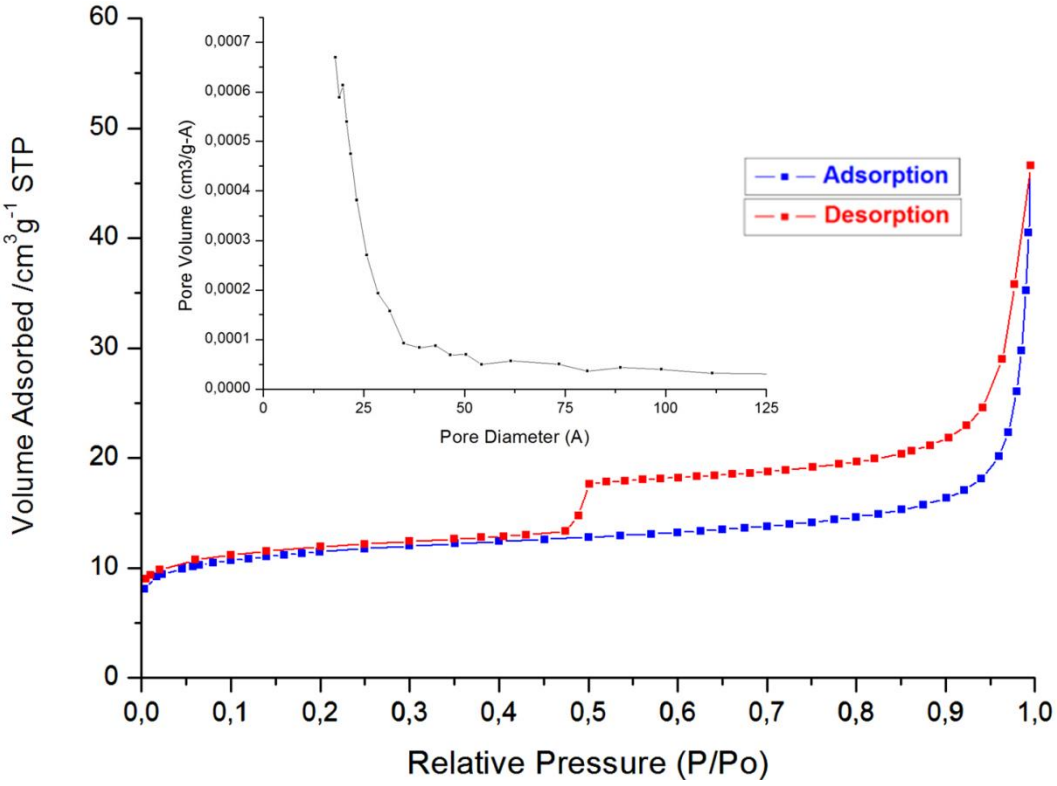

Figure B.2: BET graph of 10 CCL/ $LiFePO_4$ powders after pyrolysis.

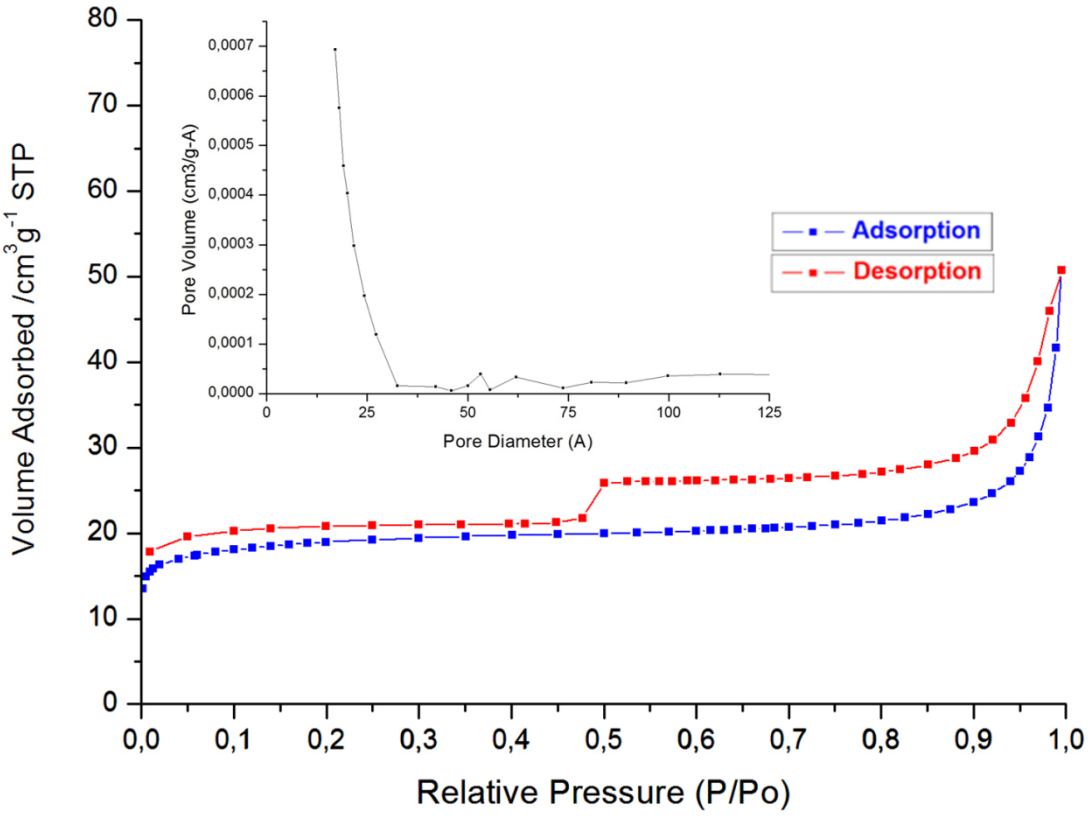

Figure B.3: BET graph of 20 CCL/ $LiFePO_4$ powders after pyrolysis.

CURRICULUM VITAE

Name Surname: Yahya TOPRAK

Place and Date of Birth: Istanbul/25-11-1987

Address: Kisikli Mah. Gemici Sok. No:18/5 Uskudar/Istanbul

E-Mail: yahya.toprak@gmail.com

B.Sc.: Material Science and Engineering/Gebze Institute of Technology

Projects

1) Production and characteriazation of $LiMO_x$ cathode materials for rechargable lithium-ion batteries using aluminum oxide templates-33996-ITU-BAP Project-November 2010-June 2012.

2) Production and characterization of nano pored CuSn and CuSi anode alloys materials obtained with electron beam technique- 110M148 TUBITAK Project - January 2011- June 2012.

3) Production and characterization of $LiFePO_4$ nano powders produced in non aqueous solutions, Istanbul Technical University/Jagielloian Universitesi (Poland) project- October 2012-September 2013.